CHAIN COLLAPSE, AGGREGATION AND MEMBRANE-INDUCED FOLDING OF AMYLOIDOGENIC PROTEINS

NEHA JAIN

Thesis submitted for the partial fulfillment of the degree of

DOCTOR OF PHILOSOPHY

Department of Biological Sciences

Indian Institute of Science Education and Research (IISER) Mohali

March 2013

CHAIN COLLAPSE, AGGREGATION AND MEMBRANE-INDUCED FOLDING OF AMYLOIDOGENIC PROTEINS

NEHA JAIN

Thesis submitted for the partial fulfillment of the degree of

DOCTOR OF PHILOSOPHY

Department of Biological Sciences

Indian Institute of Science Education and Research (IISER) Mohali

March 2013

Dedicated

to

my parents

Declaration

The work presented in this thesis has been carried out by me under the supervision of Dr. Samrat Mukhopadhyay at the Department of Biological Sciences, Indian Institute of Science Education and Research (IISER) Mohali.

This work has not been submitted in part or full for a degree, a diploma, or a fellowship to any other university or institute.

Whenever contributions of others are involved, every effort is made to indicate this clearly, with due acknowledgement of collaborative research and discussions. This thesis is a bona fide record of original work done by me and all sources listed within have been detailed in the bibliography.

Date Place Neha Jain

In my capacity as supervisor of the candidate's thesis work, I certify that the above statements by the candidate are true to the best of my knowledge.

Dr. Samrat Mukhopadhyay

(Supervisor)

Acknowledgements

The work described in this thesis is a result of contribution from a large number of people over the past few years of my stay at IISER Mohali. It gives me immense pleasure to convey my gratitude to all of them.

I feel fortunate to be a graduate student of Dr. Samrat Mukhopadhyay. Words/sentences are just insufficient to describe his unflinching encouragement, support, and guidance throughout my research. I thank him for providing an excellent scientific environment with state-of-the-art equipments, teaching me rigors of the lab work, stimulating discussions, and immense faith in me. My strong work ethics and enthusiasm for my research, is attributed entirely to my supervisor. He gave me the intellectual freedom to direct and expand my own projects to new horizons. He allowed me to dabble in some different and exciting projects leading to the use of new techniques and possibilities. His single sentence "There is always some light at the end of the tunnel" kept me motivated and instilled courage to pass over the frustration of failures. He has created and given a number of opportunities to interact and discuss with the eminent scientists in the field. I truly appreciate the countless hours he has spent to teach me, to think critically and communicate my ideas effectively. He has always been open to discuss not only the science, but life in general as a graduate student.

I owe my deepest gratitude to Dr. Mily Bhattacharya (DST Woman Scientist, IISER Mohali) for unremitting encouragement, generous help, friendship, active involvement, fruitful discussions and constructive feedback for the scientific improvement of my work. I dumped all my problems, questions, fear, anger on to her and she took care of them with enormous patience and enthusiasm. My Ph.D. would have been much tougher and longer in her absence. I duly acknowledge her for helping me analyze the Raman spectroscopic data used in Chapter 4 and

performing time-resolved experiments at TIFR Mumbai, included in Chapter 5 of this thesis. The AFM images used in Chapter 4 were recorded and analyzed by Mily.

I am grateful to all the former and present members of The Mukhopadhyay Lab for their cordiality and contribution to make my stay a memorable one. This includes Mily, Pushpender, Vijit, Dominic, Shruti, Karishma, Arpana, Hemaswasthi, Ritu, Shwetha, Priyanka, Anubhuti and Anshu. It was a pleasure working with all of them. I owe special thanks to Ritu, Karishma, Anubhuti and Hemaswasthi for their continuous and unconditional help that accelerated my thesis progress towards the end.

I would also like to thank my doctoral committee members, Dr. Lolitika Mandal and Dr. Kausik Chattopadhyay for giving critical comments and valuable suggestions on my thesis. The enormous support from the members of other laboratories at IISER Mohali is greatly appreciated and acknowledged particularly people from Prof. Bachhawat's Lab, Prof. Guptasarma's Lab, Dr. Chattopadhyay's Lab and Dr. Chaba's Lab. I would also like to thank the official staff at IISER Mohali for their support and taking care of all the paper-work.

I would like to acknowledge Prof. Vinod Subramaniam (University of Twente, Netherlands) for providing with α-synuclein plasmid. I am thankful to Prof. G. Krishnamoorthy (TIFR Mumbai) for providing us access to time-resolved fluorescence instrumentation. I would like to thank Mr. Supratim Banerjee (I.I.Sc., Bangalore) for recording TEM images, Ms. Sharanjeet Kaur (IMTECH, Chandigarh) for her help in circular dichroism experiments and Ms. Shikha Singh (IMTECH, Chandigarh) for helping in dynamic light scattering experiments.

I am thankful to Prof. N. Sathyamurthy, the Director of IISER Mohali, for being supportive and providing all the facilities. I would like to acknowledge Mrs. S. Sathyamurthy (Honorary Counselor, IISER Mohali) for her suggestions, caring and encouraging words that

kept me motivated during my stay at IISER Mohali. I am also thankful to IISER Mohali for the financial support throughout my thesis.

I would like to express my sincere appreciation to all my friends and past mentors around the globe. Their constant moral support pushed me through the difficult routes. I thank my childhood friend, Manish for preparing the graphical model used in Chapter 6.

Last but not the least, I want to express all my thanks and love to my parents, sister, brother-in-law and two little nephews for their incessant love and prayers which gave me strength to finish this thesis. It would have been impossible to complete this journey without the caring words my family has given me over the years.

List of Publications:

1. N. Jain, M. Bhattacharya and S. Mukhopadhyay (2011) Kinetics of surfactant-induced aggregation of lysozyme studied by fluorescence spectroscopy. *J. Fluorescence* 21:615-625.

2. M. Bhattacharya, N. Jain, K. Bhasne, V. Kumari and S. Mukhopadhyay (2011) pH-induced conformational isomerization of bovine serum albumin studied by extrinsic and intrinsic protein fluorescence. *J. Fluorescence* 21:1083-1090.

3. M. Bhattacharya, N. Jain and S. Mukhopadhyay (2011) Insights into the mechanism of aggregation and fibril formation from bovine serum albumin. *J. Phys. Chem. B* 115: 4195-4205.

4. N. Jain, M. Bhattacharya and S. Mukhopadhyay (2011) Chain collapse of an amyloidogenic intrinsically disordered protein. *Biophys. J.* 101:1720-1729.
   Featured as a 'Must Read' article in *Faculty of 1000*.

5. M. Bhattacharya,* N. Jain,* P. Dogra, S. Samai and S. Mukhopadhyay (2013) Nanoscopic amyloid pores formed via stepwise protein assembly. *J. Phys. Chem. Lett.* 4:480-485.
   *Joint first author

6. N. Jain, K. Bhasne and S. Mukhopadhyay. Dynamic hydration map illuminates the key structural features of membrane-bound α-synuclein. (Manuscript in preparation)

7. N. Jain, K. Bhasne, R. Roy Chowdhury and S. Mukhopadhyay. Mapping conformational dynamics of micelle-bound α-synuclein. (Manuscript in preparation).

Presentations and Abstracts:

1. Presented a poster entitled "Study of Protein Misfolding and Aggregation by Fluorescence Spectroscopy". **N. Jain**, M. Bhattacharya and S. Mukhopadhyay at 1st South-East Asian Course on F-techniques: FCS, FCCS, FLCS, FRET, FLIM and FRAP held in Singapore. (June 2011).

2. Presented a poster entitled "Study of Protein Misfolding and Aggregation Using Fluorescence Spectroscopy". **N. Jain**, M. Bhattacharya and S. Mukhopadhyay at National Fluorescence Workshop, FCS 2011 held in New Delhi, India. (Nov 2011).

3. Presented a poster entitled "Amyloidogenic Intrinsically Disordered Proteins: From Chain Collapse to Amyloid Assembly". **N. Jain**, M. Bhattacharya and S. Mukhopadhyay at the Gordon Research Conference on Intrinsically Disordered Proteins held at Vermont, USA (July 2012).

4. Presented a poster entitled "Gaining Structural Insights into the Binding-induced Folding of α-synuclein by Extracting Dynamical Signatures". **N. Jain**, R. Roy Chowdhury, and S. Mukhopadhyay at International Symposium on Protein Folding and Dynamics held at National Centre for Biological Sciences (NCBS) Bangalore, India. (Oct. 2012).

Synopsis

Chain Collapse, Aggregation and Membrane-induced Folding of Amyloidogenic Proteins

Neha Jain

Department of Biological Sciences

Indian Institute of Science Education and Research (IISER) Mohali

Thesis supervisor: Samrat Mukhopadhyay

Chapter 1: Introduction

Proteins are molecular workhorses that adopt native folded structures to execute a myriad of biological functions. However, in the cellular milieu, due to a variety of reasons, the protein folding process can go wrong resulting in the formation of aberrant or misfolded form of proteins. Protein misfolding is manifested as one of the key pathogenic events in many neurodegenerative disorders such as Alzheimer's, Parkinson's and prion diseases that are characterized by the accumulation of proteinaceous deposits comprising cross β-rich ordered aggregates known as amyloid fibrils. The precise molecular mechanism that triggers the misfolding and determines the arrangement of misfolded proteins within amyloid fibrils still remains elusive. In this thesis, efforts were directed towards delineating the early as well as the late molecular events of chain collapse, aggregation and binding-induced folding of a variety of model amyloidogenic proteins using a combination of biophysical techniques such as fluorescence, circular dichroism, dynamic light scattering, Raman spectroscopy and atomic force microscopy (Figure 1). Taken together, the findings described in this thesis may facilitate to uncover the underlying molecular mechanisms of protein amyloidogenesis.

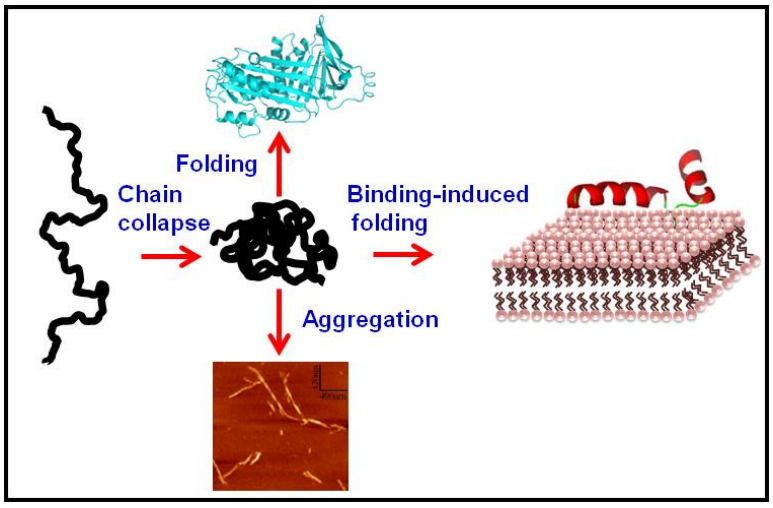

Figure 1. Chain collapse at the crossroad of folding, binding-induced folding and aggregation.

Chapter 2: Mechanism of Surfactant-induced Aggregation of Lysozyme

The study of protein conformational changes in the presence of surfactants and lipids is important in the context of membrane-induced protein aggregation. In this work, we have investigated the mechanism of the protein conformational change coupled with aggregation leading to size growth of hen egg white lysozyme (HEWL) in the presence of an anionic detergent such as sodium dodecyl sulphate (SDS) in alkaline pH. We have utilized intrinsic and extrinsic fluorescent probes to follow the protein conformational change in real-time. The kinetic parameters reveal that aggregation proceeds with an initial fast-phase (conformational change) followed by a slow-phase (self-assembly). Our results indicate that, at sub-micellar concentration, SDS induces conformational expansion that triggers the aggregation process at a micromolar protein concentration range (Figure 2).

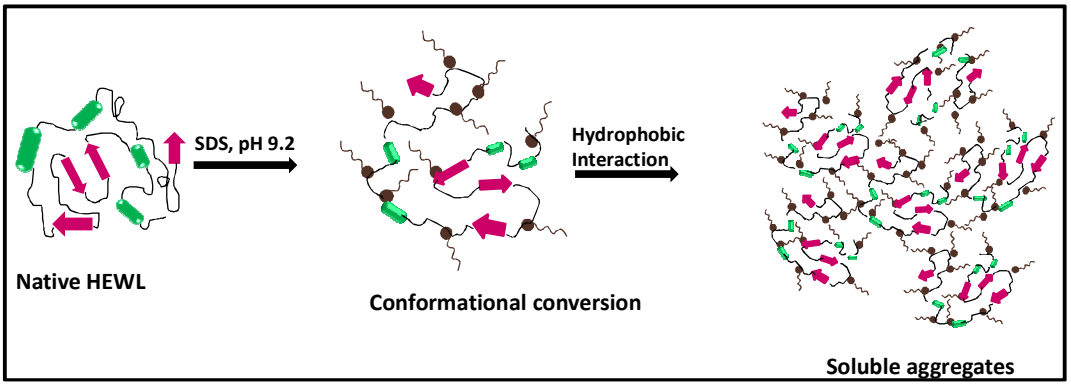

Figure 2. Proposed mechanism of surfactant-induced lysozyme aggregation.

Chapter 3: Mechanism of Amyloid Formation from Bovine Serum Albumin

Serum albumins are multi-domain, all α-helical proteins that are present in the circulatory system and aid in the transport of a variety of biomolecules. Herein, we have investigated the structural features of the pH-dependent conformers of bovine serum albumin. Our results indicate that at pH 3, a partially-folded, 'molten-globule-like' state is populated which unfolds in a non-cooperative fashion and is thermodynamically less stable than the native state. Next, we investigated the fibrillation propensity of this conformer at low pH and high temperature and observed that the partially-folded conformers associate to form oligomers that matured into ordered amyloid-like fibrils. We have elucidated the mechanism of fibril formation by monitoring changes in the kinetics of structural probes during the aggregation process. Our findings suggest that the conformational conversion occurs in the oligomers that serve as precursors to amyloid fibrils and precedes the overall fibrillar growth (Figure 3).

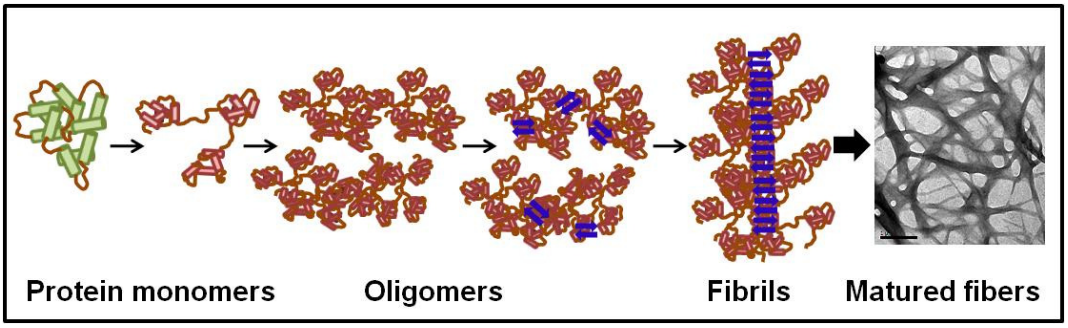

Figure 3. Proposed pathway for amyloid fibril formation from bovine serum albumin.

Chapter 4: Organization of Protein Molecules within the Amyloid Pores Revealed by Raman Spectroscopy

In the present study, we have used ovalbumin as a model protein to delineate the organization of protein molecules within the nanoscopic amyloid pores using atomic force microscopy and Raman spectroscopy. Raman spectroscopic investigations illuminated in-depth molecular details into the structural changes of the protein by monitoring both the amide backbone and the side chains of a several amino acid residues during amyloid assembly and pore formation (Figure 4). Additionally, Raman measurements indicated the presence of antiparallel β-sheets in the amyloid core.

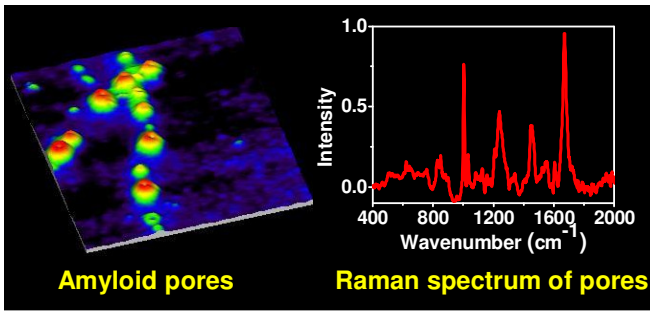

Figure 4. Raman spectroscopy of amyloid pores.

Chapter 5: Chain Collapse of an Amyloidogenic Intrinsically Disordered Protein

Polypeptide chain collapse of amyloidogenic natively unfolded or intrinsically disordered proteins (IDPs) is believed to play a key role in protein misfolding, oligomerization, and aggregation leading to amyloid fibril formation. In this work, we have used bovine κ-casein as an archetypal model protein for amyloidogenic IDPs. Using a variety of biophysical tools we first established that monomeric κ-casein adopts a collapsed premolten-globule-like conformational ensemble under physiological conditions. Our time-resolved fluorescence and light-scattering data indicate a change in the mean hydrodynamic radius from ~4.6 nm to ~1.9 nm upon chain collapse. We then covalently labeled two cysteines using thiol-reactive pyrene maleimide. This dual-labeled protein demonstrated a strong excimer formation upon renaturation from urea- and acid-denatured states under both equilibrium and kinetic

conditions, providing compelling evidence of polypeptide chain collapse under physiological conditions (Figure 5).

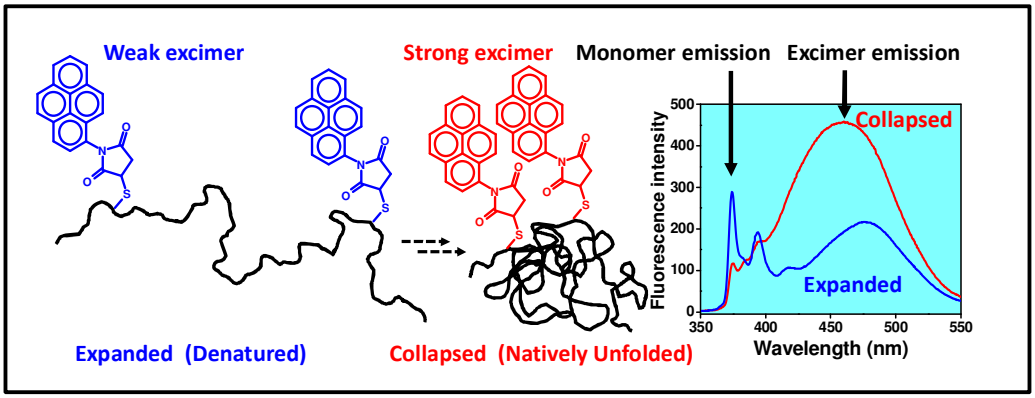

Figure 5. Chain collapse of an amyloidogenic IDP observed by pyrene excimer formation.

<u>Chapter 6:</u> Dynamic Hydration Map Reveals Key Structural Insights into Membrane-bound α-synuclein

The membrane-assisted folding and aggregation of α-synuclein, a natively unfolded soluble neuronal protein, is believed to be involved in both the normal cellular functions and the etiology of Parkinson's disease. Since α-synuclein is devoid of tryptophan, we have generated a number of single tryptophan mutants that behaved like the wild-type protein. Using these mutants, we have shown the residue-specific conformational rearrangement of α-synuclein from random coil to a helical-state on the membrane surface by monitoring both fluorescence anisotropy and hydration dynamics along the sequence of α-synuclein. Our fluorescence data illuminate the key structural details on the proximal positioning of residues on the membrane surface comprising negatively charged lipids (Figure 6). We believe that the structural arrangement of α-synuclein on the membrane will have implications in its function and disease progression.

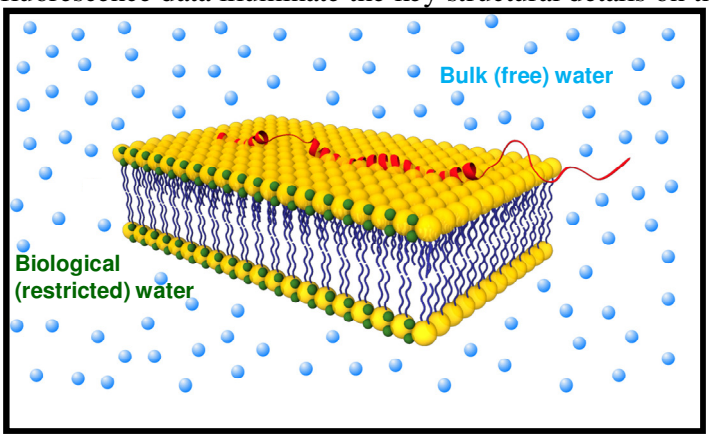

Figure 6. Structure of membrane-bound α-synuclein elucidated by measuring the dipolar relaxation of water molecules at the membrane interface.

Table of Contents

Chapter: 5 Chain Collapse of an Amyloidogenic Intrinsically Disordered Protein

Chapter: 6 Dynamic Hydration Map Reveals Key Structural Insights into Membrane-Bound α-Synuclein

Chapter 1

Introduction

1.1 Protein misfolding and aggregation

Proteins are the molecular workhorses capable of performing a myriad of cellular functions. For most proteins the polypeptide chain must fold into a specific structure to perform the function[1]. However, the question of how an unstructured linear sequence of amino acids can rapidly and efficiently fold from the countless alternatives has perplexed the scientists for past many decades. The process is not random but has been selected to have specific characteristics which would help in folding and hence gives enormous ability to generate selectivity and diversity in their functions.[2]

Inside the cell, the folding process is assisted by molecular chaperons that prevent unwanted interactions and assist in maintaining folding-competent conformation of a protein. When a protein fails to adopt its native conformation or undergoes misfolding, it can result in the formation of various types of aggregates. Under the controlled cellular environment, misfolded proteins are degraded through special mechanisms and thus protein aggregation is prevented. However, despite multiple preventative and corrective mechanisms, misfolding of proteins does occur and can have dire consequences.[3] Aggregation of misfolded proteins that elude the quality-control mechanisms lead to progression of highly debilitating diseases such as Alzheimer's, Parkinson's, Huntington's and prion diseases and a variety of other systemic amyloidosis. These pathologies are associated with the accumulation of ordered protein aggregates known as amyloid fibrils and therefore are collectively termed as "amyloidosis".[4,5]

1.2 Structure and genesis of amyloids

The term "amyloid" was given by Rudolf Virchow in 1854 to refer the abnormal deposit within the brain slice which appeared violet due to iodine staining property specific to cellulose, however, it was later demonstrated that amyloids are composed of protein aggregates.[6] By definition, amyloids can be described as 'a highly-ordered protein aggregate with an unbranched filamentous morphology'.[7] The hallmark of amyloid fibrils is the typical X-ray diffraction pattern where the repeating cross-β motif shows two distinct signals, one at 4.7 Å corresponding to the hydrogen bonding distance between the strands in each sheet and one between 6-11 Å indicates the spacing between different interacting sheets. Under electron microscopy (EM), the fibrils appear as long, non-branched filaments with diameters of 6–12 nm (Figure 1.1).[8,9] Upon binding with amyloidophilic dye Congo Red, the fibrils give rise to an apple-green birefringence under cross polarized light.[10]

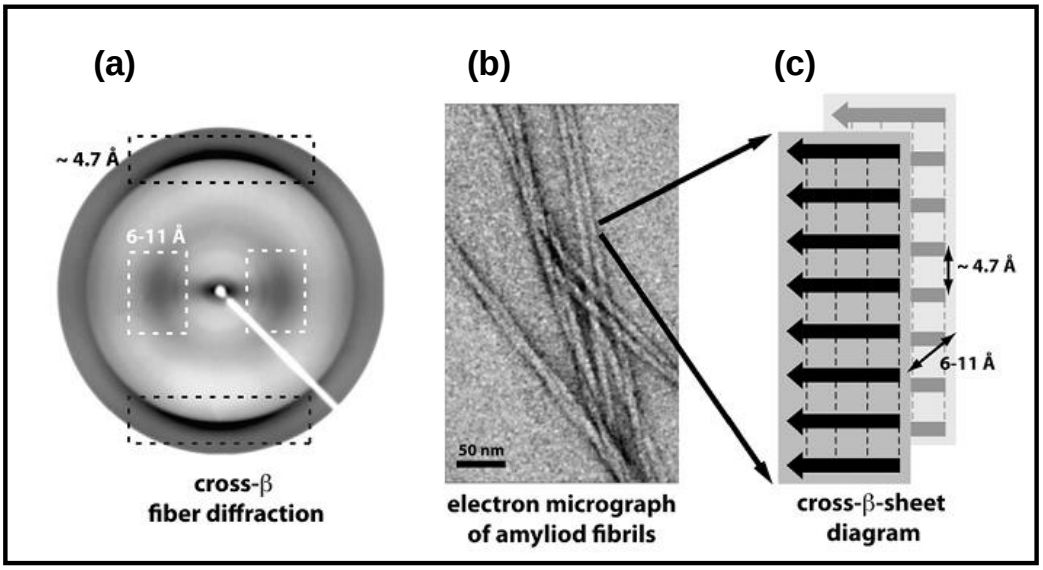

Figure 1.1 (a) X-ray fiber diffraction (b) Electron Micrograph (c) Proposed cross-β structural arrangement of amyloid fibrils. Reproduced with permission from Ref. 9.

This class of protein assembly is composed of highly ordered cross-β sheet wherein the β-strands are oriented perpendicular to the fibril axis and the inter-strand hydrogen bonds as well as the amino acid side chains are aligned parallel to the fibril axis (Figure 1.2).[11,12] These structures are highly stable, resistant to proteolysis and the cellular machinery is unable to degrade them.[13]

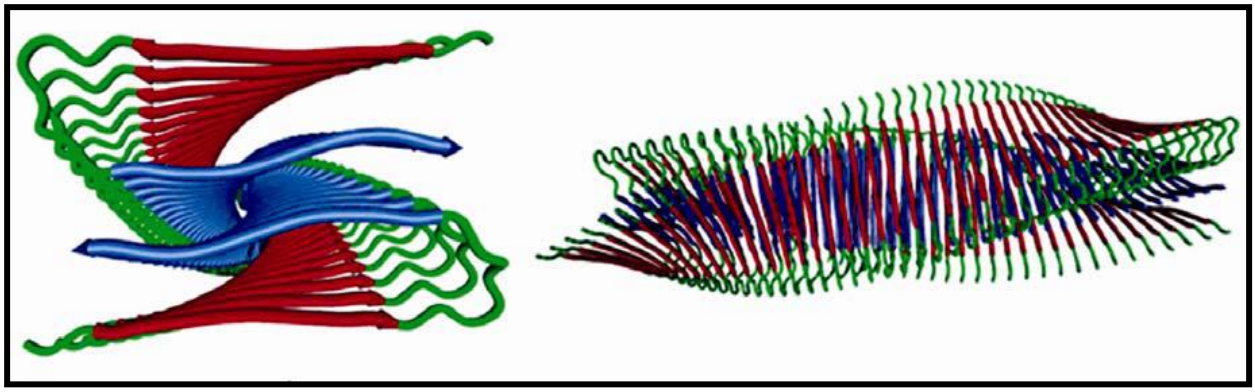

Figure 1.2 Arrangement of β-sheets in fibril. Adapted from Ref. 12.

The structural information on fibrils obtained for many of the amyloidogenic polypeptides and proteins is suggestive of differences in packing of the protofilaments. The heterogeneity in the morphology of mature fibrils generated due to differential packing leads to a phenomenon called "amyloid polymorphism".[14,15] The different aspects related to fibril organization and assembly are significantly influenced by the amino acid sequence and the environmental conditions. The fact that any protein can form amyloids under carefully designed conditions is leading to the consensus that the formation of amyloid is an inherent property of polypeptide chain and is fairly independent of sequence, size and the native structure of the protein.[16]

The precise mechanism of amyloid formation is yet to be elucidated. The pathway by which a polypeptide chain misfolds and aggregates is complex which varies with different proteins and the conditions. The fibril formation is considered as a stochastic process which is initiated by the generation of transient intermediates with heterogeneous conformations. These transient species, often oligomeric, eventually assemble into β-sheet-rich amyloids.[13] The properties and structures of these oligomeric aggregates are of immense interest to understand the mechanism of amyloid formation and its association with disease. Furthermore, cell culture studies have revealed higher toxicity of oligomers as compared to mature amyloid fibrils.[17] The amyloid formation process is usually modelled as a nucleation-elongation polymerization process, where the fibril formation is preceded by a lag phase and is concentration-dependent, indicating the formation of critical-oligomeric nucleus that facilitates the association and sequestration of other monomers into fibrils (Figure 1.3).[18,19] However, occasionally amyloid formation can be devoid of a lag phase and the initial oligomers drives the aggregation. Such a phenomenon has been demonstrated for many proteins like barstar[20] and prion protein[21] which can be explained by a few available kinetic models such as "random association",[22] "supercritical concentration driven fibril formation",[23] and "downhill polymerization".[24]

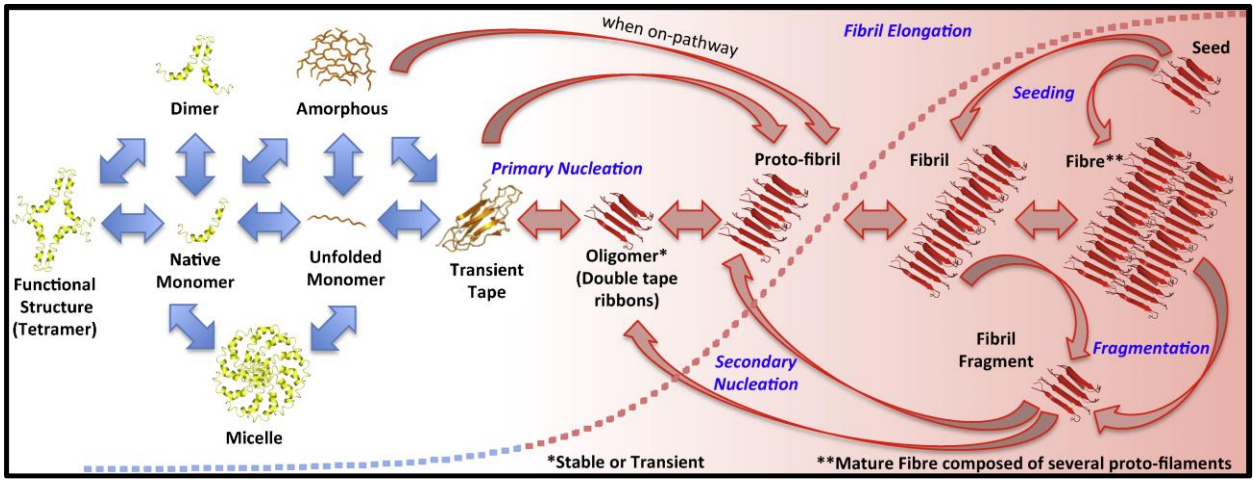

Figure 1.3 Schematic overview of amyloid assembly. Reproduced with permission from Ref. 19.

Amyloids are under intense scrutiny and a considerable progress is being made to understand the process using a combination of theoretical and experimental tools. A growing number of studies have now shown that the amyloids are not only associated with diseases but also have putative beneficial roles. This class of amyloids falls under the category of "functional amyloids".[25,26,27]

The structural diversity of amyloidogenic proteins and close similarity of the final fibrils imply that the key step in the amyloid fibril formation involves alterations in protein's native conformation, induced by the changes in the environmental conditions like pH, temperature, and ionic strength, etc., which initiate and promote the formation and accumulation of partially folded intermediates/conformers which are otherwise inaccessible under normal conditions. Considerable structural rearrangements in these intermediates are required in order to form mature fibrils. Therefore, it has been proposed that fibrillation of a globular protein requires the destabilization of its rigid native structure leading to the formation of a partially-unfolded and/or collapsed conformer. This collapsed or disordered state is believed to drive the aggregation process in the forward direction.[24] The implication of collapsed state in protein aggregation is discussed in the following section.

1.3 Intrinsically Disordered Proteins (IDPs)

Recent years have witnessed burgeoning interest in the class of proteins that lacks stable 3D structure under physiological conditions and exists as a dynamic ensemble of fluctuating conformers. These flexible proteins are commonly termed as Natively Unfolded or Intrinsically Disordered Proteins (IDPs).[28] IDPs can be empirically classified into pre-molten globule, structured-molten globule, collapsed disordered ensemble and extended disorder ensemble.[29] IDPs are known to perform a variety of crucial biological functions and thus defy the general

structure–function paradigm that correlates protein function with a well-defined structure. Several IDPs are known to be associated with amyloid formation that are involved in neurodegenerative disorders (Parkinson's and Alzheimer's)[30] as well as in functional amyloids (yeast prion proteins[31] and pMel[26]). It is demonstrated that the amyloidogenic IDPs under monomeric state can adopt a collapsed structural ensemble to avoid unfavourable chain-water interactions. At higher protein concentrations, polypeptide chains can associate to form oligomers that drive the amyloid assembly.[32] Also, the aggregation propensity of IDPs is substantially increased in the presence of a surface which may be provided by the biological membranes under physiological conditions.[33] In the next section, a brief description of membrane-induced aggregation is provided.

1.4 Membrane-induced protein misfolding and aggregation

Protein aggregation on the membrane surface proceeds through a series of events including binding, folding, insertion and association. It is becoming increasingly evident that protein fibrillization *in vivo* can also be induced and modulated at the membrane-water interface where lipid bilayer can act as an effective catalyst. Membrane-assisted fibrillogenesis is initiated by protein adsorption onto lipid bilayer followed by structural transition of the polypeptide chain into highly aggregation-prone conformers or oligomers which lead to fibril assembly and elongation.[33,34] These oligomers are known to be involved in disruption and permeabilization of membranes either by pore formation or by decreasing the lipid order ultimately culminating in cell death.[35,36] A recent review gives a comprehensive account on the interaction of membranes with amyloidogenic proteins with a perspective that the mechanism of these interactions have a some resemblance with those of pore-forming toxins derived from microorganisms.[37] It is

conceived that IDPs may adopt a stable structure upon membrane binding. For instance, α-synuclein, an IDP associated with etiology of Parkinson's disease, undergoes profound conformational transition from random coil to α-helix upon interaction with membranes which can further lead to fibrillation under suitable conditions.[38] The exact mechanism of membrane-induced fibrillation and cell death still remains an area of active research. Therefore, the elucidation of amyloidogenesis in membranes is crucial to ascertain the role of membranes in amyloid disorders.

1.5 Biophysical techniques to study aggregation mechanism

In this section, I summarize an array of biophysical tools that are used in the present work. A large number of tools are now available to monitor the kinetics of protein aggregation.[39] Here, we provide an overview of few *in vitro* biophysical techniques that are being used to monitor the different stages of protein misfolding leading to fibril formation with a greater emphasis on monitoring the changes in the early events of the process.

1.5.1 Conformational and size change probed by fluorescence spectroscopy

Fluorescence spectroscopy has proved to be a heuristic tool to extract information on protein folding, dynamics, assembly, membrane interaction and misfolding leading to amyloid formation.[40] Apart from being extremely sensitive, this technique has an advantage of capturing the protein conformational changes simultaneously with size changes.[40] Being a multiparametric technique, fluorescence spectroscopy can provide information about intensity, anisotropy, spectral shifts, lifetimes etc. of fluorophore(s) which can be used as specific markers for the monitoring monomeric, oligomeric and large-sized aggregated species formed during the process

of amyloid formation.[41] The following fluorescence parameters can be utilized to shed light on the local environment surrounding the fluorophore which in turn can provide unique structural information on aggregation process in a detailed fashion.

Fluorescence intensity and spectral shift:

The environmental effects on proteins can be monitored by intensity change and/or spectral shift of a fluorophore. These properties are also sensitive to presence of certain molecules (quenchers) that can quench the fluorescence of an exposed fluorophore. Tryptophan and tyrosine serves as intrinsic fluorophores in proteins which can be utilized to probe conformational changes during aggregation. Usually an increase in fluorescence intensity with a concomitant blue-shift in the emission maximum is an indication of the probe getting progressively buried during the aggregation.[41] Apart from intrinsic fluorophores, many extrinsic fluorophores can also be used which can bind covalently or non-covalently to the protein aggregates. Another strategy to monitor the aggregation process is the covalent modification of specific sites of a protein by a desired fluorophore. This wide range of fluorescent probes provides a handle to detect and distinguish between the prefibrillar oligomers and mature amyloid fibrils unambiguously leading to a better understanding of the events involved in amyloid formation.[42]

Fluorescence anisotropy:

Fluorescence anisotropy measurements are used to decipher the overall size and rigidity of the fluorophore attached to the biomolecules. Since anisotropy relies on the rate of reorientation of a fluorophore, therefore, larger size protein/aggregate will tumble slower and thus will have higher anisotropy.[41] Fluorescence anisotropy has been proven as an efficient tool

to differentiate monomeric protein from oligomers and fibrils since the rotational motion of a fluorophore is dampened during the growth of aggregates. The steady state fluorescence anisotropy (r_{ss}) is defined as

$r_{ss} = (I_{\parallel} - I_{\perp}G)/(I_{\parallel} + 2I_{\perp}G)$

where $I_{\parallel}$ and $I_{\perp}$ represent the fluorescence intensities when the orientation of the emission polarizer is parallel and perpendicular to the orientation of the excitation polarizer respectively. G is the geometry factor. The steady-state anisotropy is routinely used to probe the increase in the average aggregate size, whereas, time-resolved anisotropy measurements allow one to delineate the local and global rotational dynamics.

Fluorescence resonance energy transfer (FRET):

It is a common biophysical tool to study the alterations in biomolecular distance as a function of conformational changes and dynamics of a protein undergoing aggregation. FRET relies on the distance-dependent transfer of energy from a donor fluorophore to an acceptor fluorophore where donor's emission spectrum overlaps with the absorption of acceptor. The energy is transferred from the donor to the acceptor through dipole–dipole coupling. It is also known as 'Spectroscopic Ruler' or proximity indicator as it allows measurement of changes in distance ranging from 20Å to 100 Å.[41] The distance at which RET is 50% efficient is called the Förster distance, which is typically in the range of 20 to 60 Å. By suitably labelling the protein with donor and acceptor fluorophores, FRET measurements in combination with other spectroscopic techniques can be used to investigate conformational distributions in the monomeric protein due to change in solution conditions leading to oligomerization and aggregation.

1.5.2 Structural information from Raman spectroscopy

Raman spectroscopy can provide detailed structural insight into the biomolecules and has been used to unravel molecular structure within protein fibrils.[43] The Raman spectra of proteins arises from the bond vibrations of either the backbone chains or the side chains and lies in a region between 200 cm^{-1} and 3000 cm^{-1}. The frequencies of the Amide I and Amide III vibration bands allow determination of the average conformation of their backbone chain.[44] Although Raman spectroscopy is relatively insensitive, the advent of new developments such as tip enhanced Raman spectroscopy (TERS)[45] and coherent anti-stokes Raman scattering (CARS)[46] has significantly expanded the scope of this technique in biology.

1.5.3 Change in secondary structure observed by circular dichroism (CD)

CD is a powerful technique as it provides information about the changes in protein conformation.[47] In CD spectroscopy, the difference in absorbance of right- and left-circularly polarized light is measured. This phenomenon is very sensitive to the secondary structure and tertiary structure of proteins. The CD spectra of proteins can be used to estimate the contribution of different types of secondary structures such as α-helix, β-sheet and turns. The near-UV region is used to determine the tertiary structure of globular proteins where the chromophores are aromatic amino acids and disulfide bonds. During amyloid formation, CD can be used to monitor the changes in the secondary structure and the evolution of β-structure.

1.5.4 Variation in size of particles measured by dynamic light scattering (DLS)

DLS along with other fluorescent techniques have been used to elucidate complex aggregation kinetics and to reveal multiple stages of amyloid fibril formation.[48] It is a laser scattering technique capable of measuring size distributions of the diffusing particles in the nanometer to micron size range. DLS a powerful technique for systems with heterogeneous species since it allows the analysis of the samples containing broad distributions of species of widely differing molecular masses and to detect very small amounts of the higher mass species.

The spectroscopic techniques mentioned in the previous section give information related to changes in conformation and size during the fibril formation. In order to visualize the progressive changes in the nanoscale morphology, numerous high-resolution microscopic techniques have been developed in past few years. In the following section, a brief description of some of the imaging techniques used in this work is provided.

1.5.5 Nanoscale imaging of aggregates and fibrils

The present knowledge of the structural details of amyloid aggregates has greatly enhanced by the use of a diverse biophysical techniques. However, the molecular understanding of several important phenomena in amyloid biology remains largely elusive due to the limitations associated with the conventional imaging. Therefore, there is a pressing need to apply non-traditional super-resolution optical imaging that will map fibrils at a high spatial resolution as well retain the wealth of optical information. Electron microscopy (EM) provides high resolution and can be applied to obtain atomic resolution but the stringent and harsh requirements make it unapproachable for biological imaging. High-resolution scanning probe

microscopy (SPM)-based imaging technique such as atomic force microscopy (AFM) has been extremely useful in gaining in-depth insight into the nanoscale morphology of various kinds of aggregates and fibrils. AFM imaging provides very high-resolution topographic information but does not provide any optical signals. Near-field scanning optical microscopy (NSOM) breaks the far-field diffraction limit and allows both topographic and optical mapping simultaneously. Recently, NSOM has been used to resolve amyloid fibrils that were spatially separated by ~ 75nm.[49] Further, direct stochastic optical reconstruction microscopy (dSTORM) has been applied to achieve a nanoscopic resolution in fluorescence imaging of β-amyloid fibrils.[50] These newly developed high resolution imaging techniques could be utilized to address various interesting and important problems in amyloid biology.

1.6 Thesis perspective

The study of protein conformational change, kinetics, growth and morphological properties of amyloid aggregates is required to understand how all these characteristics are associated with human disorders. Further progress on the two following key questions is necessary in order to develop strategies to prevent misfolding and aggregation. How soluble proteins begin to misfold under physiological conditions? How the resultant oligomers/fibrils initiate cell dysfunction? Therefore, understanding the fundamental principles of normal and aberrant protein folding and their assembly can provide a connecting link between molecular physics and cell physiology. To highlight these factors, this thesis aims at uncovering the underlying biophysical mechanisms of chain collapse, membrane-induced protein folding and misfolding leading to aggregation in a diverse class of proteins (Figure 1.4). Taken together, I

believe that the work embodied in this thesis will enhanced our understanding towards the complex mechanisms of protein aggregation. The structural insights and mechanisms proposed herein may be useful in laying the groundwork to develop rational strategies to combat the deadly neurodegenerative diseases.

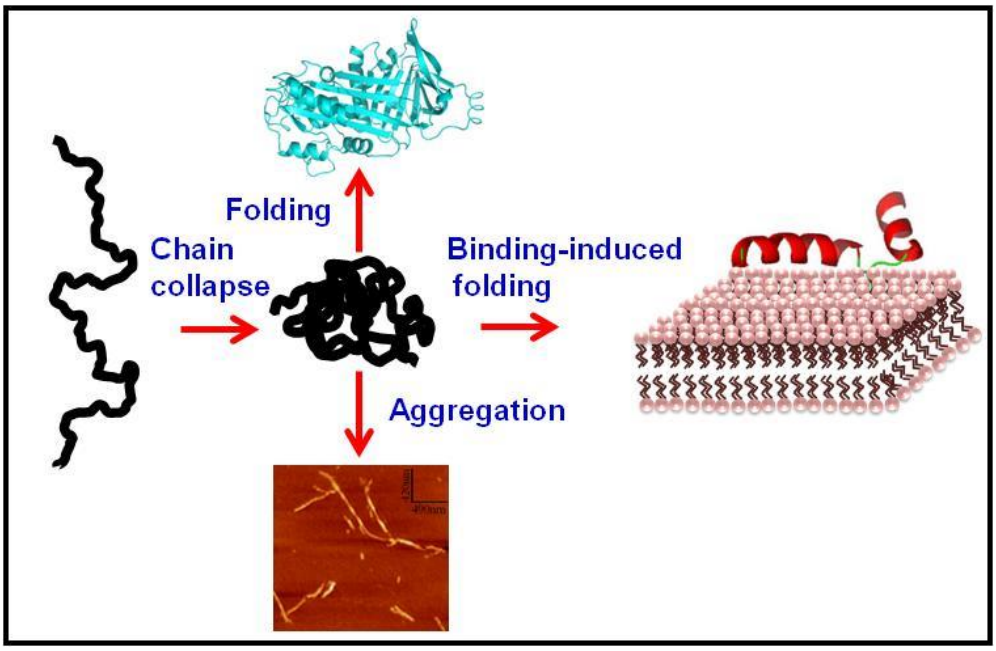

Figure 1.4 Chain collapse at the crossroad of folding, binding-induced folding and aggregation.

1.7 References

1. Udgaonkar, J. B. (2008) Multiple routes and structural heterogeneity in protein folding. *Annu. Rev. Biophys.* 37:489-510.

2. Vendruscolo, M.; Zurdo, J.; MacPhee, C. E.; Dobson, C. M. (2003) Protein folding and misfolding: a paradigm of self-assembly and regulation in complex biological systems. *Phil. Trans. R. Soc. Lond. A* 361:1205-1222.

3. Dobson, C. M. (2004) Experimental investigation of protein folding and misfolding. *Methods* 34:4-14.

4. Miranker, A. D. (2004) Unzipping the mysteries of amyloid fiber formation. *Proc. Natl. Acad. Sci. U.S.A.* 101:4335-6.

5. Eisenberg, D.; Jucker, M. (2012) The amyloid state of proteins in human diseases. *Cell* 148:1188-203.

6. Sipe, J. D.; Cohen, A. S. (2000) Review: history of the amyloid fibril. *J. Struct. Biol.* 130:88-98.

7. McGlinchey, R. P.; Yap, T. L.; Lee, J. C. (2011) The yin and yang of amyloid: Insights from α-synuclein and repeat domain of Pmel17. *Phys. Chem. Chem. Phys.*13:20066-20075.

8. Sunde, M.; Blake, C. (1997) The structure of amyloid fibrils by electron microscopy and X-ray diffraction. *Adv. Protein Chem.* 50:123-159.

9. Greenward, J.; Riek, R. (2010) Biology of amyloid: structure, function, and regulation. *Structure* 18:1244-60.

10. Westermark, G. T.; Johnson, K. H.; Westermark, P. (1999) Staining methods for identification of amyloid in tissue. *Methods Enzymol.* 309:3-25.

11. Geddes, A. J.; Parker, K. D.; Atkins, E. D.; Beighton, E. (1968) "Cross-beta" conformation in proteins. *J. Mol. Biol.* 32:343-58.

12. Petkova, A. T.; Yau, W.-M.; Tycko, R. (2006) Experimental constraints on quaternary structure in Alzheimer's β-amyloid fibrils. *Biochemistry* 45:498-512

13. Kumar, S; Udgaonkar, J. B. (2010) Mechanisms of amyloid formation by proteins. *Curr. Sci.* 96:1053-1070.

14. Wetzel, R. (2006) Kinetics and thermodynamics of amyloid fibril assembly. *Acc. Chem. Res.* 39:671-79.

15. Fändrich, M.; Meinhardt, J.; Grigorieff, N. (2009) Structural polymorphism of Alzheimer Aβ and other amyloid fibrils. *Prion* 3:89-93.

16. Chiti, F.; Webster, P.; Taddei, N.; Clark, A.; Stefani, M.; Ramponi, G.; Dobson, C. M. (1999) Designing conditions for in vitro formation of amyloid protofilaments and fibrils. *Proc. Natl. Acad. Sci. U.S.A.* 96:3590-4.

17. Glabe, C. G. (2008) Structural classification of toxic amyloid oligomers. *J. Biol. Chem.* 283:29639- 29643.

18. Jahn, T. R.; Radford, S. E. (2008) Folding versus aggregation: Polypeptide conformations on competing pathways. *Arch. Biochem. Biophys*. 469:100-117.

19. Invernizzi, G.; Papaleo, E.; Sabate, R.; Ventura, S. (2012) Protein aggregation: Mechanisms and functional consequences. *The Int. J. Biochem. Cell Biol.* 44:1541-1554.

20. Kumar, S.; Mohanty, S. K.; Udgaonkar, J. B. (2007) Mechanism of formation of amyloid protofibrils of barstar from soluble oligomers: Evidence for multiple steps and lateral association coupled to conformational conversion. *J. Mol. Biol.* 367:1186-1204.

21. Jain, S.; Udgaonkar, J. B. (2008) Evidence for stepwise formation of amyloid fibrils by the mouse prion protein. *J. Mol. Biol.* 382:1228-1241.

22. Thusius, D.; Dessen, P.; Jallon, J.-M. (1975) Mechanism of bovine liver glutamate dehydrogenase self-association I. Kinetic evidence for a random association of polymer chains. *J. Mol. Biol.* 92:413-432.

23. Powers, E. T.; Powers, D. L. (2006) The kinetics of nucleated polymerizations at high concentrations: Amyloid fibril formation near and above the "supercritical concentration". *Biophys. J.* 91:122-132.

24. Pappu, R. V.; Wang, X.; Vitalis, A.; Crick, S. L. (2008) A polymer physics perspective on driving forces and mechanisms for protein aggregation. *Arch. Biochem. Biophys*. 469:132-141.

25. Chapman, M. R.; Robinson, L. S.; Pinkner, J. S.; Roth, R.; Heuser, J.; Hammar, M.; Normark, S.; Hultgren, S. J. (2002) Role of Escherichia coli curli operons in directing amyloid fiber formation. *Science* 295:851-5.

26. Fowler, D. M.; Koulov, A.V.; Balch, W. E.; Kelly, J. W. (2007) Functional amyloid--from bacteria to humans. *Trends Biochem. Sci.* 32:217-24.

27. Otzen, D. (2010) Functional amyloid: turning swords into plowshares. *Prion* 4:256-64.

28. Tompa, P. (2010) Structure and function of intrinsically disordered proteins. CRC Press, Boca Raton, FL. U. S. A.

29. Uversky, V. N. (2002) Natively unfolded proteins: a point where biology waits for physics. *Protein Sci.* 11:739–756.

30. Uversky, V. N. (2008) Amyloidogenesis of natively unfolded proteins. *Curr. Alzheimer Res.* 5:260-287.

31. Scheibel, T.; Lindquist, S. L. (2001) The role of conformational flexibility in prion propagation and maintenance for Sup35p. *Nat. Struct. Biol.* 8:958-962.

32. Vitalis, A.; Pappu, R.V. (2011) Assessing the contribution of heterogeneous distributions of oligomers to aggregation mechanisms of polyglutamine peptides. *Biophys. Chem.* 159:14-23.

33. Gorbenko, G. P.; Paavo K.J. Kinnunen, P. K. J. (2006) The role of lipid–protein interactions in amyloid-type protein fibril formation. *Chem. Phys. Lipids* 141:72-82.

34. Murphy, R. M. (2007) Kinetics of amyloid formation and membrane interaction with amyloidogenic proteins. *Biochim. Biophys. Acta* 1768:1923-1934.

35. van Rooijen, B. D.; Claessens, M. M. A. E.; Subramaniam, V. (2009) Lipid bilayer disruption by oligomeric α-synuclein depends on bilayer charge and accessibility of the hydrophobic core. *Biochim. Biophys. Acta* 1788:1271-1278.

36. Martin T. Stöckl, M. T.; Zijlstra, N.; Subramaniam, V. (2012) α-Synuclein Oligomers: an Amyloid Pore? *Mol. Neurobiol*. doi:10.1007/s12035-012-8331-4.

37. Butterfield, S. M.; Lashuel, H. A. (2010) Amyloidogenic protein–membrane interactions: Mechanistic insight from mModel systems. *Angew. Chem. Int. Ed.* 49:5628-5654.

38. Pfefferkorn, C. M.; Jiang, Z.; Lee, J. C. (2012) Biophysics of α-synuclein membrane interactions. *Biochim. Biophys. Acta* 1818:162-171.

39. Nilsson, M. R. (2004) Techniques to study amyloid fibril formation in vitro. *Methods* 34:151-160.

40. Bhattacharya, M.; Mukhopadhyay, S. (2011) Studying protein misfolding and aggregation by fluorescence spectroscopy. *Reviews in Fluorescence* (Ed. Chris Geddes)

41. Lakowicz, J. R. (2006) *Principles of fluorescence spectroscopy*, 3rd edn. Kluwer Academic/Plenum, New York.

42. Munishkina, L. A.; Fink, A. L. (2007) Fluorescence as a method to reveal structures and membrane-interactions of amyloidogenic proteins. *Biochim. Biophys. Acta* 1768:1862-1885.

43. Yu, N.-Y.; Liu, C.; O'Shea, D. C. (1972) Laser Raman spectroscopy and the conformation of insulin and proinsulin. *J. Mol. Biol.* 70:117-132.

44. Tuma, R. (2005) Raman spectroscopy of proteins: from peptides to large assemblies. *J. Raman Spectrosc.* 36:307-319.

45. Deckert-Gaudig, T.; Deckert, V. (2010) Tip-enhanced Raman scattering (TERS) and high-resolution bio nano-analysis-a comparison. *Phys. Chem. Chem. Phys.* 12:12040-9.

46. Perney, N. M.; Braddick, L.; Jurna, M.; Garbacik, E. T.; Offerhaus, H. L.; Serpell, L. C.; Blanch, E.; Holden-Dye, L.; Brocklesby, W. S.; Melvin, T. (2012) Polyglutamine aggregate structure in vitro and in vivo; new avenues for coherent anti-Stokes Raman scattering microscopy. *PloS One* 7:e40536.

47. Kelly, S. M.; Jess, T. J.; Price, N. C. (2005) How to study proteins by circular dichroism. *Biochim. Biophys. Acta* 1751:119-139.

48. Streets, A. M.; Sourigues, Y.; Kopito, R. R.; Melki, R.; and Quake, S. R. (2013) Simultaneous measurement of amyloid fibril formation by dynamic light scattering and fluorescence reveals complex aggregation kinetics. *PLoS One* 8: e54541.

49. Dalal, V.; Bhattacharya, M.; Sharma, P. K.; Narang, D.; Mukhopadhyay, S. (2012) Nanoscale fluorescence imaging of single amyloid fibrils. *J. Phys. Chem. Lett.* 3:1783-1787.

50. Schierle, G. S. K.; van de Linde, S.; Erdelyi, M.; Esbjörner, E. K.; Klein, T.; Rees, E.; Bertoncini, C. W.; Dobson, C. M.; Sauer, M.; Kaminski, C. F. (2011) In Situ

measurements of the formation and morphology of intracellular β-amyloid fibrils by super-resolution fluorescence imaging. *J. Am. Chem. Soc.* 133:12902-12905.

Chapter 2

Mechanism of Surfactant-induced Aggregation of Lysozyme

This work has been published in *Journal of Fluorescence*

Reference: **N. Jain**, M. Bhattacharya and S. Mukhopadhyay. Kinetics of surfactant-induced aggregation of lysozyme studied by fluorescence spectroscopy. *J. Fluoresc.* **2011**, *21*, 615-625.

2.1. Introduction

Hen Egg White Lysozyme (HEWL) is an archetypal protein which has been extensively used to understand the mechanism of protein folding, misfolding and amyloid formation.[1-4] It is an attractive protein to use as a model because (i) it is a small single-domain protein with 129 amino acids and the molecular weight of 14.6 kDa (ii) it contains diverse secondary structures such as α-helix, β-sheet and random coil (Figure 2.1a) and (iii) it has a high degree of sequence and structural homology with human lysozyme that has been implicated in human amyloidosis.[5,6] Lysozyme forms fibrils under different conditions like high temperature and low pH[7], mutations,[8] proteolytic cleavage[9] and chemical modification.[10] It has been reported that aggregates of HEWL are toxic to cell cultures.[11,12] Aggregation of HEWL is shown to be a nucleation-dependent phenomenon which gives rise to a lag-phase and an assembly phase.[13]

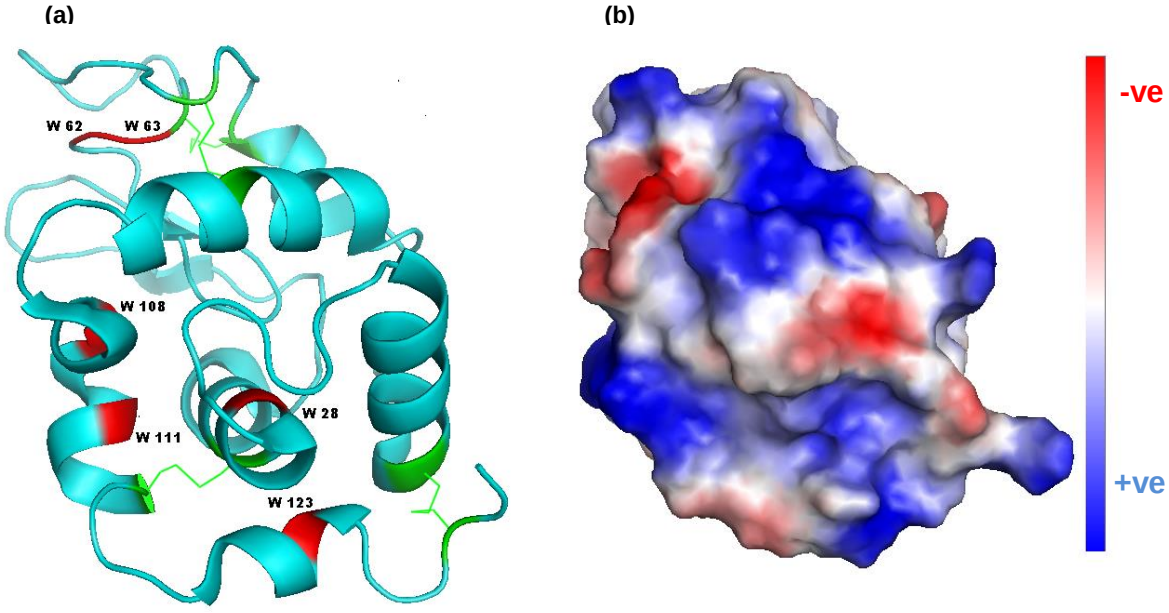

Figure 2.1 (a) Structure of Hen Egg White Lysozyme (HEWL; protein data bank ID: 1GWD; drawn using PyMol) showing tryptophans (red) and disulfide bonds (green) (b) Distribution of surface charge on HEWL (positive: blue and negative: red) charge.

Lysozyme also interacts with surfactants[14,15] and denaturants[16] to form amyloid fibrils under carefully-controlled *in vitro* conditions. The most commonly used surfactant is sodium dodecyl sulfate (SDS) which is an anionic detergent and mimics many features of biological membranes. SDS can bind to a variety of proteins and depending on its concentration, it may either induce or inhibit the aggregation.[17,18] The lysozyme-SDS complex has been studied in the context of biopolymer-surfactant interaction.[19,20] At pH lower than isoelectric point (pI 11), SDS interacts with positively charged exterior surface of HEWL and causes turbidity which is reduced with an increase in pH.[21] It was also shown that HEWL behaves differently in the presence of SDS at pH 9.2, where it leads to the formation of amyloid-like fibrils.[14]

The mechanism of the interaction of HEWL with SDS leading to oligomerization and aggregate formation is poorly understood. The present investigation aims at probing the mechanism of early conformational- and size changes during the course of aggregation in HEWL at pH 9.2 in the presence of SDS using fluorescence spectroscopy. We have utilized various reporters to shed light into the aggregation mechanism. Steady-state fluorescence intensity and anisotropy of different fluorescent reporters were used to extract information about the protein conformational change and the overall size growth that lead to the formation of soluble aggregates. The kinetic parameters recovered from the fluorescence kinetics have been used to suggest a mechanistic model of surfactant-induced aggregation of lysozyme.

2.2 Experimental Section

2.2.1 Materials

Hen Egg White Lysozyme (HEWL), 8-anilinonaphthalene-1-sulfonic acid ammonium salt (ANS) and Fluorescein-5-(6)-isothiocyanate (FITC) were purchased from Sigma-Aldrich. 5-Dimethylaminonaphthalene-1-sulfonyl chloride (Dansyl Chloride) was obtained from Molecular Probes (Invitrogen). All other chemicals were of analytical grade and were used as received.

2.2.2 Sample preparation

HEWL with a concentration of 1 mM was prepared in Milli-Q water and stored at 4 °C. Protein concentration was determined by measuring the absorbance at 280 nm using Perkin Elmer Lambda 25 UV-Vis Spectrophotometer. The extinction coefficient of HEWL is 38,000 $M^{-1}cm^{-1}$.[22] For all the experiments, a final concentration of 5 μM HEWL was used except for concentration dependence studies, where it ranged from 1 μM to 5 μM. Buffers with stock of 500 mM were prepared in Milli-Q water: Sodium phosphate pH (7-8) and Glycine-NaOH (pH 9, 9.2, and 10) and stored at 4 °C. Buffers were diluted 10-fold to yield a final concentration of 50 mM. pH of each buffer was adjusted using Cyberscan 510 pH meter procured from Eutech Pvt. Ltd with an accuracy of ±0.02. A stock of 100 mM Sodium Dodecyl Sulphate (SDS) was prepared in Milli-Q water. SDS stock was stored at room temperature (~ 24 °C). FITC solution was prepared in DMSO (dimethyl sulfoxide) and Dansyl chloride solution was prepared in DMF (dimethyl formamide) with a concentration of 5 mM. All probes were freshly dissolved in the required solvent and used in the labeling reaction immediately.

2.2.3 Fluorescence labeling of HEWL with different fluorophores

Surface labeling of HEWL was performed with Fluorescein isothiocyanate that reacts with the accessible amino groups of proteins. The procedure recommended by Molecular Probes was followed with slight modifications. Labeling was performed in freshly prepared 0.1M Na_2CO_3-$NaHCO_3$ buffer of pH 9 with equimolar proportions of HEWL and probe. The reaction was stirred on a stirrer in dark for 90 min at room temperature. Once the reaction was over, free dye was removed from labeled protein by transferring it into MICROCON YM 3 (cutoff 3000 Da; procured from Millipore) and centrifuging in Eppendorf 5230 centrifuge with 11,000 rpm at 10 ºC. The absorbance of filtrates and concentrated labeled protein were measured as a ratio at 280 nm and 488 nm for FITC labeled HEWL. Finally, the degree of labeling was determined using the molar extinction coefficient of 64,000 $M^{-1}cm^{-1}$ for FITC.[23] The protein was also labeled separately with dansyl chloride which covalently reacts with the amino groups of the surface residues of protein. Equimolar concentration of HEWL and dansyl chloride (500 μM) was taken in 0.1M Na_2CO_3-$NaHCO_3$ buffer (pH 9). The reaction mixture was allowed to stand for two hours at room temperature in the dark with intermittent mixing. After the reaction was over, it was stored at 4 °C in the dark.

2.2.4 Tryptophan fluorescence

Perkin Elmer LS 55 spectrofluorimeter was used to record steady-state fluorescence in a cuvette having pathlength of 10.0 mm. Following parameters were adjusted to monitor tryptophan intensity during aggregation: λ_{ex} = 280 nm with an excitation bandpass of 2.5 nm; λ_{em} = 350 nm with an emission bandpass of 2.5 nm. The kinetic data were collected at an interval of 10 seconds with an integration time of 5 seconds. For the equilibrium data, the emission spectra

were recorded after 30 min of incubation with a scan speed of 10 nm/min and averaged over five scans. Fluorescence anisotropy was recorded with λ_{ex} = 300 nm, bandpass = 2.5 nm; λ_{em} = 350 nm, bandpass 9 nm with the G-factor correction. For anisotropy measurements, an integration time of 30 seconds was used to obtain a satisfactory signal-to-noise.

2.2.5 ANS fluorescence

A stock of 10 mM ANS in Milli-Q water was prepared and stored in the dark at 4 ºC. For all the experiments, a 1000-fold dilution of the stock was used to yield the final concentration of 10 μM ANS. The time-course of the ANS fluorescence intensity was used to characterize the aggregation kinetics. The following parameters were adjusted during the kinetic runs: λ_{ex} = 350 nm with an excitation bandpass of 2.5 nm; λ_{em} = 475 nm with an emission bandpass of 5 nm. The kinetic data were collected at an interval of 10 seconds with an integration time of 5 seconds. For the equilibrium data, the emission spectra were recorded after 30 min of incubation with a scan speed of 10 nm/min and averaged over five scans. The ANS fluorescence anisotropy was monitored with an excitation and emission bandpass of 2.5 nm and 8 nm, respectively with an integration time of 30 seconds. Perpendicular intensity components were corrected using the G-factor.

2.2.6 Aggregation conditions

Aggregation reaction with unlabeled protein was initiated by adding 5 μM HEWL to 150 μM SDS at pH 9.2 with a manual mixing dead-time of 10 seconds and the process was monitored over a period of time. Concentration dependence studies were performed as a function of (i) varying SDS concentration from 25 μM-200 μM (ii) varying HEWL concentration from 1 μM-5

μM. Control experiments were performed at pH 7, 8, 9 and 10 under similar conditions. All the experiments were carried out at room temperature (24-25 °C).

2.2.7 Aggregation with fluorescein labeled protein

The fluorescein-labeled protein was mixed thoroughly with the unlabeled protein under native non-aggregating condition at pH 7. The labeled protein concentration was 2% of the total protein used in the reaction mixture. A total protein concentration of 5 μM having 100 nM of the labeled protein was used to monitor the changes in the fluorescence intensity and anisotropy upon addition of SDS (150 μM) at pH 9.2. The following parameters were used: λ_{ex} = 488 nm with an excitation bandpass of 2.5 nm; λ_{em} = 514 nm with an emission bandpass of 4 nm (for intensity) and 7 nm (for anisotropy). The integration time was 5 and 30 seconds for the measurement of fluorescence intensity and anisotropy, respectively. The error in fluorescence anisotropy was below 0.01.

2.2.8 Aggregation with dansyl labeled protein

The dansyl-labeled protein was mixed thoroughly with the unlabeled protein under native non-aggregating condition at pH 7. The labeled protein concentration was 20% of the total protein used in the reaction mixture. A total protein concentration of 5 μM having 1 μM of the labeled protein was used to monitor the changes in the fluorescence intensity and anisotropy upon addition of SDS (150 μM) at pH 9.2. The following parameters were used: λ_{ex} = 340 nm with an excitation bandpass of 2.5 nm; λ_{em} = 500 nm with an emission bandpass of 5 nm (for intensity) and 8 nm (for anisotropy). The integration time was 5 and 30 seconds for the measurement of fluorescence intensity and anisotropy, respectively.

2.2.9 Circular Dichroism (CD) spectroscopy

The far-UV CD spectra of the protein samples were recorded on an Applied PhotoPhysics Chirascan CD spectrometer at room temperature. For the acquisition of CD spectra, the protein sample solutions were taken in a quartz cuvette of 2 mm pathlength and the secondary structural changes were recorded in the range of 190-260 nm. The scan rate was 1nm/sec and the final spectrum was the average of four scans. The spectra were corrected with buffer baseline subtraction and were smoothened using Chirascan software. For kinetic experiments, HEWL at pH 9.2 was taken in a quartz cuvette of 10 mm pathlength and SDS was added with a manual mixing deadtime of 10 seconds. The loss of helicity was monitored by change in ellipticity at 222nm.

2.2.10 Data analysis

The data were plotted and analyzed with non-linear curve fitting method using commercially available OriginPro Version 8.0 Software. All the plots were fitted to more than one functions and the best fit was used to explain the kinetics of the process. The goodness of the fit was determined by the adjusted R^2 and residual analysis.

2.3 Results

2.3.1 Intrinsic and extrinsic fluorescence of Lysozyme in the presence of SDS

The native monomeric form of hen egg white lysozyme (HEWL) converts into insoluble amyloid-like aggregates upon incubation with sodium dodecyl sulfate (SDS) at pH 9.2 at room temperature.[14] Our interest in the mechanism of protein aggregation led us to investigate the early events of the protein conformational change and aggregation that converts the monomeric protein into soluble oligomers. We have used three different fluorescent reporters namely tryptophan (intrinsic fluorophore), ANS (non-covalently bound fluorophore) and dansyl and fluorescein (covalently attached fluorophore) to observe the structural changes of HEWL in the presence of SDS at pH 9.2. Figure 2.2 shows the fluorescence emission spectra and the steady-state anisotropy plots of different fluorescent reporters in HEWL under different solution conditions at equilibrium. Upon addition of SDS, there was a substantial increase in the tryptophan, ANS and dansyl fluorescence intensity with a concomitant blue shift in the emission wavelength. Since protein aggregation in water is largely driven by hydrophobic interaction of exposed hydrophobic patches, ANS-fluorescence provides a useful readout of the aggregation process.

Our results indicate that under the aggregating condition, HEWL may undergo a conformational transition to partially unfolded 'molten globule'-like state comprising hydrophobic binding pockets for ANS. This expanded conformer associates to form oligomeric aggregates as evident from the increase in the steady-state fluorescence anisotropy for all three probes for the protein at pH 9.2 in the presence of SDS. Large fluorescence anisotropy revealed the increase in overall size due to protein aggregation leading to soluble oligomer formation.

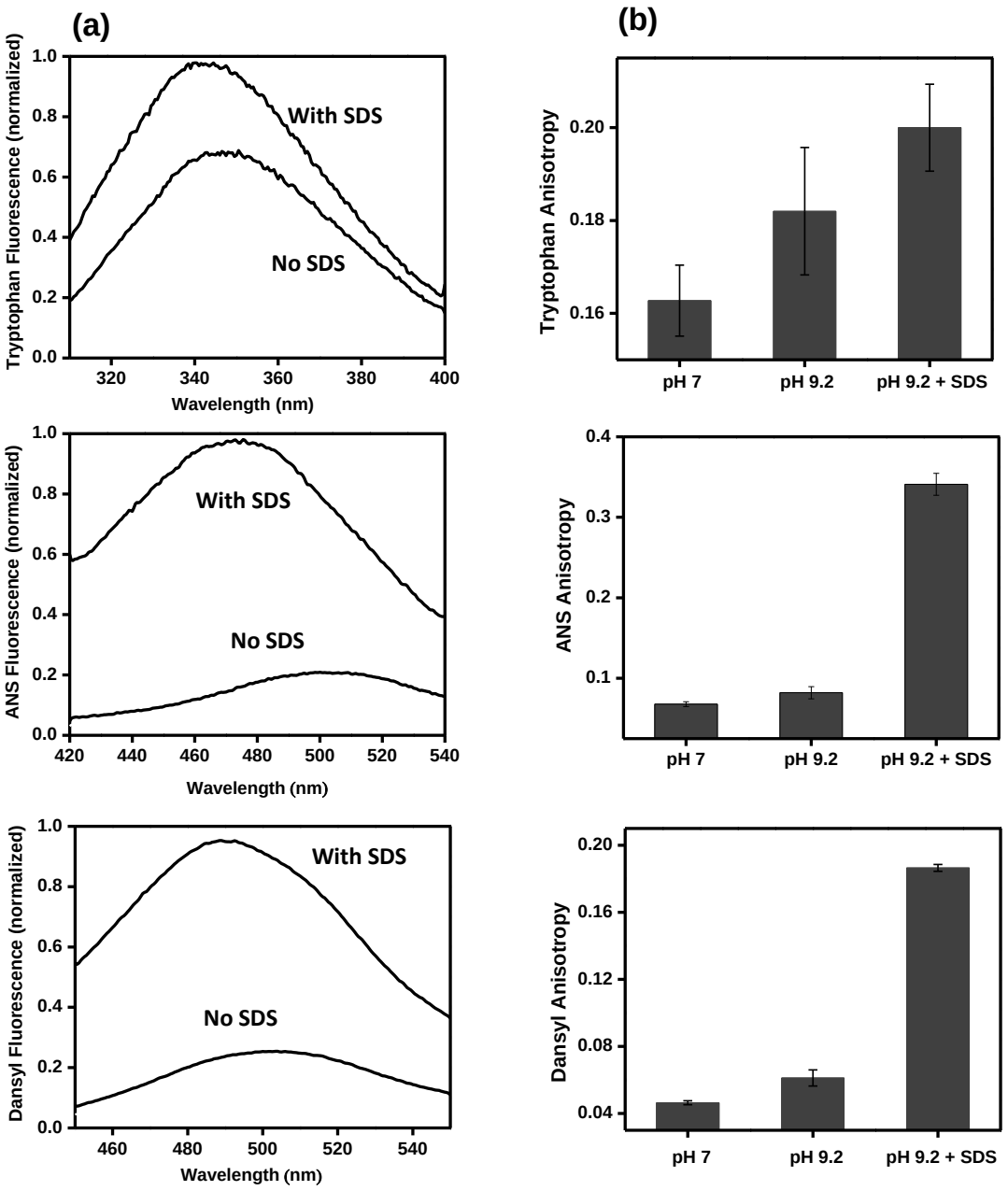

Figure 2.2 Surfactant-induced changes in (a) fluorescence spectrum and (b) anisotropy of different probes (intrinsic tryptophan, ANS and dansyl) upon addition and incubation of 5 μM HEWL with 150 μM SDS at pH 9.2 at room temperature.

Upon prolonged incubation, aggregates further grew in size and could be visually seen form the increase in the turbidity. These observations prompted us to devise fluorescence-based kinetic experiments to investigate the mechanism of lysozyme aggregation in the presence of SDS.

2.3.2 Dependence of pH, surfactant concentration and protein concentration

In order to ascertain the emergence of hydrophobic regions as a result of conformational changes during the course of HEWL aggregation, we used ANS that is widely used to characterize partially unfolded 'molten-globule' states of the protein.[24] It is an environment-sensitive dye which is weakly fluorescent in aqueous solution but fluoresces strongly when it is non-covalently bound to a hydrophobic microenvironment. ANS has also been used previously as a reporter to probe protein aggregation.[25] In order to investigate whether HEWL aggregation occurs at other pH where negatively charged SDS can interact with positively charged lysozyme (Figure 2.1b), the change in ANS fluorescence intensity in the presence of HEWL and SDS (150 μM) was monitored over a period of time at several pH ranging from the neutral to alkaline (Figure 2.3a). In the presence of HEWL at pH 9.2, ANS fluorescence was very low. A 10-fold increase in the fluorescence was observed within a few minutes of addition of SDS which reached saturation after 40 min whereas at other pHs (7, 8, 9 and 10) the extent and the rate of increase in the ANS fluorescence was much less significant. To identify the optimal concentration of SDS required for HEWL aggregation, we performed concentration dependent studies whereby the concentration of SDS was varied from 50 μM to 200 μM. Figure 2.3b shows an increase in the ANS fluorescence intensity with an increase in SDS concentration. At higher SDS concentrations (viz. 500 μM), ANS fluorescence initially increased as observed at lower SDS concentrations and then it decreased. Our further studies were made at the range of SDS

concentration from 50 μM to 200 μM. It is worth mentioning here that the concentration of SDS used for the aggregation experiments is significantly lower than its critical micelle concentration (~ 8 mM).[26] Additionally, we performed protein concentration dependent studies to identify the optimal concentration of HEWL for aggregation since protein concentration plays a crucial role in the aggregation processes. In this set of experiments, ANS fluorescence intensity was monitored at various HEWL concentrations (from 1-5 μM) in the presence of 150 μM SDS at pH 9.2 (Figure 2.3c). At higher protein concentrations, the solutions turned turbid immediately and therefore, reliable fluorescence measurements could not be performed. Therefore, the optimal condition for aggregation experiments was set at 150 μM of SDS with 5 μM of HEWL at pH 9.2. To confirm the decisive role of SDS in protein aggregation further, a triggering experiment (Figure 2.3d) was performed in which no detectable fluorescence intensity was observed for HEWL at pH 9.2 without ANS (initial part of Figure 2.3d) and with ANS (second part of Figure 2.3d). These observations indicate that there is no hydrophobic pocket available in the monomeric HEWL to which ANS can bind. Then the aggregation was triggered by adding a stock solution of SDS (final trace in Figure 2.3d). As soon as SDS was added and mixed to the protein solution, there was a time-dependent increase in the ANS fluorescence suggesting the formation of aggregates containing hydrophobic-rich regions to which ANS can bind. This set of experiments convincingly demonstrated that the protein molecules aggregate at pH 9.2 which is mediated by negatively-charged SDS. Control experiment showed that in the absence of HEWL, the ANS fluorescence was negligible at all the SDS concentrations used for the present study, thus, emphasizing the fact that upon interaction with SDS, HEWL association occurs which leads to the formation of aggregates driven by hydrophobic association of conformationally altered HEWL.

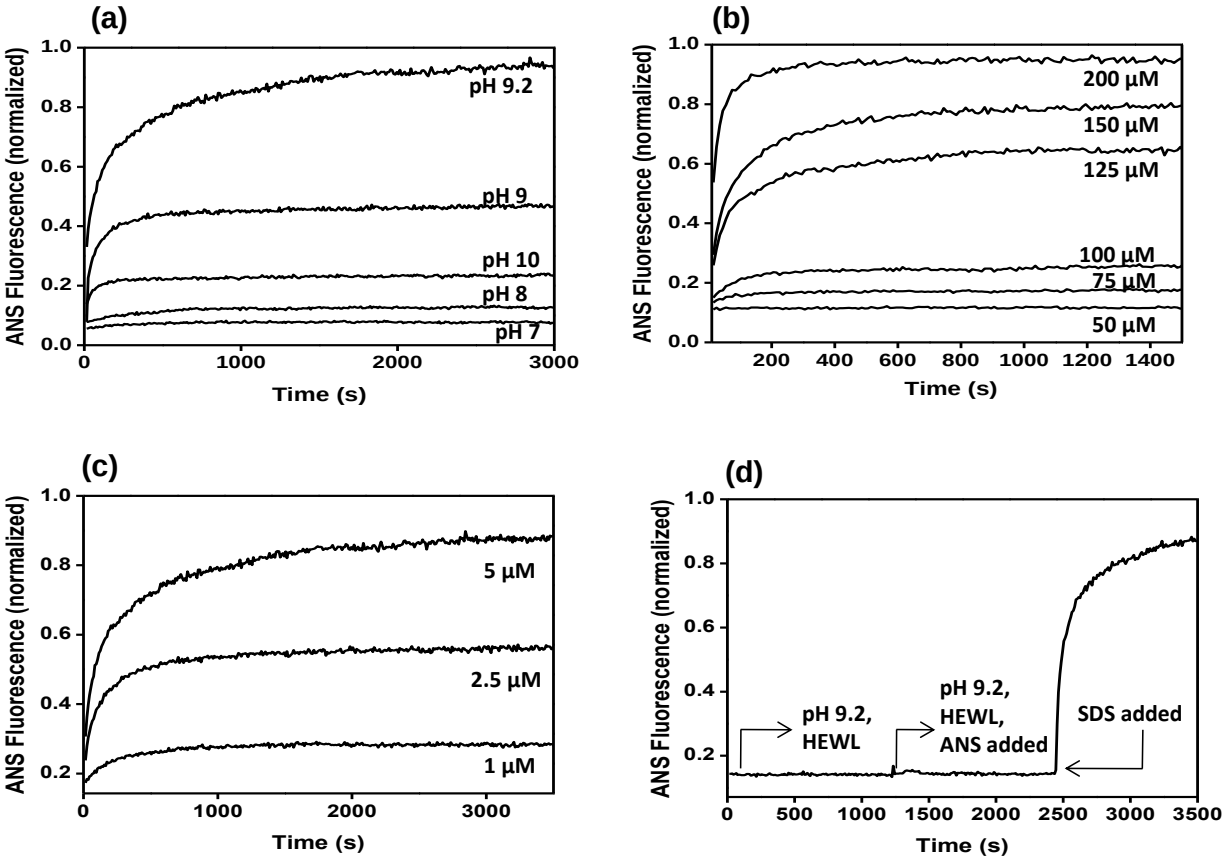

Figure 2.3 Time-course of ANS fluorescence intensity as a function of HEWL aggregation in presence of SDS with (a) variation in pH, (b) SDS concentration and (c) protein concentration. (d) A triggering experiment is shown with the addition of SDS (final concentration 150 µM).

To investigate whether the negative charge on the SDS molecules plays a crucial role in HEWL aggregation, we performed similar experiments with cationic surfactants such as, cetyl tetramethylammonium bromide (CTAB). ANS-binding experiments revealed that CTAB did not facilitate protein aggregation at pH 9.2 (data not shown) which indicated that the negatively charged SDS indeed promotes HEWL aggregation at pH 9.2. Interestingly, anionic bile salt surfactants (sodium cholate and sodium deoxycholate) did not induce aggregation under identical conditions. Next, we investigated the kinetics of a number of fluorescence observables under identical aggregation condition to shed light into the mechanism of surfactant-induced lysozyme aggregation.

2.3.3 Kinetic analysis of lysozyme aggregation using multiple fluorescent reporters

First, we carried out kinetic experiments with ANS to monitor the protein conformational change leading to a partially unfolded 'molten globule'-like state that associates to form oligomers. In the presence of 10 μM ANS, HEWL was mixed with SDS at pH 9.2 using manual mixing with a deadtime of 10 s. The time-dependence of ANS fluorescence intensity exhibited a sharp rise during the aggregation process. A single exponential kinetics was inadequate to describe the processes as revealed by non-random residuals and low adjusted R^2 value (Figure 2.4a). A double exponential kinetics was able to satisfactorily describe the time-dependent changes in the fluorescence intensity (Figure 2.4b). In all the experiments, the absence of a lag phase was observed.

The increase in ANS fluorescence was fitted to a double exponential function which suggests that the aggregation is a biphasic process where a rapid-initial phase is followed by a slow phase (Figure 2.5a). The recovered rate constants obtained from the ANS fluorescence kinetics were $k_{fast} \sim 12 \times 10^{-3}\ s^{-1}$ and $k_{slow} \sim 1.2 \times 10^{-3}\ s^{-1}$. This may suggest that upon addition of SDS, HEWL undergoes a fast conformational transition to a partially unfolded 'molten-globule'-like state that eventually associates to form soluble aggregates in slower kinetics. The decrease in the secondary structural contents during the time-course was also evident by the loss of helicity from the circular dichroism spectroscopy (Figure 2.4c,d). Next, we performed the kinetic experiments by monitoring the intrinsic tryptophan fluorescence as a function of aggregation.

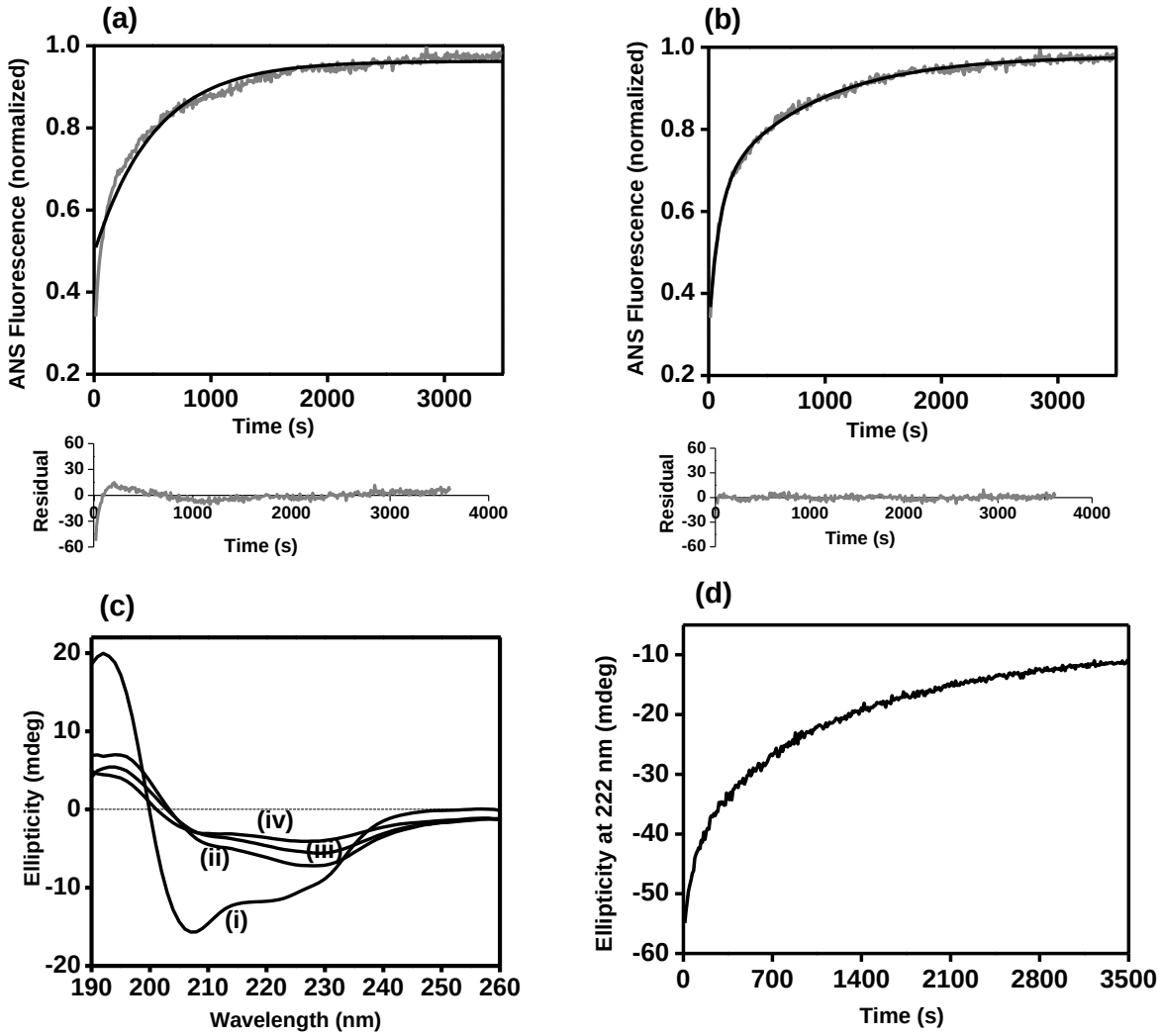

Figure 2.4 Comparison between (a) single and (b) double exponential fit for ANS-fluorescence kinetics during aggregation of HEWL (5 μM) in presence of SDS (150 μM) at pH 9.2. Residual plots obtained for the respective fits are also shown. (c) CD spectra of HEWL at pH 9.2 in the absence of SDS at pH 9.2 in (i) absence and after adding SDS (150 μM) (ii) 5 min (iii) 15 min (iv) 45 min (v).(d) Kinetics of the loss of helicity probed by CD at 222 nm during aggregation. The double exponential fit is shown in solid (black) line in (a) and (b).

Tryptophan is an intrinsic fluorophore whose emission maximum depends on the polarity of its microenvironment. The emission maximum of tryptophan, when exposed to an aqueous medium, is ~350 nm whereas it exhibits a blue-shift when buried inside a hydrophobic

environment.[27] As mentioned earlier, at pH 9.2 and in the presence of SDS, an increase in the tryptophan fluorescence intensity was observed with a concomitant blue-shift to ~340 nm with a simultaneous increase in the fluorescence anisotropy. Both the observations suggest that the aggregation of HEWL occurs in the presence of SDS whereby the tryptophans get buried inside the hydrophobic interior formed upon association. This prompted us to probe into the time-dependent changes in the tryptophan fluorescence as a function of aggregation. A sharp rise in the tryptophan fluorescence was observed which reached a quasi-plateau within 15 minutes and then attained saturation (Figure 2.5b). Here again, a double exponential kinetics was able to describe the time-dependent changes in the tryptophan fluorescence indicating a fast and a relatively slower kinetic components. The observed rate constants for the changes in tryptophan fluorescence intensity were found to be $k_{fast} \sim 22 \times 10^{-3}$ s^{-1} and $k_{slow} \sim 2 \times 10^{-3}$ s^{-1}. The initial, rapid phase may indicate the protein conformational changes to extended conformers whereas the slower phase could be ascribed to the aggregation process. HEWL contains six tryptophan residues (Figure 2.1c) among which Trp 63 and 123 are non-fluorescent due to the proximity of the tryptophans with the sulfur atoms of the disulfides.[28] The initial increase in the tryptophan fluorescence (k_{fast}) is interpreted as protein conformational expansion that diminishes the quenching of non-fluorescent tryptophan residues by the disulfides. The increase in the tryptophan fluorescence in the latter phase (k_{slow}) arises due to burial of the tryptophan residues into the core of the aggregates.

Comparison of the fast component of the rate obtained for tryptophan and ANS intensities reveals that the rate of change in tryptophan fluorescence kinetics is ~ 2-fold faster than the ANS fluorescence kinetics.

To further investigate the mechanism of aggregation, we labeled the protein surface sparsely with different fluorophores and monitored the changes in fluorescence properties during aggregation under identical condition. The protein was labeled with dansyl chloride and the aggregation was monitored by dansyl fluorescence. A rapid increase in dansyl fluorescence intensity, similar to that of tryptophan and ANS, was observed (Figure 2.5c). A double exponential function was again required to fit the kinetics of dansyl fluorescence data. The recovered rate constants were $k_{fast} \sim 24 \times 10^{-3}$ s^{-1} and $k_{slow} \sim 1 \times 10^{-3}$ s^{-1}. It is interesting to note that the fast component of rate constant of the dansyl fluorescence is similar to that of tryptophan and both tryptophan and dansyl fluorescence readouts probe the conformational change of the polypeptide chain. Next, we carried out the fluorescence anisotropy kinetics to follow the size growth of the oligomers during aggregation.

In order to observe the changes in the steady-state fluorescence anisotropy as a function of HEWL aggregation, we labeled the protein surface sparsely with another surface-modifying fluorophore, namely, fluorescein isothiocyanate. The reason for choosing fluorescein was that its fluorescence property is largely environmental insensitive[27], and therefore, the change in the steady-state fluorescence anisotropy is primarily dominated by the change in the overall rotational correlation time. The steady-state fluorescence anisotropy showed a steady increase that could satisfactorily be described by a single exponential kinetics and the recovered rate constant ($\sim 1 \times 10^{-3}$ s^{-1}, Figure 2.5d) is similar to the slower kinetic component (k_{slow}) obtained from the kinetics of ANS, tryptophan and dansyl fluorescence. This also confirms that the slower kinetic component (k_{slow}) in other fluorescence observables represents the aggregation growth.

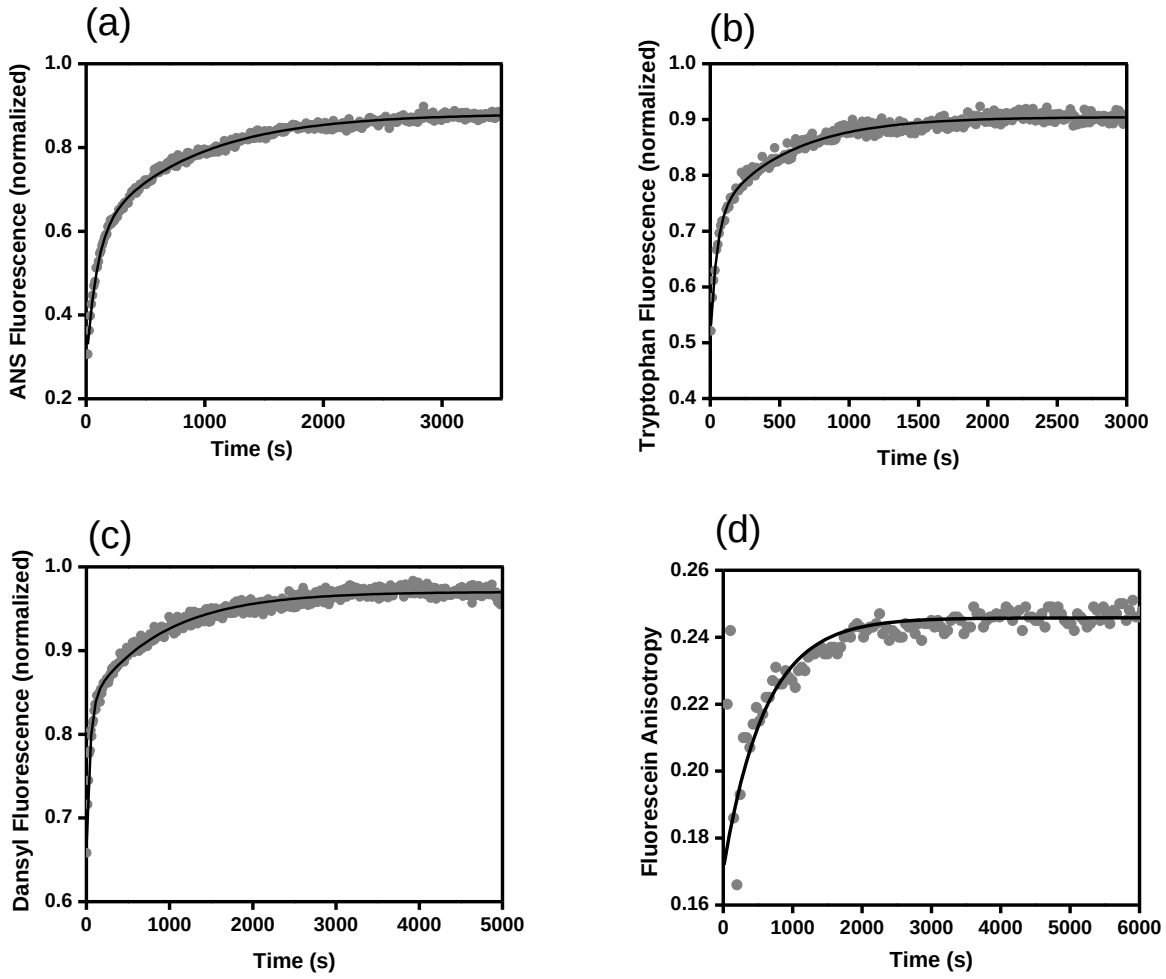

Figure 2.5 Time-course of aggregation in HEWL at pH 9.2 in presence of SDS studied with multiple fluorescent reporters in-tandem: (a) ANS intensity (b) Tryptophan intensity (c) Dansyl intensity in dansyl labeled HEWL and (d) Fluorescence anisotropy of fluorescein labeled HEWL. The solid line represents experimental fit.

As it has been discussed, we can infer that under the present set of experimental conditions, lysozyme aggregation is at least a two-step process as described by the double exponential fitting analysis. Figure 2.6 depicts a comparison between the recovered rate constants with standard deviations obtained from the analysis. The rates of change in tryptophan (k_{fast} ~ 22 x 10^{-3} s^{-1}) and dansyl fluorescence intensities (k_{fast} ~ 24 x 10^{-3} s^{-1}) are similar and faster

than the rate constants extracted for ANS intensity (k_{fast} ~ 12 x 10^{-3} s^{-1}). Such a comparison reflects that the fluorophores report two distinct aspects of aggregation. As tryptophan is more sensitive to its environment, it reports any change that affects the lysozyme's native conformation whereas, ANS reports the generation of hydrophobic sites as a consequence of conformational change and oligomerization. For all the three fluorescent reporters, the contribution from fast and slow phases was almost same (~ 50%). Fluorescence anisotropy showed a single exponential fit which resembles with the slower components of other observables demonstrating the aggregation process.

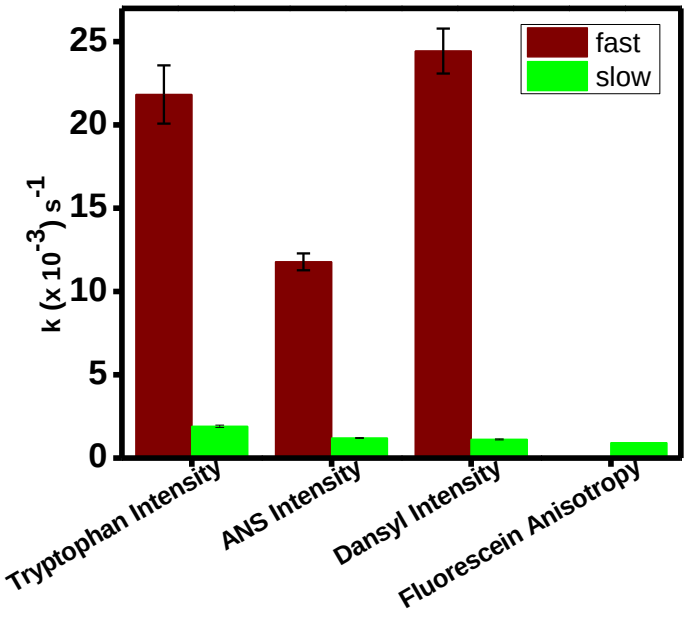

Figure 2.6

The fast and slow rate constants of different fluorescent reporters during the HEWL aggregation kinetics.

2.4 Discussion

Protein aggregation occurs through various mechanisms and different methods have been used to delineate the process.[29] In the present study, we have investigated the conformational and size change during aggregation of HEWL in the presence of SDS at alkaline pH. We have used a variety of fluorescent markers to get insights into the mechanism of aggregation. A sharp increase in the fluorescence properties of all the probes under prevailing conditions indicates that the protein conformational change is coupled with aggregation of HEWL. In the native protein and in the absence of SDS, these probes are either exposed to the solvent or to certain residues which may quench their fluorescence. Also, the probes have high degree of rotational motion and thus contribute to low fluorescence anisotropy. Upon addition of SDS at pH 9.2, conformational change in the HEWL brings them in an environment where they exhibit high fluorescence intensity and the overall rotational motion is restricted due to an increase in the overall size as a result of aggregation, thus, giving high fluorescence anisotropy. We suggest that SDS being negatively charged interacts electrostatically with positively charged surface of lysozyme (Figure 2.1b) at pH 9.2 (pI ~ 11). This interaction neutralizes surface charge on the protein and increases hydrophobicity which is in accordance with a previous study where similar mode of interaction was observed during the formation of SDS-lysozyme complex.[19] Reduction of overall protein charge facilitates penetration of negatively charged SDS into the protein-core leading to the conformational change resulting in the formation of extended conformers. It was also noticed that by changing the non-polar linear, alkyl chain of SDS to a cyclic, fused ring system such as, sodium cholate and sodium deoxycholate did not foster the formation of HEWL aggregates. We speculate that in addition to the negative charge on the head group, the linear hydrocarbon tail

might play an important role in stabilizing the surfactant-protein interaction, thus favoring the conformational expansion of the lysozyme. Such conformational change may facilitate intermolecular interaction driven by hydrophobic effects and eventually lead to the aggregation of protein molecules.[14] The remarkable feature of this aggregation is that it requires protein and SDS in very low concentrations viz. 5 μM and 150 μM, respectively. This is in contrast to most of the studies where a high concentration of protein is required for protein aggregation.[15,16]

An increase in ANS fluorescence intensity during aggregation reflects that the conformational expansion due to SDS-lysozyme interaction creates some hydrophobic pockets to which ANS can bind non-covalently and the number of hydrophobic sites increases to a certain extent as aggregation progresses. However, the initial increase in ANS intensity is slower than that of tryptophan, suggesting that the formation of hydrophobic regions and hence oligomerization, occurs as a consequence of the conformational change of the polypeptide chain. The overall increase in the fluorescence anisotropy of different probes also indicates that the conformational change in the protein facilitates association of protein molecules which restricts the rotational motion of the fluorophore, thus exhibiting large fluorescence anisotropy. The overall finding of this study involves an understanding of lysozyme aggregation in the presence of an anionic surfactant. A plausible mechanism of HEWL aggregation can be suggested based on our observations (Figure 2.7). Initially, the protein interacts with SDS by virtue of electrostatic interaction that leads to a conformational expansion in the protein. This in turn, directs the formation of oligomers mediated by hydrophobic interactions that subsequently lead to the formation of lysozyme aggregates.

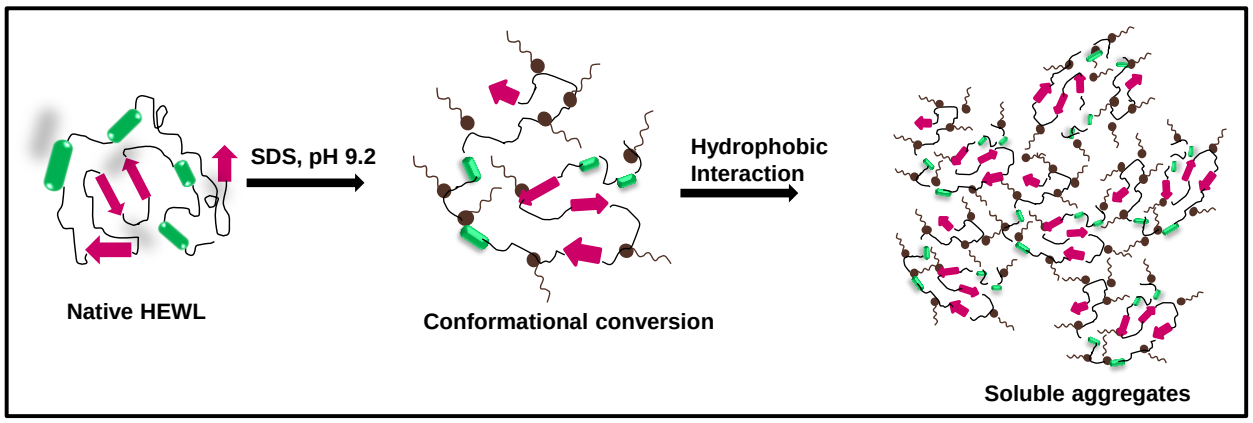

Figure 2.7 Proposed mechanism of aggregation of HEWL in presence of SDS at pH 9.2.

2.5 Conclusion

In the present study we have attempted to understand the basic mechanism of aggregation by providing insights into the change in protein conformation and size using fluorescence spectroscopy. It is important to mention that the protein concentrations used in our experiments are significantly lower than in typical aggregation experiments which are often carried out at the millimolar protein concentration range. This type of surfactant-protein interaction may be relevant in certain critical interactions between lipid membrane and proteins inside the cell leading to aggregation. We believe that our fluorescence kinetic analysis will find broad applications in the area of protein misfolding and aggregation.

2.6 References

1. Itzhaki, L.S.; Evans, P.A.; Dobson, C.M.; Radford, S.E.; (1994) Tertiary interactions in the folding pathway of hen lysozyme: Kinetic studies using fluorescent probes. *Biochemistry* 33:5212-5220.

2. Rothwarf, D.M.; Scheraga, H.A. (1996) Role of non-native aromatic and hydrophobic interactions in the folding of hen egg white lysozyme. *Biochemistry* 35: 13797-13807.

3. Bachmann, A.; Segel, D.; Kiefhaber, T. (2002) Test for cooperativity in the early kinetic intermediate in lysozyme folding. *Biophys. Chem.* 96:141-151.

4. Booth, D.R.; Sunde, M.; Bellotti, V.; Robinson, C.V.; Hutchinson, W.L.; Fraser, P.E.; Hawkins, P.N.; Dobson, C.M.; Radford, S.E.; Blake, C.C.F.; Pepys, M.B. (1997) Instability, unfolding and aggregation of human lysozyme variants underlying amyloid fibrillogenesis. *Nature* 385:787-793.

5. Dumoulin, M.; Kumita, J.R.; Dobson, C.M. (2006) Normal and aberrant biological self-assembly: Insights from studies of human lysozyme and its amyloidogenic variants. *Acc. Chem. Res.* 39:603-610.

6. Merlini, G.; Bellotti, V. (2005) Lysozyme: A paradigmatic molecule for the investigation of protein structure, function and misfolding. *Clin. Chim. Acta* 357:168-172.

7. Frare, E.; Mossuto, M.F.; de Laureto, P.P.; Tolin, S.; Menzer, L.; Dumoulin, M.; Dobson, C.M.; Fontana, A. (2009) Characterization of oligomeric species on the aggregation pathway of human lysozyme. *J. Mol. Biol.* 387:17-27.

8. Canet, D.; Sunde, M.; Last, A.M.; Miranker, A.; Spencer, A.; Robinson, C.V.; Dobson, C.M. (1999) Mechanistic studies of the folding of human lysozyme and the origin of amyloidogenic behavior in its disease-related variants. *Biochemistry* 38:6419-6427.

9. Frare, E.; de Laureto, P.P.; Zurdo, J.; Dobson, C.M.; Fontana, A. (2004) A highly amyloidogenic region of HEWL. *J. Mol. Biol.* 340:1153-1165.

10. Morshedi, D.; Ebrahim-Habibi, A.; Moosavi-Movahedi, A. A.; Nemat-Gorgani, M. (2010) Chemical modification of lysine residues in lysozyme may dramatically influence its amyloid fibrillation. *Biochim. Biophys. Acta* 1804:714-722.

11. Malisauskas, M.; Ostman, J.; Darinskas, A.; Zamotin, V.; Liutkevicius, E.; Lundgren, E.; Morozova-Roche, L. A. (2005) Does the cytotoxic effect of transient amyloid oligomers from common equine lysozyme in vitro imply innate amyloid toxicity? *J. Biol. Chem.* 280:6269-6275.

12. Gharibyan, A.L.; Zamotin, V.; Yanamandra, K.; Moskaleva, O.S.; Margulis, B.A.; Kostanyan, I.A.; Morozova-Roche, L.A. (2007) Lysozyme amyloid oligomers and fibrils induce cellular death via different apoptotic/necrotic pathways. *J. Mol. Biol.* 365:1337-1349.

13. Holley, M.; Eginton, C.; Schaefer, D.; Brown, L. R. (2008) Characterization of amyloidogenesis of hen egg white lysozyme in concentrated ethanol solution. *Biochem. Biophys. Res. Commun.* 373: 164-168.

14. Moosavi-Movahedi, A.A.; Pirzadeh, P.P.; Hashemnia, S.; Ahmadian, S.; Hemmateenejad, B.; Amani, M.; Saboury, A.A.; Ahmad, F.; Shamsipur, M.; Hakimelahi, G.H.; Tsai, F.Y.; Alijanvand, H.H.; Yousefi, R. (2007) Fibril formation of lysozyme upon interaction with sodium dodecyl sulfate at pH 9.2. *Coll. Surf. B: Biointerfaces* 60:55-61.

15. Kumar, S.; Ravi, V. K.; Swaminathan, R. (2008) How do surfactants and DTT affect the size, dynamics, activity and growth of soluble lysozyme aggregates? *Biochem. J.* 415:275-288.

16. Vernaglia, B. A.; Huang, J.; Clark, E. D. (2004) Guanidine hydrochloride can induce amyloid fibril formation from hen egg-white lysozyme. *Biomacromolecules* 5:1362-1370.

17. Pertinhez, T. A.; Bouchard, M.; Smith, R. A. G.; Dobson, C. M.; Smith, L. J. (2002) Stimulation and inhibition of fibril formation by a peptide in the presence of different concentrations of SDS. *FEBS Lett.* 529:193-197.

18. Andersen, K. K.; Oliveira, C. L.; Larsen, K. L.; Poulsen, F. M.; Callisen, T. H.; Westh, P.; Pedersen, J. S.; Otzen, D. (2009) The role of decorated SDS micelles in sub-CMC protein denaturation and association. *J. Mol. Biol.* 391: 207-226.

19. Stenstam, A.; Khan, A.; Wennerström, H. (2001) The lysozyme-dodecyl sulfate system. An example of protein-surfactant aggregation. *Langmuir* 17:7513-7520.

20. Chatterjee, A.; Moulik, S. P.; Majhib, P. R.; Sanyal, S. K. (2002) Studies on surfactant–biopolymer interaction. I. Microcalorimetric investigation on the interaction of cetyltrimethylammonium bromide (CTAB) and sodium dodecylsulfate (SDS) with gelatin (Gn), lysozyme (Lz) and deoxyribonucleic acid (DNA). *Biophys. Chemis.* 98:313-327.

21. Pirzadeh, P.; Moosavi-Movahedi, A. A.; Hemmateenejad, B.; Ahmad, F.; Shamsipur, M.; Saboury, A.A. (2006) Chemometric studies of lysozyme upon interaction with sodium dodecyl sulfate and β-cyclodextrin. *Coll. Surf. B: Biointerfaces* 52:31-38.

22. Yamashita, S.; Nishimoto, E.; Szabo, A. G.; Yamasaki, N. (1996) Steady-state and time-resolved fluorescence studies on the ligand-induced conformational change in an active lysozyme derivative, Kyn62-Lysozyme. *Biochemistry* 35:531-537.

23. Chowdhary, R. P.; Chatterji, D. (2007) Estimation of Förster's distance between two ends of Dps protein from mycobacteria: Distance heterogeneity as a function of oligomerization and DNA binding. *Biophys. Chem.* 128:19-29.

24. Semisotnov, G. V.; Rodionova, N. A.; Razgulyaev, O. I.; Uversky, V. N.; Gripas, A. F.; Gilmanshin, R. I. (1991) Study of the 'molten globule' intermediate state in protein folding by a hydrophobic fluorescent probe. *Biopolymers* 31:119-128**.**

25. Lindgren, M.; Sörgjerd, K.; Hammarström, P. (2005) Detection and characterization of aggregates, prefibrillar amyloidogenic oligomers, and protofibrils using fluorescence spectroscopy. *Biophys. J.* 88:4200-4212.

26. Fuguet, E.; Ráfols, C.; Rosés, M.; Bosch, M. (2005) Critical micelle concentration of surfactants in aqueous buffered and unbuffered systems. *Anal. Chim. Acta* 548:95-100.

27. Lakowicz JR (2006) Principles of fluorescence spectroscopy, 3rd edn. Kluwer Academic/Plenum, New York

28. Wu, L. Z.; Sheng, Y. B.; Xie, J. B.; Wang, W. (2008) Photoexcitation of tryptophan groups induced reduction of disulfide bonds in hen egg white lysozyme. *J. Mol. Struct.* 882:101-106.

29. Frieden, C. (2007) Protein aggregation processes: In search of the mechanism. *Protein Sci.* 16:2334-2344.

Chapter 3

Mechanism of Amyloid Formation from Bovine Serum Albumin

This work has been published in *Journal of Fluorescence* and *Journal of Physical Chemistry B*

References:

1. M. Bhattacharya, **N. Jain**, K. Bhasne, V. Kumari and S. Mukhopadhyay. pH-induced conformational isomerization of bovine serum albumin studied by extrinsic and intrinsic protein fluorescence. *J. Fluoresc.* **2011,** *21*, 1083-1090.
2. M. Bhattacharya, **N. Jain** and S. Mukhopadhyay. "Insights into the mechanism of aggregation and fibril formation from bovine serum albumin." *J. Phys. Chem. B* **2011,** *115*, 4195–4205.

3.1 Introduction

The formation of β-rich amyloid-like aggregates from an all α-helical protein despite having no predisposition towards β-sheet formation, has spurred a lot of interest in recent years.[1] An interesting question in this area is how an all α-helical protein transforms into β-rich conformation, in response to modification of solution conditions favoring a partially destabilized state, that ultimately culminates in amyloid fibril formation. Serum albumin is a globular, all α-helical protein present in the circulatory system which is the most abundant of all plasma proteins (~ 60 %) with an average concentration of 50 g/L. It is primarily a carrier protein that is involved in the binding and transport of fatty acids, hormones, metabolites, endogenous ligands and drug delivery in addition to the maintenance of colloid osmotic blood pressure.[2,3] It has been demonstrated that serum albumin is majorly responsible for the preservation of blood pH as changes in the plasma protein concentration can induce either acidosis or alkalosis that results in albumin-related diseases.[4]

Human serum albumin (HSA) or its bovine analogue (BSA) is a 585-residue, multi-domain, all-α-helical protein that adapts a heart-shaped structure at physiological pH (Figure 3.1). The crystal structure of HSA[5,6] shows that each of the three homologous domain (I, II and III) is further composed of two sub-domains (A and B) that contain several intra-domain disulfide bonds (17 disulfide bridges in total) which impart rigidity to the helical, globular structure but allow enough flexibility to the protein to undergo conformational changes in response to changes in pH[7] and upon interaction with fatty acids.[2]

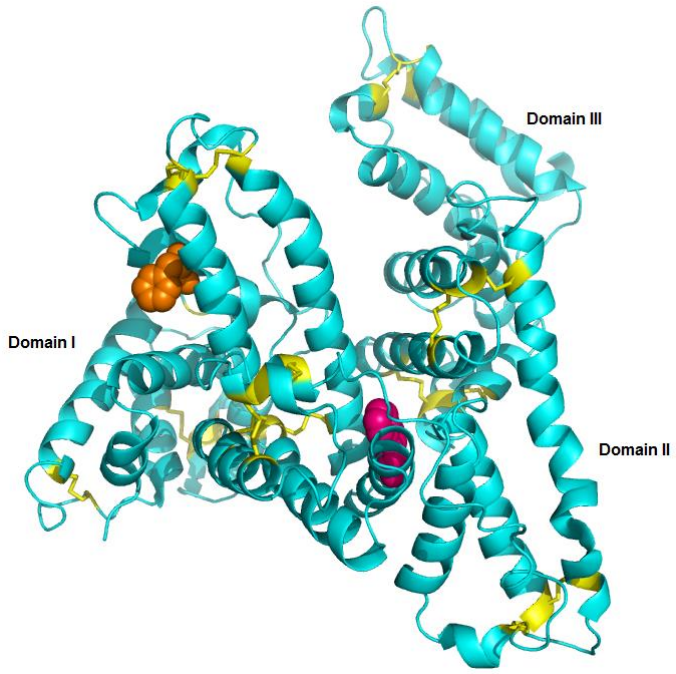

Figure 3.1

The crystal structure of human serum albumin (HSA) showing the single tryptophan (W214; magenta), phenylalanine (F134; orange) and disulfides (yellow) generated using PyMol from protein data bank (1UOR.pdb). Bovine serum albumin (BSA), structure of which is not available, contains an additional tryptophan in domain I at residue position 134 instead of the phenylalanine.

BSA shares a 76 % sequence homology with HSA, contains one more tryptophan residue in domain I (in addition to the one in domain II) and also undergoes reversible conformational isomerization as a function of pH.[8,9] Recent reports suggest that the structural organization and compactness of the tertiary structure of BSA vary as a function of pH whereby a few significant modifications in the secondary structures are also observed.[10-12] Five conformational isomers of BSA over different pH ranges have been identified namely, the E-form (Extended; pH < 3), the F-form (Fast; pH 3-5), the N-form (Native; pH 5-7), the B-form (Basic; pH 7-8.5) and the A-form (Aged; pH > 8.5). It was also suggested that the conformational isomerization of serum albumins is conserved across various species which implies that the pH-dependent isomerization might play a significant physiological role.[2] The physiological relevance of serum albumins might be linked to pH-dependent binding and release of substrates given the fact that low pH has been measured on the membrane surfaces of several tissues.[13] Various studies have been directed

towards the design of optimum conditions and probing the mechanistic aspects of both human- and bovine-serum albumin aggregation.[14-19] However, the time-course of the structural transition from the partially-unfolded monomeric conformer to the fibrillar state still remains elusive. Therefore, it is important to understand different conformations that eventually drive the aggregation process forward and to investigate the aggregation mechanism of serum albumin at other solution conditions especially at low pH.

In this work, we have carried out fluorescence-based studies on the structural changes of monomeric BSA by extracting detailed information on conformational changes coupled with the size variation to identify an amyloidogenic precursor. Following the monomeric BSA experiments, we investigated the aggregation propensity of the amyloidogenic precursor. The early key steps in the fibrillation event were deciphered by monitoring the kinetics of both conformational–and size changes simultaneously using multiple structural probes.

3.2 Experimental Section

3.2.1 Materials

Bovine Serum Albumin (BSA), glycine, sodium phosphate monobasic, sodium phosphate dibasic, citric acid, potassium chloride, Tris, urea were purchased from Sigma and used without any further purification. The fluorescent probes viz. 8-anilinonaphthalene,1-sulfonic acid (ANS), pyrene and Thioflavin-T (ThT) were obtained from Sigma and 5-((((2-iodoacetyl)amino)ethyl)amino)naphthalene-1-sulfonic acid (IAEDANS) was procured from Molecular Probes, Invitrogen Inc. and used as received. KCl-HCl (pH 1.6, 2), glycine-HCl (pH 2.5, 3), sodium citrate (pH 3-6), sodium phosphate mono-and dibasic (pH 6.5-8), Tris-HCl (pH 8.5), glycine-NaOH (pH 9-10.5) were used for buffer preparations. All the pH buffers (from pH 1.6-10.5) were always made freshly and adjusted by adding 1N HCl or NaOH prior to every pH titration experiments. The pH of the buffers was checked on Cyberscan pH 510 bench meter from Eutech Instruments. The final pH was in the range of ± 0.01 at 24-25 °C. Milli-Q water was used for the preparation of solutions and buffers.

3.2.2 Preparation of protein sample for studies on BSA monomer

To prepare a stock solution of 1 mM, BSA was dissolved in 50 mM, phosphate buffer of pH 7 and stored at 4 °C. Accurate protein concentration was determined by measuring the absorbance of tryptophans at 280 nm on Lambda 25, Perkin-Elmer UV-Visible spectrophotometer. The molar extinction coefficient of BSA at 280 nm is 43,824 $M^{-1}cm^{-1}$.[3] For pH titration experiment, the BSA stock was diluted 100-fold to a final protein concentration of

10 μM in the respective pH buffer (pH 1.6-10.5) and equilibrated for at least 2 hours at 24-25 ^{o}C prior to florescence measurement. After 2 hours, 1 mM of pyrene (in methanol) was diluted 100-fold into a protein solution and kept in the dark for 5 minutes each at 24-25 °C prior to the recording of fluorescence spectral scans. All the measurements were carried out at 24-25 °C.

3.2.3 Equilibrium unfolding studies on protein using urea

Typically, 1 mM BSA in phosphate buffer (50 mM, pH 7) was prepared in 2 sets for the unfolding experiments at pH 7 and pH 3 and stored at 4 °C. A stock solution of urea (8 M) in the respective pH buffers (phosphate buffer: pH 7, 50 mM and Gly-HCl buffer: pH 3, 50mM) was prepared separately and the pH of the urea solutions were checked and adjusted accordingly at 24-25 °C. The stock solution of BSA was then diluted 100-fold in varying concentrations (0-8 M) of urea in the respective pH buffer to yield a final protein concentration of 10 μM. The solutions were incubated at 25 °C for 2 hours to ensure partial/complete denaturation at that particular concentration of urea. The unfolding of BSA was monitored by tryptophan fluorescence intensity and anisotropy.

3.2.4 Preparation of protein sample for aggregation

BSA was dissolved in 5 mM, phosphate buffer of pH 7 to give a stock solution of 1 mM and stored at 4 °C. In a typical aggregation experiment, 1 mM of BSA (5 mM phosphate, pH 7) was diluted 10-fold using a buffer (pH 3, 50 mM Gly-HCl) to yield a final protein concentration of 100 μM (~6 mg/mL) at pH 3. The protein samples were incubated with 50mM NaCl and heated to 65 (±1) °C in a heating block preset at the required temperature without agitation. For

aggregation studies using labeled BSA, a mixture of unlabeled and labeled protein was prepared so that the labeled protein content was 5 % of the total protein concentration.

3.2.5 Fluorescence labeling of BSA

The labeling of the thiol group of cysteine was carried out in 50 mM, phosphate buffer of pH 7.4. Approximately, 10 equivalents of IAEDANS, dissolved in dry N,N-dimethylsulfoxide (DMSO), was added to BSA solution in phosphate buffer of pH 7.4 and the reaction mixture was kept in the dark for overnight under quiescent condition. After the labeling reaction was complete, the labeled protein was purified in 2 stages. In the first step, the labeled protein was passed through a desalting column whereby the free, unreacted dye was removed. To ensure complete removal of non-covalently bound IAEDANS from BSA, the labeled protein was again purified and concentrated using a Microcon centrifugal filter (30 kDa cut-off; obtained from Millipore). The concentrated protein was diluted in a phosphate buffer (50 mM, pH 7.4) and concentration was checked by measuring the absorbance at both 280 nm (tryptophan) and 337 nm (AEDANS). The concentration of the labeled protein was determined by subtracting the absorption contribution of AEDANS at 280 nm. The molar extinction coefficient of IAEDANS at 280 nm and 337 nm is 1060 $M^{-1}cm^{-1}$ [20] and 6100 $M^{-1}cm^{-1}$ [21], respectively. The AEDANS fluorescence was measured at 475 nm (excitation wavelength: 375 nm).

3.2.6 Fluorescence measurements

All the steady-state fluorescence measurements were performed on an LS 55 luminescence spectrometer from Perkin Elmer at room temperature (~ 24 °C). The following

parameters were adjusted for monitoring tryptophan fluorescence intensity and anisotropy during urea unfolding experiments: λ_{ex} = 300 nm, λ_{em} = 350 nm, excitation bandpass = 2.5 nm, emission bandpass = 4 nm (for intensity) and 5–7 nm (for anisotropy). The pyrene fluorescence intensity at different pH was recorded with the following parameters, λ_{ex} = 335 nm, excitation bandpass = 2 nm and emission bandpass = 2.5 nm.

For monitoring the tryptophan fluorescence during aggregation, aliquots of protein sample (100 μM) were taken out at regular intervals, diluted 10-fold using a buffer (50 mM, phosphate, pH 7.4) and allowed to cool at room temperature prior to fluorescence measurements. For ANS fluorescence-based aggregation experiments, ANS concentration of 10 μM was used which was obtained by suitable dilution of a stock solution (10 mM) of ANS (prepared in Milli-Q water and stored at 4°C) into protein solution prior to heating required for aggregation. Aliquots from the aggregate sample were withdrawn at regular intervals, allowed to cool at room temperature and the fluorescence properties of ANS were measured without any further dilution. For aggregation studies using labeled BSA, aliquots from the labeled sample mixture were cooled at ~ 24 °C and used without any further dilution for measuring the fluorescence intensity and anisotropy. For all the experiments, the fluorescence intensity and anisotropy were collected at constant wavelength with an integration time of 5 seconds and 30 seconds, respectively. The steady-state anisotropy is given by: $r = (I_{\parallel}-GI_{\perp}) / (I_{\parallel}+2GI_{\perp})$, where $I_{\parallel}$, $I_{\perp}$ are fluorescence intensities collected using parallel and perpendicular geometry of the polarizers, respectively and the perpendicular components were corrected using respective G-factors. The error associated with the fluorescence anisotropy measurements was below 0.01. All the emission spectra were scanned at a rate of 10 nm/min and averaged over 5 scans. The following parameters were

adjusted for monitoring tryptophan fluorescence intensity and anisotropy during aggregation experiments: λ_{ex} = 300 nm, λ_{em} = 350 nm, excitation bandpass = 2.5 nm, emission bandpass = 4 nm (for intensity) and 7-9 nm (for anisotropy). For recording ANS fluorescence intensity and anisotropy, the following parameters were used: λ_{ex} = 350 nm, λ_{em} = 475 nm, emission bandpass = 4 nm (for intensity) and 6 nm (for anisotropy). For monitoring AEDANS fluorescence anisotropy,the parameters were: λ_{ex} = 375 nm, λ_{em} = 475 nm, excitation bandpass = 2.5 nm and emission bandpass = 6-7 nm. Several data points at a given condition were collected to get an estimate of the standard deviation associated with the measurement. The graphs were plotted using commercially available OriginPro Version 8.0 software and wherever required, fitted using non-linear least square curve fitting. The goodness of the fit was determined by the adjusted R^2 value (which was typically in the range of 0.97-0.99) and the respective residual plots.

3.2.7 Thioflavin-T fluorescence assay

Thioflavin-T (ThT) fluorescence was measured to monitor amyloid aggregation of BSA (unlabeled) as a function of time. Typically, 50 μL of protein aggregate sample in Gly-HCl buffer (50 mM, pH 3) was diluted 10-fold by using a phosphate buffer (50 mM, pH 7.4) containing ThT to a final concentration of 18 μM ThT in pH 7.4 at room temperature. The following parameters were adjusted for monitoring ThT fluorescence intensity during aggregation experiments: λ_{ex} = 450 nm, λ_{em} = 480 nm, excitation bandpass = 2.5 nm, emission bandpass = 5 nm.

3.2.8 Circular Dichroism (CD) spectroscopy

The far-UV CD spectra of the protein aggregates were recorded on a J-810 Jasco CD spectrometer at room temperature. Typically, the protein sample solution at pH 3 was diluted 30-fold to a final protein concentration of 3 μM, which was taken in a quartz cuvette of 1 mm pathlength and the secondary structural changes were recorded in the range of 195-250 nm. The scan rate was 100 nm/min and the final spectrum was averaged over 5 scans. The spectra were corrected with buffer baseline subtraction.

3.2.9 Transmission electron microscopy

The sample was transferred onto a carbon-coated copper grid and dried in air for 2-3 hr and then under vacuum for 5 hr. It was then stained with 0.2 % aqueous uranyl acetate solution and dried under vacuum for 5 hr. The TEM images were recorded on an FEI Tecnai T20 microscope at an operating voltage of 200 kV.

3.3 Results

3.3.1 pH-induced conformational changes revealed by fluorescence and CD

Initial studies from our lab have demonstrated that BSA undergoes pH-induced conformational changes as revealed by detailed fluorescence and CD spectroscopic measurements. The tryptophan and ANS fluorescence observables together with the CD data indicated that BSA forms an expanded, 'molten-globule-like' state at pH 3 which is accompanied by a partial loss in helicity.

3.3.2 Pyrene fluorescence of pH-induced conformational isomers

In order to ascertain whether the pH-induced conformational isomers of BSA can also be distinguished based on their polarity index, pyrene fluorescence experiments were undertaken. Pyrene is a rigid, polycyclic aromatic hydrocarbon fluorophore whose fluorescence emission spectrum is dependent on the polarity of its microenvironment and is frequently employed to estimate the polarity of micelles and model lipid membranes.[22-24] In a non-polar medium, the fluorescence emission spectrum of pyrene exhibits five vibronic bands, namely, I_1, I_2, I_3, I_4 and I_5 at 373 nm, 378 nm, 384 nm, 389 nm and 394 nm, respectively which reduces to three bands in a polar medium (I_1, I_3 and I_5).[23,25,26] A qualitative estimate of the polarity of the pyrene microenvironment can be obtained from the ratio of the fluorescence intensities at I_3 and I_1. Higher I_3/I_1 ratio indicates that the environment surrounding the pyrene molecules is more hydrophobic. Figure 3.2a depicts representative fluorescence emission spectra of pyrene (normalized at 373 nm) bound to native BSA (pH 7) and one of the conformational isomers of

BSA at acidic pH regime (pH 3). The data clearly shows the split of the emission spectra into five vibrational peaks which clearly indicate that pyrene is bound to the hydrophobic regions of BSA, given that the serum albumins have two distinct binding sites.[2,3] The I_3/I_1 ratio of pyrene was also estimated to obtain an idea of the relative polarity of the pH-induced conformational isomers (Figure 3.2b). The ratio was higher in native BSA (~ 0.78) than that in water (~ 0.65) which is suggestive of the fact that the pyrene molecules are localized in the hydrophobic binding sites of BSA. It is noteworthy to state that the I_3/I_1 ratio in BSA at pH 3 (~ 0.90) was considerably higher than that of the native protein and all other pH-induced isomers (I_3/I_1 ratio ~ 0.78), emphasizing the existence of an expanded conformational state of BSA comprising exposed hydrophobic pockets at pH 3.

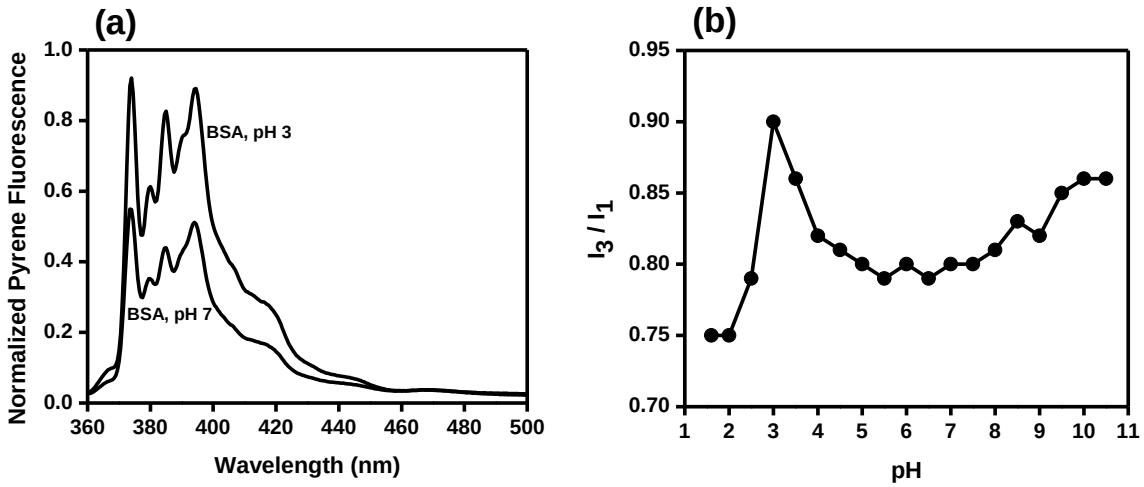

Figure 3.2 (a) Fluorescence emission spectra of pyrene in the presence of BSA at pH 7 and pH 3 at 25 °C. (b) The ratio of the third (I_3; 384 nm) and first (I_1; 373 nm) vibronic peak intensities of pyrene in BSA as a function of pH obtained from calculation of the emission spectra. All the experiments were repeated separately three times to get an estimate of the error associated with the measurements which was < 0.01.

3.3.3 Equilibrium unfolding studies of BSA at acidic and physiological solution conditions

All the fluorescence observables have indicated that the native BSA isomerizes to a partially-extended, 'molten-globule-like' state predominantly populated at pH 3. In order to compare the thermodynamic stabilities between the native and the expanded isomer of BSA, the unfolding of BSA, induced by urea, was investigated by steady-state fluorescence spectroscopy under physiological and acidic pH (pH 7 and pH 3, respectively) conditions. Changes in the fluorescence intensity and anisotropy of tryptophans were measured. The fluorescence emission maximum and steady-state anisotropy value of the tryptophan residues in the native BSA at pH 7 were found to be 350 nm and ~ 0.21 respectively. At pH 7, a cooperative transition from the native to unfolded state of BSA was evident from the sigmoidal curves for both in tryptophan fluorescence intensity and anisotropy as a function of denaturant concentration (Figure 3.3a,b). The mid-point of transition was centered around 5 M urea concentration. The chemical denaturation studies were also carried out at pH 3 where the partially-extended conformers were populated. Both tryptophan fluorescence intensity and anisotropy did not demonstrate a cooperative transition; rather they showed a continuous change as a function of denaturant concentration. No significant changes were observed after 3 M of urea (Figure 3.3a,b).

The overall fluorescence intensity plot of BSA at pH 3 suggested that, as expected, the partially-extended conformational population unfolds in a non-cooperative fashion. The conformational isomers, especially in the acidic pH, showed a decrease in helical content with an increase in the hydrophobicity which indicated the existence of 'molten-globule-like' expanded conformers and were expected to be amyloidogenic precursors. These findings set the stage for

further investigations into the structural and mechanistic aspects of the aggregation process at higher protein concentrations.

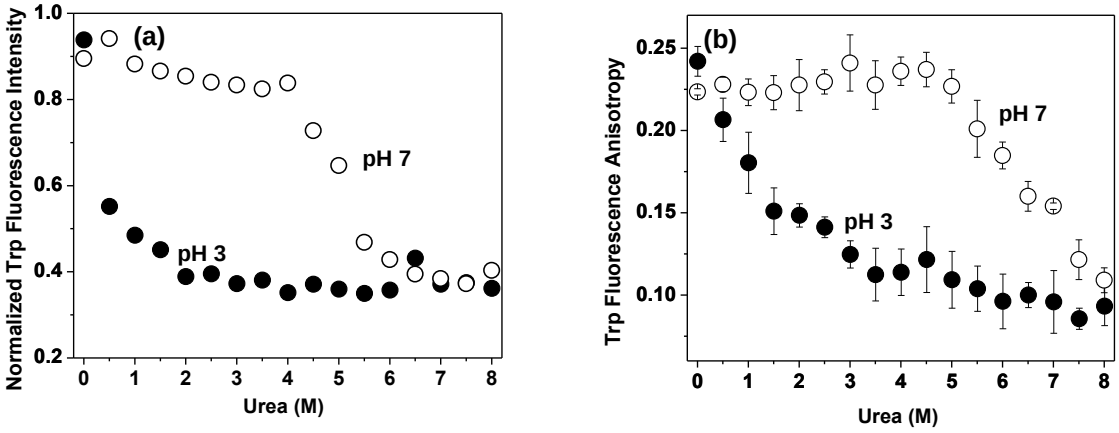

Figure 3.3 Chemical denaturation of the native BSA (pH 7: open circle) and the partially-folded conformational isomer of BSA (pH 3: filled circle) as a function of urea concentration at 25 °C. Changes in the (a) tryptophan fluorescence intensity and (b) tryptophan fluorescence anisotropy as observed during unfolding of BSA.

3.3.4 Aggregation of BSA

In order to monitor the aggregation kinetics of BSA; 50 mM NaCl, pH 3 and 65 °C were set as the optimum condition and the fibrillation was investigated by changes in the Thioflavin-T (ThT) fluorescence intensity. Figure 3.4a shows a typical evolution of ThT fluorescence spectra as a function of time indicating the formation of amyloid-like aggregates. The plot at pH 3 (Figure 3.4a inset) reveals that the ThT intensity increased very sharply within first 10 minutes of heating; approached a quasi-plateau region in 30 minutes and then appeared to be completed within an hour. Approximately, 40-fold enhancement in the ThT fluorescence intensity was observed at the end of fibrillation compared to the intensity observed before the sample was incubated at 65 °C, which indicated the formation of β-sheet-rich amyloid-like aggregates and

hence, an increase in ThT-binding sites. The average rate constant of ThT-florescence kinetics was estimated to be ~67 x 10^{-3} min^{-1}.

Nile red has been reported as a better amyloid aggregation marker compared to ThT, especially, if the aggregation studies are carried out under acidic conditions.[27] At pH 7 (the native-monomeric-form) and pH 3 (the acid-expanded-monomeric-form), the fluorescence emission of Nile red was measured at 620 nm; the latter exhibiting a 2-fold excess intensity compared to that of the native BSA. A substantial increment in the Nile red emission was observed for the unheated sample at pH 3 and 50 mM NaCl. Upon heating, a significant enhancement in the Nile red fluorescence was observed with a concomitant blue-shift to 615 nm which is an indicator of the formation of amyloid-like aggregates (Figure 3.4b).[27] The observations are in good agreement with that obtained from the ThT fluorescence assay.

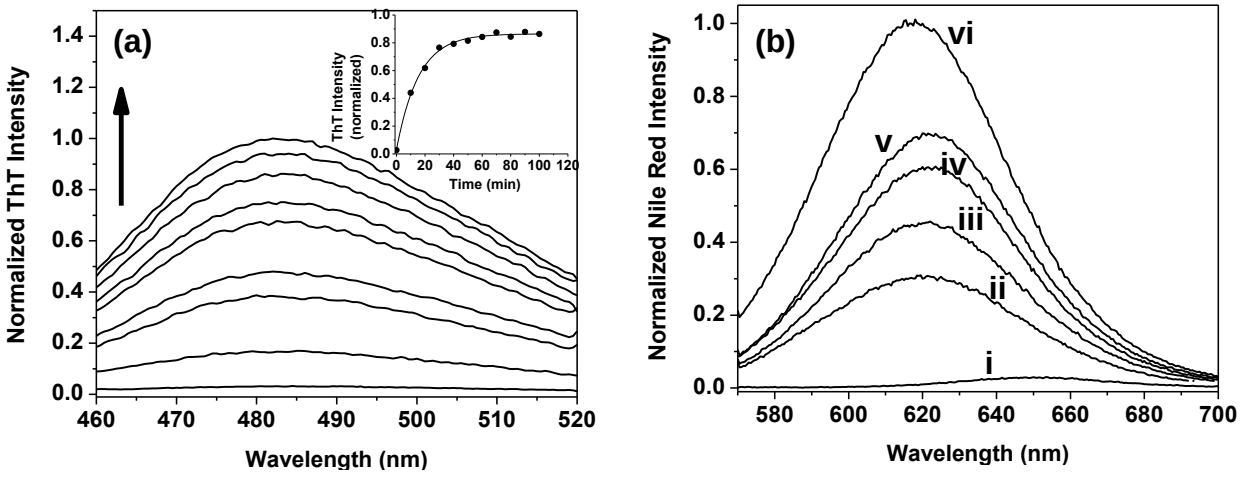

Figure 3.4 Amyloid aggregation of BSA at pH 3, 50 mM NaCl, 65 °C monitored by change in Thioflavin-T (ThT) and Nile red fluorescence. (a) Evolution of ThT emission spectra as a function of time; inset graph depicts the change in ThT intensity as a function of time. (b) Change in Nile red fluorescence emission spectra in (i) water (ii) BSA (10 μM), pH 7 (iii) BSA (10 μM), pH 3 (iv) BSA (100 μM), pH 7 (v) BSA (100 μM), pH 3 and (vi) Amyloid fibrils of BSA at pH 3, 65 °C. The spectra (ii-vi) were collected in presence of 50 mM NaCl.

Next, the amyloid fibrillation of BSA was monitored by ThT fluorescence as a function of temperature. The apparent rate of amyloid-like aggregate formation was found to be faster at higher temperature and a linear Arrhenius plot was observed when the observed rate constant was plotted *vs.* 1/T (Figure 3.5a). The activation energy was determined to be ~109 kJ/mol which is close to the reported data for aggregation of other proteins.[16,28] The structures of the BSA fibrils formed under acidic conditions were also examined under Transmission Electron Microscope. The TEM images (Figure 3.5b,c) revealed infinite stretches (in the order of microns) of a flat-ribbon and long rod-shaped, self-assembled fibrillar network intertwined together.

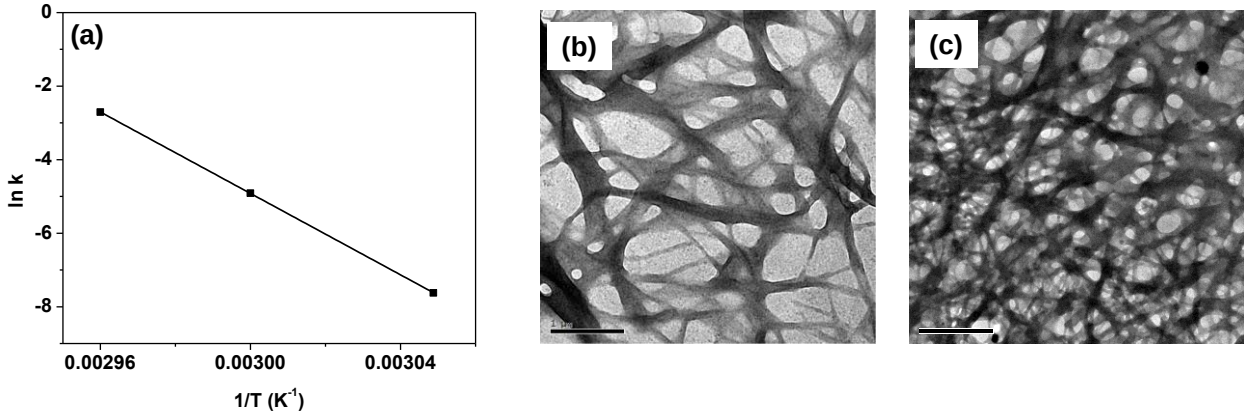

Figure 3.5 (a) Arrhenius plot of bovine serum albumin (BSA) fibrillation kinetics at pH 3, 50 mM NaCl at 55, 60 and 65 °C. The activation energy (E_{act}) of fibril formation was determined to be 109 (±7) $kcalmol^{-1}K^{-1}$. The error bars are included in the symbols. (b,c) TEM images of BSA amyloid fibrils after heating for 4 hours followed by a 30-days-long incubation at room temperature (25 °C). Scale bar: 1 μm.

3.3.5 Aggregation monitored by tryptophan fluorescence

The changes in the average fluorescence intensity and anisotropy of the two intrinsic tryptophan residues were monitored during fibrillation as a function of time. At a high protein concentration, 50 mM NaCl and room temperature, an intense tryptophanyl fluorescence at ~ 344 nm was observed which indicates that the tryptophans are present in non-polar environment. Upon heating to 65 °C, a progressive reduction in tryptophan fluorescence intensity (Figure 3.6a) accompanied by a slight blue-shift (~ 3 nm) was observed upon formation of the amyloid-like aggregates. We suggest that the observed drop in fluorescence intensity could be due to quenching of tryptophan intensity due to an increase in the number of phenylalanines, histidines and disulfides in the proximity of tryptophans that quench the emission upon aggregation mediated by both electrostatic and hydrophobic interactions. Kinetic analysis of the reduction in tryptophan fluorescence intensity yielded an average rate constant of ~ 188 x 10^{-3} min^{-1}, which is ~2.8 fold higher than that of the ThT fluorescence-monitored kinetics (k = ~ 67 x 10^{-3} min^{-1}) observed under identical conditions. Prior to heating at 65 °C, a small but measurable increase in tryptophan fluorescence anisotropy was observed as compared to that of the monomeric protein in pH 3. This could probably be attributed to the formation of soluble-oligomers at higher protein concentration from the acid-expanded conformer of BSA whereby the oligomerization could be facilitated by the presence of salt. A significant enhancement in the tryptophan fluorescence anisotropy without any lag-phase was observed upon heating that reached saturation very quickly as fibrillation progressed, suggesting formation of large-sized aggregates (Figure 3.6a). The apparent rate constant obtained for changes in tryptophan anisotropy was ~ 97 x 10^{-3} min^{-1}. Comparison of the two rate constants, monitored by tryptophan fluorescence, reveal that the

conformational changes occur at a faster rate compared to that of the overall size growth of the aggregates.

3.3.6 Aggregation monitored by ANS fluorescence

To determine whether hydrophobic regions are accessible and attainable in the oligomerization and subsequent amyloid fibrillation of protein at pH 3, the fluorescence intensity and anisotropy of 8-anilinonaphthalene-1-sulfonic acid ammonium salt (ANS) were measured. In our experiments, ANS was initially bound to the hydrophobic pockets and charged surface residues of the unheated sample at pH 3. After the temperature jump, a sharp enhancement in the ANS emission at 475 nm followed by a plateau was observed which indicated a dramatic increase in the extent of hydrophobic environment upon heating that drives the oligomerization-fibrillation reaction (Figure 3.6b). Kinetic analysis of the ANS fluorescence intensity data yielded an apparent rate constant of ~ 244 x 10^{-3} min^{-1}; slightly faster (~ 1.3 times) than that of the tryptophanyl fluorescence kinetics. At room temperature and higher protein concentration, the ANS fluorescence anisotropy was higher (0.17 ± 0.002) compared to that of the monomeric protein (0.14 ± 0.003) suggesting the existence of soluble oligomers. Upon heating to 65 °C, the ANS anisotropy showed a monotonic increase and attained saturation after 40 minutes of heating (see Figure 3.6b inset) and exhibited an average rate constant of ~ 102 x 10^{-3} min^{-1}; almost similar to that of the tryptophan fluorescence anisotropy. Taken together, these observations suggest that higher protein concentration induces a collapse of the hydrophobic patches in an otherwise expanded, 'molten-globule-like' form of the α-helical protein which is aided by the addition of salt at room temperature. During the temperature jump, both the salt and temperature

placate the formation and growth of larger aggregates with increased hydrophobicity which eventually form amyloid-like fibrillar aggregates. Here again, like tryptophan fluorescence kinetics, the rate of change in conformation, and hence, hydrophobicity monitored by ANS is much faster than that of the overall size growth.

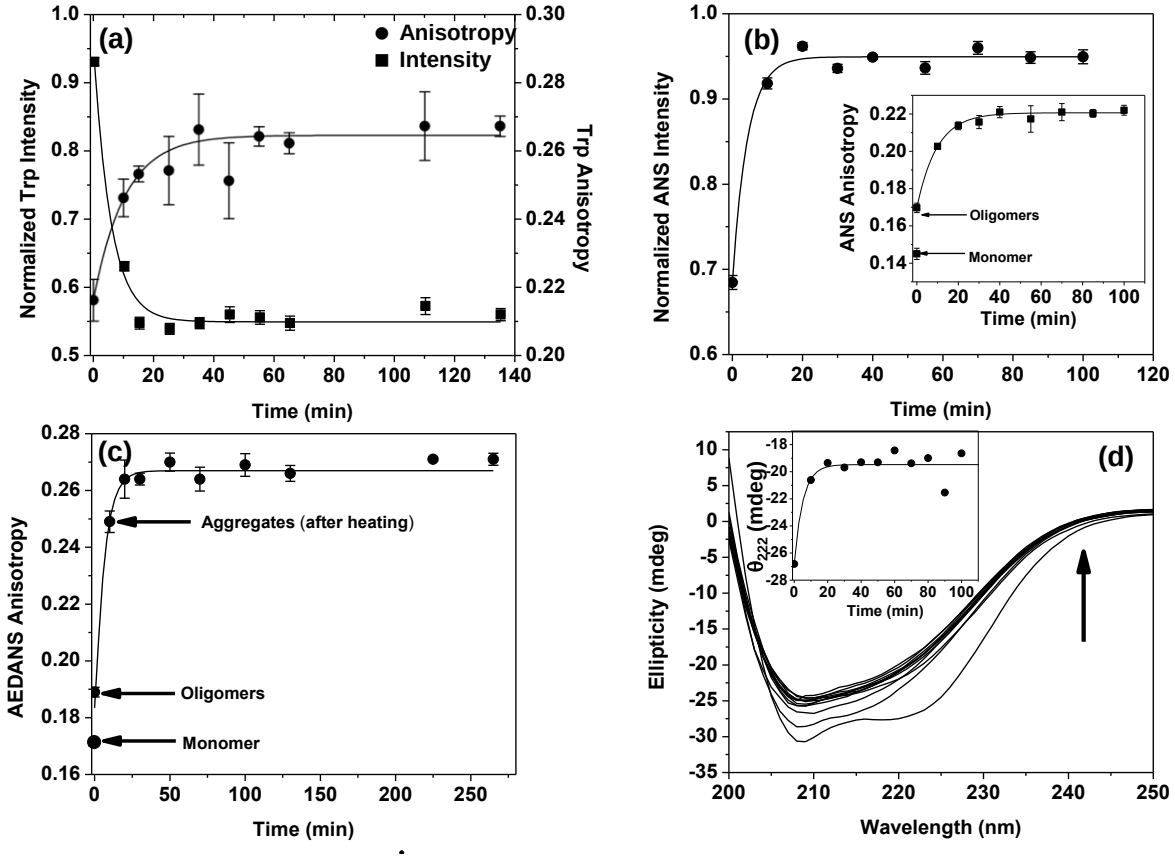

Figure 3.6 Amyloid fibrillation of BSA at pH 3, 50mM NaCl, 65 °C as a function of time monitored by (a) tryptophan fluorescence intensity (filled square) and anisotropy (filled circle) (b) ANS fluorescence intensity (filled circle) and anisotropy (inset, filled square) (c) AEDANS fluorescence anisotropy and (d) secondary structural changes monitored by far-UV CD spectra and change in ellipticity at 222 nm as a function of time (inset). The data points at 0 min represent fluorescence intensity and anisotropy of the respective structural probe at 25 °C i.e. prior to heating. The solid lines represent the fit obtained from mono-exponential function.

3.3.7 Aggregation monitored by AEDANS fluorescence

The previous set of experiments has shown that the far-UV CD spectrum of the monomeric protein indicates a considerable loss in helical content at pH 3 which was correlated to the loss of intra-domain helicity in domains I and II from the FRET efficiency data.[29] Additionally, the findings obtained from tryptophan and ANS fluorescence suggest that at room temperature, the 'molten-globule-like' isomer collapses to hydrophobic-rich oligomers at higher protein concentration and salt which eventually leads to larger aggregates. Therefore, in order to decipher the plausible involvement of domain I (largely disordered at pH 3) in oligomerization and amyloid fibrillation, following studies were carried out. The availability of a single, free cysteine residue (Cys34) in the domain I of the α-helical protein provides us with a unique advantage of carrying out a chemical modification of the cysteine. IAEDANS (5-((((2-iodoacetyl)amino)ethyl)amino)naphthalene-1-sulfonic acid) was employed to label the thiol group of the cysteine residue specifically because IAEDANS has a long fluorescence lifetime,[21] so any small change in the conformation and size can be easily and clearly detected within the lifetime of this probe. Aggregation of labeled BSA (5% of total BSA concentration) was monitored by AEDANS fluorescence anisotropy under same acidic conditions in the presence of NaCl (Figure 3.6c). The initial fluorescence anisotropy of BSA-AEDANS (before heating) was found to be 0.19 ± 0.004, again suggesting the existence of soluble-oligomers (anisotropy of BSA-AEDANS monomer at pH 3 was 0.17 ± 0.002), which enhanced rapidly upon heating and reached saturation at a value of ~ 0.26. It should be noted here that the covalently-labeled cysteine is located in domain I; hence, the observed changes in the fluorescence anisotropy of AEDANS can be correlated with only a local structural reordering of domain I. Interestingly, the

apparent rate constant obtained from the changes in AEDANS fluorescence anisotropy is ~ 142 x 10^{-3} min^{-1} which is much faster (~ 1.5 times) than that obtained from ANS and tryptophan anisotropies, respectively but again, slower than the conformational changes. Overall, the AEDANS fluorescence anisotropy data imply that the partially exposed domains in the 'molten-globule-like' form of BSA, under mildly acidic conditions, form amyloid-like aggregates wherein the sequestration of domain I into hydrophobic oligomers is one of the earliest events that takes place during the fibrillation process. Moreover, the covalently-labeled cysteine residue did not appear to obstruct the fibril formation which is congruent with a previous report.[30]

3.3.8 Aggregation monitored by CD spectroscopy

At pH 3 and 50 mM NaCl, the far-UV CD spectrum of BSA shows minima at 222 and 209 nm which is a characteristic of an α-helix rich protein. After the sample was incubated at 65 °C, there was a successive loss in the helicity at 222 and 209 nm as revealed by the far-UV CD spectra (Figure 3.6d) which may suggest that the formation of both β-sheet and unordered conformation occur at the expense of helical conformation. This also implies that partially-unfolded conformers having variable secondary structural contents exist in solution after heating which subsequently lead to the formation of β-sheet-rich amyloid aggregates as evidenced by an increase in ThT and Nile-red fluorescence. The average rate constant of loss of helicity at 222 nm (inset of Figure 3.6d) was determined to be ~ 192 x 10^{-3} min^{-1}, almost equal to that of the tryptophanyl and ANS fluorescence intensity kinetics and corroborates the changes in conformations at a faster rate compared to the overall size growth.

The kinetic analysis of all the structural probes suggests that the aggregation is likely to be devoid of a nucleation step that is typically characterized by a lag-phase. The initial rise in fluorescence anisotropy of the structural probes at room temperature indicated that at a higher protein concentration, oligomerization occurs which is facilitated by the presence of salt. Figure 3.7 depicts a comparison between the rate of conformational changes and that of the overall size growth which suggests that the conformational conversion in the preformed oligomers occurs considerably faster than the growth of higher-order aggregates. Association of these aggregates subsequently leads to the formation of amyloid-like fibrils with increasing β-sheet content.

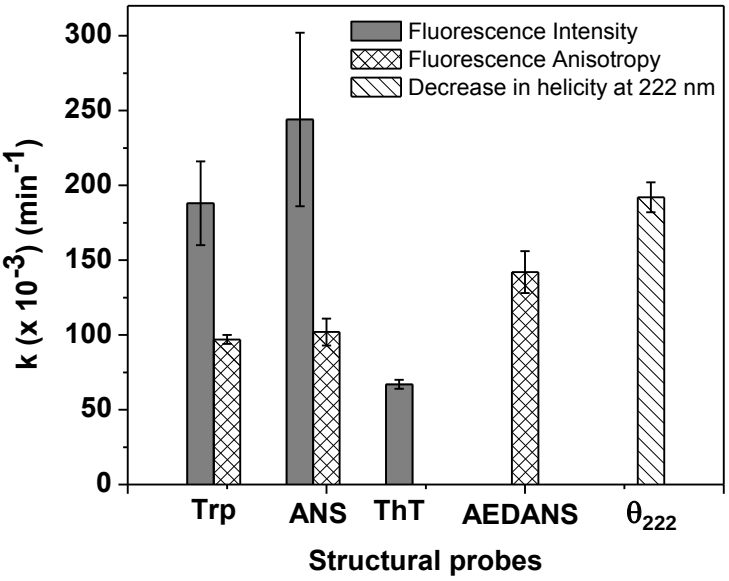

Figure 3.7 Comparison of the rate constants of amyloid fibrillation kinetics of multiple structural probes as depicted by changes in conformation and size to delineate the steps involved in the fibrillation event.

3.4 Discussion

We initially characterized the partially-folded 'molten-globule-like' of BSA at low pH. Then we studied the structural transformation and aggregation propensity of this molten globule conformer in the presence of salt and observed that one of the conformational isomers, formed at pH 3, predominantly forms amyloid-like aggregates at 50 mM NaCl when heated to 65 °C. Although the aggregation reactions are endowed with inherent complexity, all the kinetic traces could be fitted to a single-exponential function. The sample incubated at 100 μM of BSA remained as a clear solution even after heating for 4 hours and keeping at room temperature for a period over days to months indicative of the fact that the oligomers and the subsequent fibrillar aggregates are soluble. It has been pointed out that the soluble oligomers and fibrillar aggregates are cytotoxic and seem to be responsible for the onset of neurodegeneration whereas fibrils appear to be relatively harmless unless they assemble to very high levels causing organ malfunction and subsequent failure.[31]

There have been several reports suggesting that in the absence of seeding, accruement of oligomeric assemblies drives the spontaneous fibrillation of several proteins under acidic conditions.[14,28,32] As discussed previously, the acid-expanded, 'molten-globule-like' isomer of BSA forms oligomers immediately at high protein concentration and in the presence of salt. Such phenomenon is discernible given the fact that there is a substantial loss in intra-domain helicity of domain I when BSA forms an expanded, 'molten-globule-like' state at pH 3,[29] giving rise to a considerable fraction of extended structures. At a higher protein concentration, these exposed, disordered segments (both from domain I and the remaining inherent extended structures)

assemble via hydrophobic interactions and form soluble (molten) oligomers at room temperature. This observation is consistent with a recent report on HSA fibrillation.[18]

In our present investigation, various structural probes in-tandem were utilized to decipher the temporal evolution of both conformational and size changes during the aggregation (Figure 3.6 & 3.7). The rate of conformational changes observed by tryptophan fluorescence and CD spectroscopy are almost similar but markedly higher than that monitored by ThT fluorescence. One of the salient features of fluorescence anisotropy kinetics is that the rate of change in AEDANS anisotropy is higher than that of tryptophan which implies that the sequestration of domain I into the aggregate is likely to be the earliest event in the oligomerization and self-assembly process (Figure 3.7). However, comparison of the kinetics of conformational changes and fluorescence anisotropy indicate that the rate of conformational change is higher than that of the overall size growth of the aggregates (Figure 3.7). We suggest that conformational conversion from α-helices to extended regions and β-sheets in the pre-formed molten-oligomers occurs faster compared to the aggregate size growth and subsequent formation of β-sheet-rich amyloid-like aggregates at higher temperature. The kinetics monitored by ThT-fluorescence is comparable to the anisotropy kinetics probed by different fluorescent markers, which indicates that the size increase and the formation of β-sheet-rich fibrillar aggregates occur simultaneously. Also, ThT appears to be the slowest of all probes used in this study, suggestive of the fact that ThT exhibits the strongest signal when it is bound to mature fibrils.[33]

Typically, fibrillation occurs by a nucleation-dependent polymerization mechanism whereby the fibril formation is preceded by a lag-phase and is strongly concentration-dependent, denoting the formation of critical-oligomeric nucleus that facilitates the association and sequestration of

other monomers into fibrils.[34,35,36] In our study, a common observation obtained from multiple probes is that the conversion of BSA monomers to fibrils proceeds without any lag-phase (Figure 3.6). This observation is in line with the reports on HSA and BSA fibrillation.[15,16] The non-existent lag-phase has been found to be independent of protein concentration and seeding in earlier studies.[16,18] This suggests that BSA fibrillation neither solely follows the classical nucleated polymerization kinetics[34] nor it is dominated by the secondary nucleation phenomenon.[37] The characteristic absence of lag-phase has also been demonstrated in the amyloidogenesis of β_2-microglobulin,[38,39] transthyretin,[40] prion protein[28] and barstar.[41] The absence of lag-phase has been attributed to the formation of "propagation-competent nucleus-like structures"[30] that do not require the formation of high-energy, critical-and-unstable nucleus.[40] Such a phenomenon can be explained by a few available kinetic models such as 'random association',[42] 'supercritical concentration driven fibril formation'[43] and 'downhill-polymerization'.[44] Given the inherent complex nature of aggregation kinetics,[45] although it is difficult to assign any particular kinetic pathway for serum albumin fibrillation, we speculate that the overall kinetics observed is a complex combination of either some or all the three 'lag-phase-independent' mechanisms mentioned above. Complete kinetic analyses of protein aggregation processes have yielded several prominent models such as template assembly,[45,46] monomer-directed conversion,[47] nucleated polymerization[48-50] and nucleated conformational conversion (NCC).[51] The NCC-model states that the conformational conversion occurs within the 'molten' oligomeric intermediate and forms nuclei that drive the assembly rapidly. In our case, we suggest a plausible molecular mechanism of BSA fibrillation (Figure 3.8) that mostly echoes the central

theme of the NCC model, while incorporating the features of both downhill- and irreversible polymerization to account for the absence of lag-phase.

At room temperature and low pH, the protein forms a 'molten-globule-like' state that gives rise to exposed hydrophobic regions at a low protein concentration. An increase in the protein concentration induces (intermolecular) self-association whereby the domain I is sequestered into the oligomers. At elevated temperature, a conformational conversion from α-helix and random coil structures to β-rich structures is facilitated in these pre-formed oligomers that serve as precursors of matured amyloid fibrils. In summary, our present investigation reveals multiple and kinetically distinct steps such as conformational changes-and size changes followed by fibril formation as depicted in a simplistic model (Figure 3.8).

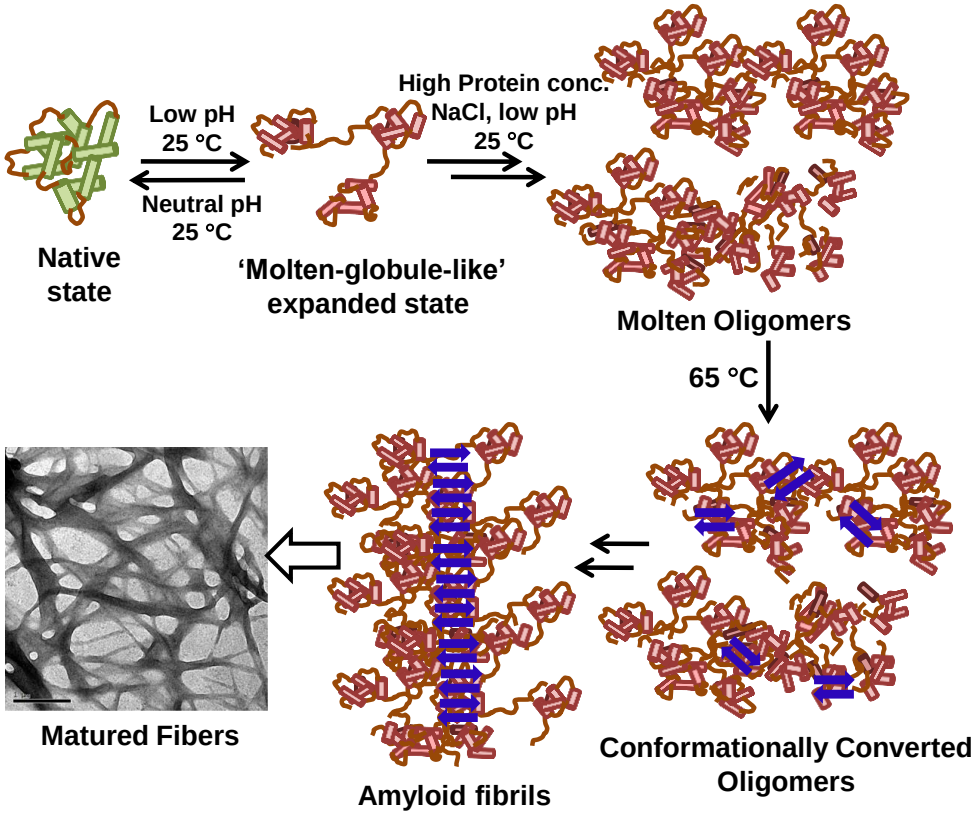

Figure 3.8 Suggested molecular mechanism of amyloid formation from all α-helical serum albumins.

3.5 Conclusion

The present work describes the identification and characterization of multiple pH-dependent conformational isomers of BSA. Our findings indicated that BSA forms a partially-folded, 'molten-globule-like' form in the acidic pH regime. Our results demonstrate that the acid-expanded, 'molten-globule-like' isomer of BSA forms amyloid-like fibrils under carefully designed conditions. The conformational rearrangement in the early (molten) oligomers precedes the formation of larger aggregates leading to the formation of β-rich fibrils. The mechanistic insights gained from the present work would be useful in the design of anti-amyloid therapeutics by targeting various stages of the aggregation process. Additionally, we believe that the combination of methodologies used in this work will find broad application in the study of misfolding and aggregation of other physiologically important proteins.

3.6 References

1. Fandrich, M.; Fletcher, M. A.; Dobson, C. M. (2001) Amyloid fibrils from muscle myoglobin *Nature* 410:165-166.

2. Carter, D. C.; Ho, J. X. (1994) Structure of serum albumin. *Adv. Protein Chem.* 45:153-203.

3. Peters Jr., T. (1985) Serum Albumin. *Adv. Protein Chem.* 37:161-245.

4. Rossing, T. H.; Maffaeo, N.; Fencl, V. (1986) Acid–base effects of altering plasma protein concentration in human blood in vitro. *J. Appl. Physiol.* 61:2260-2265.

5. He, X. M.; Carter, D. C. (1992) Atomic structure and chemistry of human serum albumin. *Nature* 358:209-215.

6. Sugio, S.; Kashima, A.; Mochizuki, S.; Noda, M.; Kobayashi, K. (1999) Crystal structure of human serum albumin at 2.5Å resolution. *Protein Engg.* 12:439-446.

7. Luetscher, J. A. Serum Albumin. II. (1939) Identification of more than one albumin in horse and human serum by electrophoretic mobility in acid solution. *J. Am. Chem. Soc.* 61:2888-2890.

8. Williams, E. J.; Foster, J. F. (1960) The aggregation of bovine plasma albumin at low pH. *J. Am. Chem. Soc.* 82:3741-3745.

9. Foster, J. F. (1977) *Some aspects of the structure and the conformational properties of serum albumin* in Albumin structure, function and uses (Rosenoer, V. M.; Oratz, M.; Rothschild, M. A. Eds.) pp 53-84, Oxford, Pergamon.

10. Era, S.; Sogami, M. (1998) ^{1}H-NMR and CD studies on the structural transition of serum albumin in the acidic region-the N$\rightarrow$F transition. *J. Peptide Res.* 52:431-442.

11. Li, Y.; Lee, J.; Lal, J.; An, L.; Huang, Q. (2008) Effects of pH on the interactions and conformation of bovine serum albumin: comparison between chemical force microscopy and small-angle neutron scattering. *J. Phys. Chem. B* 112:3797-3806.

12. Kadi, N. E.; Taulier, N.; Huérou, J. Y. L.; Gindre, M.; Urbach, W; Nwigwe, I.; Kahn, P.C.; Waks, M. (2006) Unfolding and refolding of bovine serum albumin at acid pH: ultrasound and structural studies. *Biophys. J.* 91:3397-3404.

13. Wilting, J.; Kremer, J. M. H.; Ijzerman, A. P.; Schulman, S. G. (1982) The kinetics of the binding of warfarin to human serum albumin as studied by stopped-flow spectrophotometry. *Biochim. Biophys. Acta.* 706:96-104.

14. Militello, V.; Vetri, V.; Leone, M. (2003) Conformational changes involved in thermal aggregation processes of bovine serum albumin. *Biophys. Chem.* 105:133-141.

15. Taboada, P.; Barbosa, S.; Castro, E.; Mosquera, V. (2006) Amyloid fibril formation and other aggregate species formed by human serum albumin association. *J. Phys. Chem. B* 110:20733-20736.

16. Holm, N. K.; Jespersen, S. K.; Thomassen, L. V.; Wolff, T. Y.; Sehgal, P.; Thomsen, L. A.; Christiansen, G.; Andersen, C. B.; Knudsen, A. D.; Otzen, D. E. (2007) Aggregation and fibrillation of bovine serum albumin. *Biochim. Biophys. Acta* 1774:1128-1138.

17. Vetri, V.; Librizzi, F.; Leone, M.; Militello, V. (2007) Thermal aggregation of bovine serum albumin at different pH: comparison with human serum albumin. *Eur. Biophys. J.* 36:717-725.

18. Juarez, J.; Taboada, P.; Mosquera, V. (2009) Existence of different structural intermediates on the fibrillation pathway of human serum albumin. *Biophys. J.* 96:2353-2370.

19. Juarez, J.; Lopez, S. G.; Cambon, A.; Taboada, P.; Mosquera, V. (2009) Influence of electrostatic interactions on the fibrillation process of human serum albumin. *J. Phys. Chem. B* 113:10521-10529.

20. Atanasiu, C.; Su, T.-J.; Sturrock, S. S.; Dryden, D. T. F. (2002) Interaction of the ocr gene 0.3 protein of bacteriophage T7 with EcoKI restriction/modification enzyme. *Nucl. Acids Res.* 30:3936-3944.

21. Hudson, E. N.; Weber, G. (1973) Synthesis and characterization of two fluorescence sulfhydryl reagents. *Biochemistry* 12:4154-4161.

22. Graetzel, M.; Thomas, J. K. (1973) Dynamics of pyrene fluorescence quenching in aqueous ionic micellar systems. Factors affecting the permeability of micelles. *J. Am. Chem. Soc.* 95:6885-6889.

23. Glushko, V.; Thaler, M. S. R.; Karp, C. D. (1981) Pyrene fluorescence fine structure as a polarity probe of hydrophobic regions: Behavior in model solvents. *Arch. Biochem. Biophys.* 210:33-42.

24. Chaudhuri, A.; Haldar. S.; Chattopadhyay, A. (2009) Organization and dynamics in micellar structural transition monitored by pyrene fluorescence. *Biochem. Biophys. Res. Commun.* 390:728-732.

25. Dong, D. C.; Winnik, M. A. (1982) The P*y* scale of solvent polarities. Solvent effects on the vibronic fine structure of pyrene fluorescence and empirical correlations with the E_T and Y values. *Photochem. Photobiol.* 35:17-21.

26. Haque, M. E.; Ray, S.; Chakrabarti, A. (2000) Polarity estimate of the hydrophobic binding sites in erythroid spectrin: a study by pyrene fluorescence. *J. Fluoresc.* 10:1-6.

27. Mishra, R.; Sörgjerd, K.; Nyström, S.; Nordigården, A.; Yu, Y.-C.; Hammarström, P. (2007) Lysozyme amyloidogenesis is accelerated by specific nicking and fragmentation but decelerated by intact protein binding and conversion. *J. Mol. Biol.* 366:1029-1044.

28. Jain, S.; Udgaonkar, J. B. (2008) Evidence for stepwise formation of amyloid fibrils by the mouse prion protein. *J. Mol. Biol.* 382:1228-1241.

29. Bhattacharya, M.; Jain, N.; Bhasne, K.; Kumari, V.; Mukhopadhyay, S. (2011) pH-induced conformational isomerization of bovine serum albumin studied by extrinsic and intrinsic protein fluorescence. *J. Fluoresc.* 21:1083-1090.

30. Holm, N. K.; Jespersen, S. K.; Thomassen, L. V.; Wolff, T. Y.; Sehgal, P.; Thomsen, L. A.; Christiansen, G.; Andersen, C. B.; Knudsen, A. D.; Otzen, D. E. (2007) Aggregation and fibrillation of bovine serum albumin. *Biochim. Biophys. Acta* 1774:1128-1138.

31. Pepys, M. B.; Hawkins, P. H.; Booth, D. R.; Vigushin, D. M.; Tennent, G. A.; Soutar, A. K.; Totty, N.; Bguyen, O.; Blake, C. C.; Terry, C. J.; Feest, T. G.; Zalin, A. M.; Hsuan, J. J. (1993) Human lysozyme gene mutations cause hereditary systemic amyloidosis. *Nature* 362:553-557.

32. Harper, J. D.; Lansbury Jr., P. T. (1997) Models of amyloid seeding in Alzheimer's disease and scrapie: mechanistic truths and physiological consequences of the time-dependent solubility of amyloid proteins. *Annu. Rev. Biochem.* 66:385-407.

33. Lindgren, M.; Sörgjerd, K.; Hammarström, P. (2005) Detection and characterization of aggregates, prefibrillar amyloidogenic oligomers and protofibrils using fluorescence spectroscopy. *Biophys. J.* 88:4200-4212.

34. Oosawa, F.; Asakura, S.; Hotta, K.; Nobuhisa, I.; Ooi, T. (1959) G-F transformation of actin as a fibrous condensation. *J. Polym. Sci.* 37:323-336.

35. Jahn, T. R.; Radford, S. E. (2008) Folding versus aggregation: polypeptide conformations on competing pathways. *Arch. Biochem. Biophys.* 469:100-117.

36. Wetzel, R. (2006) Kinetics and thermodynamics of amyloid fibril assembly. *Acc. Chem. Res.* 39:671-679.

37. Knowles, T. P. J.; Waudby, C. A.; Devlin, G. L.; Cohen, S. I. A.; Aguzzi, A.; Vendruscolo, M.; Terentjev, E. M.; Welland, M. E.; Dobson, C. M. (2009) An analytical solution to the kinetics of breakable filament assembly. *Science* 326:1533-1537.

38. Radford, S. E.; Gosal, W.S.; Platt, G. W. (2005) Towards an understanding of the structural and molecular mechanism of β2-microglobulin amyloid formation in vitro. *Biochim. Biophys. Acta* 1753:51-63.

39. Sasahara, K.; Yagi, H.; Sakai, M.; Naiki, H.; Goto, Y. (2008) Amyloid nucleation triggered by agitation of β2-microglobulin under acidic and neutral pH conditions. *Biochemistry* 47:2650-2660.

40. Hurshman, A. R.; White, J. T.; Powers, E. T.; Kelly, J. W. (2004) Transthyretin aggregation under partially denaturing conditions is a downhill polymerization. *Biochemistry* 43:7365-7381.

41. Kumar, S.; Mohanty, S. K.; Udgaonkar, J. B. (2007) Mechanism of formation of amyloid protofibrils of barstar from soluble oligomers: evidence for multiple steps and lateral association coupled to conformational conversion. *J. Mol. Biol.* 367:1186-1204.

42. Thusius, D.; Dessen, P.; Jallon, J.-M. (1975) Mechanism of bovine liver glutamate dehydrogenase self-association I. Kinetic evidence for a random association of polymer chains. *J. Mol. Biol.* 92:413-432.

43. Powers, E. T.; Powers, D. L. (2006) The kinetics of nucleated polymerizations at high concentrations: amyloid fibril formation near and above the "supercritical concentration". *Biophys. J.* 91:122-132.

44. Pappu, R. V.; Wang, X.; Vitalis, A.; Crick, S. L. (2008) A polymer physics perspective on driving forces and mechanisms for protein aggregation. *Arch. Biochem. Biophys.* 469:132-141.

45. Morris, A. M.; Watzky, M. A.; Finke, R. G. (2009) Protein aggregation kinetics, mechanism and curve-fitting: a review of the literature. *Biochim. Biophys. Acta* 1794:375-397.

46. Uratani, Y.; Asakura, S.; Imahori, K. (1972) A circular dichroism study of Salmonella flagellin: evidence for conformational change on polymerization. *J. Mol. Biol.* 67:85-98.

47. Prusiner, S. B. (1982) Novel proteinaceous infectious particles cause scrapie. *Science* 216:136-144.

48. Beaven, G. H.; Gratzer, W. B.; Davies, H. G. (1969) Formation and structure of gels and fibrils from glucagon. *Eur. J. Biochem.* 11:37-42.

49. Hofrichter, J.; Ross, P. D.; Eaton, W. A. (1974) Kinetics and mechanism of deoxyhemoglobin S gelation: a new approach to understanding sickle cell disease. *Proc. Natl. Acad. Sci. U.S.A.* 71:4864-4868.

50. Jarrett, J. T.; Lansbury Jr., P. T. (1993) Seeding one-dimensional crystallization of amyloid: a pathogenic mechanism in Alzheimer's disease and scrapie. *Cell* 73:1055-1058.

51. Serio, T. R.; Cashikar, A. G.; Kowal, A. S.; Sawicki, G. J.; Moslehi, J. J.; Serpell, L.; Arnsdorf, M. F.; Lindquist, S. L. (2000) Nucleated conformational conversion and the

replication of conformational information by a prion determinant. *Science* 289:1317-1321.

Chapter 4

Organization of Protein Molecules within the Amyloid Pores Revealed by Raman Spectroscopy

This work has been published in *Journal of Physical Chemistry Letters*

M. Bhattacharya*, **N. Jain***, P. Dogra, S. Samai and S. Mukhopadhyay. Nanoscopic amyloid pores formed via stepwise protein assembly. *J. Phys. Chem. Lett.* **2013**, *4*, 480-485.

*Joint first author

4.1 Introduction

In the present study, we have used ovalbumin which is a model non-inhibitory member of the serpin superfamily. It is present in the chicken egg-white and is commonly used as a gelling agent, emulsifier etc. in the food industry.[1-3] It is a 385-residue, 45 kDa glycoprotein comprising nine α-helices and three β-sheets that harbor three tryptophans (Trp 148, Trp 184, Trp 267), four free cysteines (Cys 11, Cys 30, Cys 367, Cys 382), and one solvent accessible disulfide bond (Cys 73-Cys 120) (Figure 4.1). The structural similarity between ovalbumin and other archetypal serpins (α-antitrypsin, neuroserpin) coupled with the ease of availability makes ovalbumin an attractive candidate for investigating the mechanistic aspects of serpinopathies. These serpinopathies are described as a range of physiological diseases that occur as a consequence of misfolding and self-assembly of serpins (serine protease inhibitors).[4-6] Both the wild-type and mutants of the archetypal serpins have been reported to aggregate at elevated temperatures and under acidic conditions.[7-8] Similarly, several reports have demonstrated earlier that the native ovalbumin, upon heat-denaturation, undergoes irreversible aggregation that involves a profound conformational change from largely α-helical to β-sheet-rich structure that is reminiscent of the conformational switch that triggers amyloid formation.[9-10] Few other reports have also indicated that the acid-triggered molten-globule state of ovalbumin also tends to aggregate at a very high temperature of 80-90 °C.[11-14] However, the mechanism of amyloid aggregation as well as the organization of individual protein molecules within the supramolecular amyloid assembly are poorly understood.

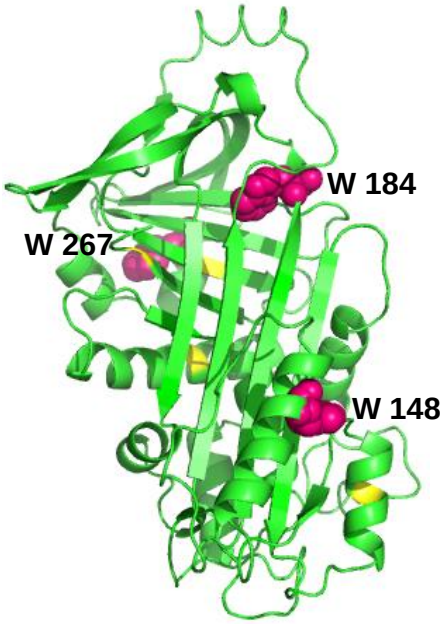

Figure 4.1

Crystal structure of ovalbumin (PDB ID: 1OVA) generated using PyMol (DeLano Scientific, LLC, CA). The tryptophans, free cystines and the single disulfide bond are shown as magenta spheres, yellow ribbons and yellow stick, respectively.

In addition to the quest of a comprehensive molecular mechanism of amyloid formation, there is a pressing need to delineate the cascade of molecular events during protein self-assembly coupled to cytotoxicity. An increasing body of evidences suggests that the oligomeric or prefibrillar intermediates are more cytotoxic compared to the matured amyloid fibrils.[15,16] Among various oligomeric structures, annular pore-based morphology is prevalent. Several hypotheses suggest that amyloid pores permeabilize cell membranes by a mechanism, conjectured to be similar to that of pore-forming bacterial toxins,[15] though other types of membrane disruption mechanisms are also proposed to be quite effective in causing neurodegeneration.[16] However, molecular insights into the transition of a soluble monomeric protein into doughnut-shaped supramolecular amyloid pores leading to nanoscopic amyloid assemblies are quite limited.

In the present study, Raman spectroscopy was employed to investigate the changes in secondary structure of the ovalbumin at the molecular level during time-dependent evolution

of the amyloid fibrils. It provides a wealth of information about both the polypeptide backbone and the amino acid residues involved in aggregation.[17] The backbone amide group markers such as amide I and amide III regions as well as a few aromatic side-chain markers such as, tryptophans and tyrosines could be monitored to probe the changes (and/or shift) in the respective band positions and intensities as a function of aggregation. The amide I (~1640-1690 cm^{-1}) band represents primarily the carbonyl (>C=O) stretching frequency that has smaller contributions from both –C-N stretching and –N-H bending frequencies whereas the amide III (~1230-1300 cm^{-1}) band corresponds to the in-phase combination of N-H in-plane bending and –C-N stretching frequencies.[18,19] Both the amide regions denote the presence of secondary structural elements such as α-helix, β-sheet and random coils. More importantly, these regions also provide information about (i) whether the β-sheet is parallel or anti-parallel and (ii) whether the cross-β-sheet-rich structure at ~1670 cm^{-1}, a potent hallmark of amyloid fibril formation, evolves as a function of aggregation.[20,21] Additionally, residue-specific information about the changes in the environment around tryptophans and tyrosines during aggregation can also be obtained.

4.2 Experimental Section

4.2.1 Materials

Ovalbumin, sodium phosphate monobasic dehydrate, glycine and salt (NaCl) were purchased from Sigma (St. Louis, MO). Solutions of protein, buffers and salt were prepared using Milli-Q water.

4.2.2 Atomic Force Microscopy

The morphology and topography of the ovalbumin aggregates were investigated using atomic force microscopy (AFM). A stock solution of ovalbumin (1 mM) was prepared in pH 7, 5 mM phosphate buffer and accurate concentration was estimated on a Chirascan CD spectrometer (Applied Photophysics, UK) using a reported molar extinction coefficient of 30,957 M^{-1} cm^{-1}.[22] Typically, a stock solution of ovalbumin was diluted 10-fold into an aggregation buffer containing 50 mM NaCl and Gly-HCl, pH 2.2 to a final protein concentration of 100 µM. The protein sample was then incubated and heated to 65±1 °C in a heating block preset at the required temperature under quiescent condition. Prior to AFM imaging, the aggregation buffer (50 mM Gly-HCl, pH 2.2) was filtered using 0.22 µm membrane filter (Millipore). Aliquots from the aggregation mixture were withdrawn at regular time intervals viz. 0 minute (before heating), 15 minutes and 4 hours (after heating) and diluted 40-100-fold using the filtered aggregation buffer. 10 µL of the diluted aggregate sample was loaded on freshly cleaved, buffer-washed muscovite mica (Grade V-4 mica from SPI, PA) and was allowed to incubate for 15-20 minutes. The AFM images were collected on

a Multiview[2000] scanning probe microscope (Nanonics Imaging, Israel) and processed using WSxM version 4 develop 11.6 software[23] available with the AFM set-up.

4.2.3 Raman spectroscopy

Sample preparation: The native ovalbumin stock solution (1 mM in pH 7, 5 mM phosphate buffer) was diluted 10-fold into an aqueous solution containing 50 mM NaCl and the pH of the resulting solution was adjusted to 2.2 at room temperature using 1 N HCl. The total protein concentration was 100 μM and the total volume of the solution was 8 mL that was concentrated further to a volume of ~800 μL (final protein concentration ~1 mM) using 10 kD cutoff AMICON filter (Millipore) prior to the collection of Raman spectra. For the 0 min sample (i.e. before heating was started), the protein solution was incubated for 30 minutes at room temperature prior to concentrating it. For all other samples at different time intervals (i.e. after heating was initiated), the freshly prepared protein solution was heated to 65 °C in a water-bath without agitation. The aggregation reaction was quenched/stopped at a desired time interval and the mixture was cooled to room temperature followed by concentrating the sample before Raman spectra were collected.

Raman spectroscopic measurements: The solution Raman spectra of the ovalbumin aggregates were collected on an inVia Raman microscope (Renishaw, UK) at ~24 ºC. 500 μL of the concentrated protein solution was taken into one of the transparent wells of a Lab-Tek chamber (Nunc, Sigma) and placed on the microscope's sample stage. A laser line of 514 nm (50 mW) from a tunable Ar^+ laser was selected as an excitation source that was focussed into the sample solution by a 50X long working distance objective (Nikon, Japan). Utmost care was taken to eliminate any possible scattering from either the inner or the outer surface of the

well. Both the Rayleigh and the Raman scattered light were collected through the inverted microscope and the incident radiation was blocked using an edge filter of 514 nm whereas the Raman scattering was passed through. The scattered light was then dispersed using a diffraction grating (1800 lines/mm) which was then collected by an air-cooled CCD detector and the spectral resolution was found to be ~ 1 cm^{-1}. All the Raman spectra were collected using Wire 3.1 software provided with the instrument. The full spectral range (400-2000 cm^{-1}) of the protein samples was averaged over 25 scans whereas the desired specific ranges (1640-1700, 1200-1300, 950-1400 and 750-950 cm^{-1}) were averaged over 100 scans with an exposure time of 30 seconds in each scan. Phenylalanine, present in the protein, was used as an internal standard which showed a Raman band at ~1003 cm^{-1}. The band at ~1003 cm^{-1} is assigned to phenyl ring breathing mode that has been reported to be insensitive to the protein conformation.[24] Similarly, the Raman spectra of the solvent background (aqueous solution containing 50 mM NaCl and pH adjusted to 2.2) were collected at all the spectral ranges mentioned above under the same conditions with identical number of scans as used for the samples. The averaged sample and solvent spectra were corrected separately for the observed baseline tilt using cubic spline interpolation method (available in the Wire 3.1 software). Following the baseline corrections, the sample spectra were further corrected by subtracting the respective solvent spectra (baseline corrected) to remove any Raman contribution from the solvent. The resultant protein aggregate spectra were also smoothened using the Wire 3.1 software. The same procedure was applied for collecting the Raman spectrum of the native ovalbumin whereby both the sample and the solvent spectra, devoid of any NaCl, were recorded in an aqueous solution with pH adjusted to 7. The final Raman spectra of the native and the aggregated protein were also plotted later using the Origin Pro version 8.5 software.

Deconvolution of the Raman spectra: Changes in the secondary structural content were estimated by deconvoluting and analyzing the amide peaks obtained in the desired spectral ranges that were collected from 1640-1700 (amide I) and 1200-1300 (amide III) cm^{-1}. The deconvolutions were carried out using the peak analyzer option (listed in the peak and baseline analysis) available in the Origin Pro version 8.5 software and the amide regions (amide I and III) were fitted by at least four component bands representing major structural components viz. (i) α-helix (1645-1654 cm^{-1} and 1264-1272 cm^{-1} & 1300 cm^{-1}), β-sheet (1665-1674 cm^{-1} and 1230-1240 cm^{-1}), random coil (1660-1665 cm^{-1} and 1245-1255 cm^{-1}) and extended (1680-1690 cm^{-1}) conformations. Fitting was carried out using the Levenberg-Marquadt non-linear least squares method to obtain multiple fitted Gaussian curves whose bandwidth (FWHM) varied between 12-40 cm^{-1} and the fitting parameters were kept variable in order to prevent any bias during the fitting procedure. The standard errors in the analyses for peak positions and peak widths are ≤3 cm^{-1} and ≤5 cm^{-1}, respectively. The percentage contents of various secondary structural elements (with respect to the cumulative peak fit with a total area of 100%) were obtained during the fitting analysis.

Protocol for Solution Raman Spectroscopy of amyloids

- Sample: ~ 1 mM homogeneous
- Solvent: water (pH adjusted to desired value)
- Sample holder: Labtek chambers (low scattering)
- LASER: 514 nm (no interference from fluorescence)
- Laser spot focus: Avoid scattering from surface or liquid-air interface
- Acquisitions: 25-100 scans for 30 sec each (better signal to noise ratio)
- Baseline Correction: to remove any tilt in the spectrum
- Background Correction: same set of experiment without protein
- Data analysis: Deconvolution of amide regions

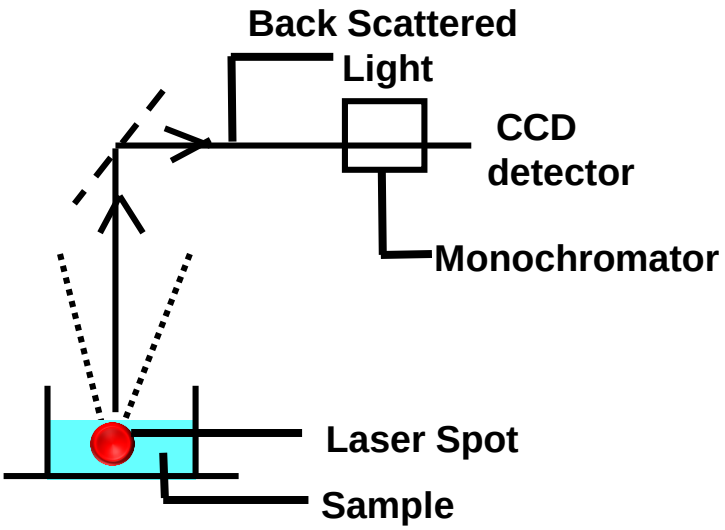

Schematic for data collection for solution Raman spectroscopy

4.3 Results

4.3.1 Structural characteristics of ovalbumin aggregates revealed by AFM

Prior to embarking on the Raman spectroscopic investigation of ovalbumin aggregation, efforts were directed to ascertain whether the molten globule state (previously characterized)[25] can form amyloid aggregates under suitable *in vitro* conditions. The aggregation reaction was triggered by incubating ovalbumin at pH 2.2 and 65 ºC in the presence of 50 mM NaCl. Before the sample was incubated, spherical oligomeric aggregates were observed (Figure 4.2a) that revealed a height distribution centered at ~3.5 nm. Upon thermal incubation, the nanoscale morphology of the sample (after 15 min) showed a heterogeneous distribution predominated by the presence of annular pore-like aggregates (height: 20-40 nm) in addition to worm-like structures (height: 10-15 nm; Figure 4.2a). The average diameter of the pores was ~50 nm (54±9 nm). Upon prolonged incubation, the proportion and the dimensions of these annular pores increased further (Figure 4.2a) and the topographical distribution reflected an average height of ~50−60 nm, whereas the proportion of aggregates with height of ~10 nm reduced by ~50%. Therefore, AFM images of the overall assembly process revealed that the spherical oligomers, formed at room temperature, associate to form both small annular pores and worm-like fibrils (upon heating) that served as templates for further nanoscale assembly of annular pores (Figure 4.2a) into higher-order supramolecular amyloid pores that remained soluble even for several days. The morphological changes observed by AFM prompted us to delineate the protein structural changes at the molecular level.

4.3.2 Raman Spectroscopy: Conformational fingerprints of the aggregates

Raman spectroscopy was employed to investigate ovalbumin conformational changes during the course of aggregation. Figure 4.2b (i) shows the Raman spectrum of the native ovalbumin which corroborated well with that reported earlier.[26,27] Deconvolution of the spectrum followed by percentage analysis yielded the secondary structural contents that agreed well with that extracted from the respective CD spectrum.[25] The Raman spectrum of the oligomers was recorded under the identical conditions (Figure 4.2b (ii)). Analysis of the amide I and III regions of the oligomeric species indicated a small but significant decrease in the α-helical and β-sheet contents whereas an increase in the random-coil content was observed as expected. Following this observation, the sample was heated at 65 °C to trigger the aggregation process which was subsequently monitored by Raman spectroscopy. Figures 4.2b (iii) and (iv) show the representative spectra of ovalbumin aggregates obtained after 15 minutes and 4 hours of heating. In all the cases, a peak/shoulder at ~1208 cm^{-1} was observed due to the aromatic ring vibrations of the tryptophans, tyrosines and phenylalanines.[17,18] Moreover, a progressive decrease in the band intensity at 935 cm^{-1} (due to α-helix backbone) was observed as a function of aggregation that confirmed the reduction in α-helical content.[18] A careful look at all the spectra revealed that upon heating, the peak maximum of the amide I band shifted from ~1666 cm^{-1} (observed in both the native and molten-globule-oligomers of ovalbumin) to ~1670 cm^{-1} suggestive of the formation of cross-β-sheet-rich amyloid aggregates as a function of time (Figure 4.2b inset). Also, the amide I band which was initially broad, became sharper after 4 hours of heating. Deconvolution (Figure 4.3c) and percentage analysis of the amide I region suggested a decrease in both the α-helical (reduced further) and random-coil contents in the amyloid aggregates as compared to the oligomers.

On the contrary, the β-sheet content which decreased in the molten-globule-oligomers, increased upon heating as aggregation progressed thus, supporting the evolution of Raman band at ~1670 cm^{-1}. Next, similar careful consideration was given for the amide III Raman band analysis. The amide III band, that appeared broad initially, became sharper during the course of aggregation, similar to that observed for the amide I band. Analysis of the amide III region (Figure 4.2d) corroborated the same trend; an increase in β-sheet content was observed while both the α-helical and random-coil contents decreased. Additionally, the band at ~1240 cm^{-1} gained prominence and became sharper indicating the rearrangement of β-strands into anti-parallel β-sheets similar to that observed in heat-denatured ovalbumin aggregates at pH 7[26] and insulin filaments.[28] Therefore, combining the results obtained from the analysis of amide I and III regions, we propose that the ovalbumin aggregation proceeds via loss in the secondary structural content with a concomitant increase in random-coil structure which eventually leads to the formation of cross-β-sheet-rich amyloid aggregates that constitute anti-parallel β-sheets in the amyloid core.

Another remarkable aspect related to the amide region is that the value of Ramachandran ψ dihedral angle of the amyloid aggregates could be estimated from the amide III Raman band (at ~1240 cm^{-1}) representing the anti-parallel β-sheets.[29] It has been demonstrated earlier that the amide III frequency is extremely sensitive to the peptide bond conformation and exhibits strong ψ dihedral angle dependence whereas the dependence on Ramachandran ϕ dihedral angle is moderate.[30] Additionally, the "conformational sensitivity" of the amide III frequency depends on the extent of coupling between the N-H and $C-C^{\alpha}-H$ bending modes. A strong coupling in a β-strand is observed due to an approximate cis-

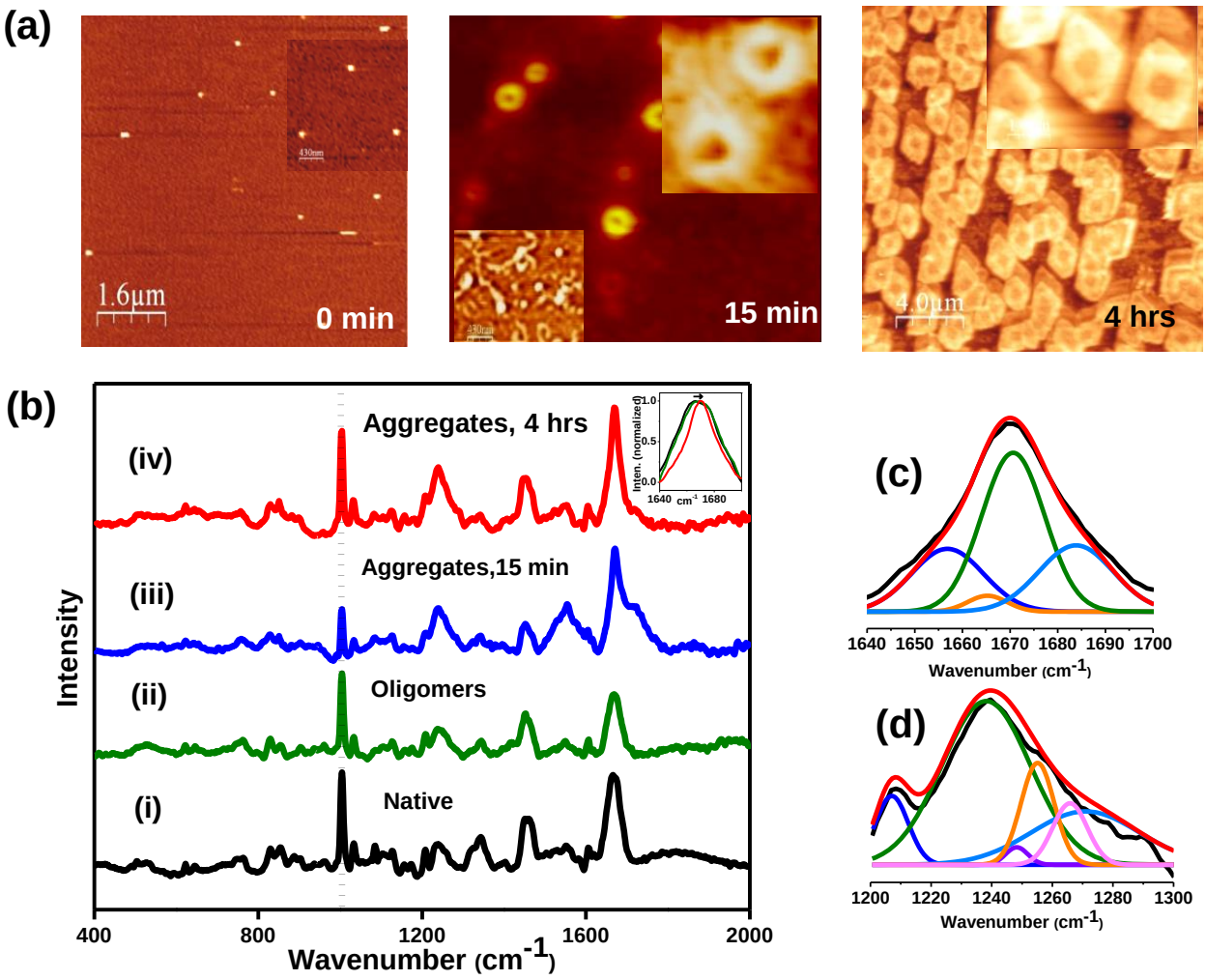

Figure 4.2 (a) AFM images of aggregates at different time points (b) Solution Raman spectra of ovalbumin in the (i) native form (black solid line) at pH 7 and (ii-iv) aggregates formed at pH 2.2 (green, blue and red solid lines for 0 minute, 15 minutes and 4 hour, respectively) as a function of time. The peak observed at ~1003 cm^{-1} due to phenylalanine present in the protein was taken as an internal standard (black short dotted line). The inset graph shows the shift of amide I band from ~1666 cm^{-1} to ~1670 cm^{-1} (depicted by an arrow) indicating the evolution of cross β-sheet structure during ovalbumin amyloid assembly. Gaussian deconvolution of the (c) amide I and (d) amide III regions, collected after 4 hours of heating, to analyze the percentage composition of various secondary structures. The black and the red solid lines, in both the spectra (c,d) represent the actual data and the cumulative fit, respectively. The other colored solid lines represent the Gaussian peaks obtained after deconvolutions.

geometry of the N-H and C-H bonds whereas the coupling disappears in an α-helix conformer due to the trans geometry.[31] Using the following equation: $\nu_{\text{Amide III}}(\psi) = \{1239\ \text{cm}^{-1} - 54\ \text{cm}^{-1} \sin(\psi+26°)\}$,[31,32] the average Ramachandran ψ dihedral angle for the ovalbumin amyloid aggregates was determined to be ~ +135° that agrees well with the results obtained for amyloid fibrils derived from Alzheimer's Aβ peptide.[32]

After the backbone conformational analysis, efforts were directed towards extracting information about the possible orientation and environment around the aromatic side-chain markers such as tyrosines and tryptophans. It is known that tyrosine exhibits two bands at ~830 and ~850 cm^{-1} that are designated as Fermi doublet arising out of the vibrational mode of the benzene ring.[17,18] The ratio of intensities at 850 to 830 cm^{-1} denoted as I_{850}/I_{830}, serves as an indicator of the hydrogen bonding strength between the phenolic hydroxyl moiety (of tyrosine) and the solvent molecules.[18,33] It has been reported that the tyrosine band at ~850 cm^{-1} might shift to ~855 cm^{-1} depending on the protein's environment.[33] In our case, we observed the tyrosine doublet at ~829 and ~855 cm^{-1} at all the stages namely, native, oligomeric and aggregated ovalbumin. Ratio analysis (I_{855}/I_{829}) followed by a comparison suggested that the hydrogen bonding strength between the phenolic hydroxyl and the surrounding water molecules varied from strong (1.7 in the native) to moderate (1.0 in the aggregated species). However, we must emphasize that the nature of hydrogen bonding mentioned here is an average estimate since ovalbumin contains ten tyrosines.[33] We can only infer that the tyrosines became partially buried and formed transient hydrogen bonds with the aqueous surroundings[34] as aggregation progressed, which was reflected in the diminution of the average hydrogen bonding strength.

Another aromatic amino acid that is used as an important Raman conformational marker is tryptophan. It is well-documented that like tyrosine, tryptophan also exhibits a Fermi doublet at ~1340 and ~1360 cm^{-1}.[17,18] The ratio of band intensities at 1360 to 1340 denoted as I_{1360}/I_{1340} is a measure of strong hydrophobic interactions between the indole ring (of tryptophan) and the neighbouring aliphatic groups.[35,36] In our study, we observed a continuous increase in the I_{1360}/I_{1340} ratio as we moved from the native (0.3) to the aggregated states (1.0) thus indicating an increase in the average hydrophobicity of the environment around the tryptophans. Similar sequestration of tryptophans has been commonly observed in the amyloid fibrils formed from other globular proteins.[37] Here again, we mention an average hydrophobic environment since ovalbumin contains three tryptophan residues. Additionally, tryptophan exhibits another Raman band at ~880 cm^{-1} that is assigned to the hydrogen bonding strength between the –N-H of the indole ring and the surrounding solvent molecules.[18] It has been shown that this band at ~880 cm^{-1} shifts to ~871 cm^{-1} if the hydrogen bonding is quite strong whereas a lack of any hydrogen bond shifts the band to ~883 cm^{-1}.[18,36,38] A careful scrutiny of the band position was carried out for all the states of ovalbumin. For native ovalbumin, the band appeared at ~877 cm^{-1} indicative of moderately strong hydrogen bonds which is in accordance with its crystal structure.[1] On the other hand, the oligomeric species revealed two bands at ~877 and ~886 cm^{-1} suggesting that at least one of the three tryptophans forms moderately strong hydrogen bonds with its neighbouring water molecules.[38] Interestingly, both the aggregated species formed after 15 minutes and 4 hours of heating exhibited Raman band at ~881 cm^{-1} thus, indicating the absence of any hydrogen bonds. This also implied that the tryptophans get progressively buried which renders the

indole group inaccessible to form hydrogen bonds with the water molecules, hence corroborating the results obtained from the I_{1360}/I_{1340} ratio.

We also observed an additional Raman band of tryptophan at ~1550 (native and oligomeric states) and ~1553 cm^{-1} (aggregated species). It has been suggested and shown earlier that the occurrence of tryptophanyl indole ring vibrational band at ~1550 cm^{-1} is a measure of an absolute value of the $C_\alpha C_\beta$-C_2C_3 torsion angle ($|\chi^{2,1}|$) that is observed strongly when a visible light is used as an excitation source (514 nm used in our study).[39] The band position can vary between ~1542-1557 cm^{-1} depending on the protein's environment and such variation results in a range of torsional angles ($|\chi^{2,1}|$ range: 60º-120º) owing to the varying orientation of the indole ring with respect to the polypeptide backbone.[39] Therefore, according to our study, the average absolute value of the torsional angle was estimated to be ~95° (in the native and oligomeric state) that increased to ~100° during the amyloid aggregation of ovalbumin.

4.4 Discussion

In the present work, we have demonstrated that the predominantly α-helical molten-globule state of ovalbumin undergoes a profound conformational rearrangement, presumably by a previously described mechanism,[40] and self-associates in a stepwise manner to form cross β-rich amyloid pores. These nanoscopic pores further serve as templates for the genesis of higher order supra-molecular pores. However, we cannot completely eliminate the possibility of dissociation of pores and worm-like fibrils which can serve as templates for monomers to generate fibrils. Additionally, Raman spectra distinctly revealed the presence of

antiparallel β-sheets in the amyloid core of ovalbumin, similar to that observed in heat-denatured ovalbumin aggregates at pH 7[26] and insulin filaments.[28] These data are in accordance with the FTIR spectra of ovalbumin fibrils, formed at neutral pH, whereby FTIR bands of β-sheets at 1625 and 1680 cm^{-1} were observed and confirmed to be different than that present in the native ovalbumin.[41] Therefore, the overall process of ovalbumin aggregation suggests a profound conformational change in the molten-globule oligomers involving an initial loss in the α-helical and β-sheet contents with a concurrent gain in the random-coil structure that eventually undergoes a conformational switch from predominantly α-helical to β-sheet-rich amyloid annular pores.

In many instances of protein aggregation and amyloid assembly, it has been demonstrated that both electrostatic and hydrophobic interactions play a very vital role in promoting aggregation.[42-44] Ovalbumin has an isoelectric point of ~ 4.5[2] which acquires a net charge of + 43 at pH 2.2.[45] At higher protein concentration and upon thermal incubation, addition of salt screens the electrostatic repulsions between the positively charged polypeptide chains and favours hydrophobic association of the thermally-unfolded regions. Previous studies on ovalbumin aggregation at neutral pH have proposed that the exposure of hydrophobic surfaces and formation of intermolecular disulfide bonds drive the aggregation forward.[9] We believe that the aggregation of ovalbumin at low pH (in the present study) does not involve the formation of intermolecular disulfide linkages[46] that has been suggested earlier.[9] The evidence favouring an increase in hydrophobicity was also provided by the Raman spectra of aggregates that showed an increase in the tryptophan hydrophobicity ratio (I_{1360}/I_{1340}) that has been commonly observed in the amyloid fibrils formed from other globular proteins.[37] Therefore, the Raman hydrophobicity ratio pertaining to tryptophan

suggests that the tryptophans get progressively buried into the hydrophobic regions of the ovalbumin aggregates. The possible sequestration of tryptophans was also validated by an average reduction in the hydrogen bonding strength of tryptophanyl indole ring with the neighbouring water molecules as indicated by the Raman spectra. Additionally, the tyrosines also get partially buried into the ovalbumin aggregates as depicted by the moderate hydrogen bonding strength revealed by the Raman spectra. Taken together, ovalbumin aggregation involves sequestration of the tryptophans and possibly, tyrosines into the hydrophobic cross-β amyloid core during the supramolecular assembly of amyloid annular pores.

4.5 Conclusion

In summary, we have shown that ovalbumin, a model non-inhibitory serpin, forms β-sheet-rich nanoscopic amyloid annular pores at low pH mediated by non-covalent interactions. Additionally, an in-depth insight into the protein secondary structural changes at the molecular level was obtained by Raman spectroscopy that revealed the formation of cross β-sheet-rich amyloid aggregates while tryptophans and tyrosines get sequestered into the amyloid core comprising antiparallel β-sheets.

4.6 References

1. Stein, PE .; Leslie, A. G. W.; Finch, J. T.; Carrell, R. W. (1991) Crystal structure of uncleaved ovalbumin at l.95 Å resolution. *J. Mol. Biol.* 221:941-959.

2. Donnell, E.R.-O. (1993) The ovalbumin family of serpin proteins. *FEBS Letts.* 315:105-108.

3. Mine, Y. (1995) Recent advances in the understanding of egg white protein functionality. *Trends Food Sci. Tech.* 6:225-232.

4. Gooptu, B.; Lomas, D. A. (2009) Conformational pathology of the serpins: themes, variations and therapeutic strategies. *Annu. Rev. Biochem.* 78:147-176.

5. Knaupp, A. S.; Bottomley, S. P. (2009) Serpin polymerization and its role in disease-the molecular basis of α1-antitrypsin deficiency *IUBMB Life* 61:1-5.

6. Kaiserman, D.; Whisstock, J. C.; Bird, P. I. (2006) Mechanisms of serpin dysfunction in disease. *Expert Rev. Mol. Med.* 8:1-19.

7. Dafforn, T. R.; Mahadeva, R.; Elliott, P. R.; Sivasothy, P.; Lomas, D. A. (1999) A kinetic mechanism for the polymerization of α1-antitrypsin. *J. Biol. Chem.* 274:9548-9555.

8. Ricagno, S.; Pezzullo, M.; Barbiroli, A.; Manno, M.; Levantino, M.; Santangelo, M.G.; Bonomi, F.; Bolognesi, M. (2010) Two latent and two hyperstable polymeric forms of human neuroserpin. *Biophys. J.* 99:3402-3411.

9. Sun, Y.; Hayakawa, S. (2002) Heat-induced gels of egg white/ovalbumins from five avian species: thermal aggregation, molecular forces involved and rheological properties. *J. Agric. Food Chem.* 50:1636-1642.

10. Weijers, M.; Barneveld, P. A.; Stuart, M. A. C.; Visschers, R. W. (2003) Heat-induced denaturation and aggregation of ovalbumin at neutral pH described by irreversible first-order kinetics. *Protein Sci.* 12:2693-2703.

11. Azakami, H.; Mukai, A.; Kato, A. (2005) Role of amyloid type cross β-structure in the formation of soluble aggregate and gel in heat-induced ovalbumin. *J. Agric. Food Chem.* 53:1254-1257.

12. Tani, F.; Murata, M.; Higasa, T.; Goto, M.; Kitabatake, N.; Doi, E. (1995) Molten globule state of protein molecules in heat-induced transparent food gels. *J. Agric. Food Chem.* 43:2325-2331.

13. Hu, H. Y.; Du, H .N. (2000) α-to-β structural transformation of ovalbumin: heat and pH effects. *J. Protein Chem.* 19:177-183.

14. Alting, A. C.; Weijers, M.; de Hoog, E. H. A.; van de Pijpekamp, A. M.; Stuart, M. A. C.; Hamer, R. J.; de Kruif, C. G.; Visshchers, R. W. (2004) Acid-induced cold gelation of globular proteins: effects of protein aggregate characteristics and disulfide bonding on rheological properties. *J. Agric. Food Chem.* 52:623-631.

15. Lashuel, H. A.; Lansbury Jr., P. T. (2006) Are amyloid diseases caused by protein aggregates that mimic bacterial pore-forming toxins? *Q. Rev. Biophys.* 39:167-201.

16. Butterfield, S. M.; Lashuel, H. A. (2010) Amyloidogenic protein-membrane interactions: mechanistic insight from model systems. *Angew. Chem. Int. Ed.* 49:5628-54.

17. Tuma, R. (2005) Raman spectroscopy of proteins: from peptides to large assemblies. *J. Raman Spectrosc.* 36:307-319.

18. Němeček, D.; Thomas Jr. G. J. (2009) Handbook of Molecular Biophysics; Bohr, H.G. Ed.; Wiley-VCH Verlag: Weinhem.

19. Oladepo, S. A.; Xiong, K.; Hong, Z.; Asher, S. A.; Handen, J.; Lednev, I. K. (2012) UV resonance Raman investigations of peptide and protein structure and dynamics. *Chem. Rev.* 112:2604-2628.

20. Carrotta, R.; Vetri, V.; Librizzi, F.; Matrorana, V.; Militello, V.; Leone, M. (2011) Amyloid fibrils formation of concanavalin A at basic pH. *J. Phys. Chem. B* 115:2691-2698.

21. Mason, B. D.; Schoneich, C.; Kerwin, B. A. (2012) Effect of pH and light on aggregation and conformation of an IgG1 mAb. *Mol. Pharm.* 9:774-790.

22. Naeem, A.; Khan, T. A.; Muzaffar, M.; Ahmad, S.; Saleemuddin, M. (2011) A partially folded state of ovalbumin at low pH tends to aggregate. *Cell Biochem. Biophys.* 59:29-38.

23. Horcas, I.; Fernández, R.; Gómez-Rodríguez, J. M.; Colchero, J.; Gómez-Herrero, J.; Baro, A. M. (2007) WSxM: A software for scanning probe microscopy and a tool for nanotechnology. *Rev. Sci. Instrum.* 78:013705.

24. Krafft, C.; Hinrichs, W.; Orth, P.; Saenger, W.; Welfle, H. (1998) Interaction of Tet repressor with operator DNA and with tetracycline studied by Infrared and Raman spectroscopy. *Biophys. J.* 74:63-71.

25. Bhattacharya, M.; Mukhopadhyay, S. (2012) Structural and dynamical insights into the molten-globule form of ovalbumin. *J. Phys. Chem. B* 116:520-531.

26. Painter, P. C.; Koenig, J. L. (1976) Raman spectroscopic study of the proteins of egg white. *Biopolymers* 15:2155-2166.

27. Koenig, J. L.; Frushour, B. G. (1972) Raman scattering of chymotrypsinogen A, ribonuclease, and ovalbumin in the aqueous solution and solid state. *Biopolymers* 11:2505-2520.

28. Zako, T.; Sakono, M.; Hashimoto, N.; Ihara, M.; Maeda, M. (2009) Bovine insulin filaments induced by reducing disulfide bonds show a different morphology, secondary structure, and cell toxicity from intact insulin amyloid fibrils. *Biophys. J.* 96:3331-3340.

29. Shashilov, V.A.; Sikirzhytski, V.; Popova, L.A.; Lednev, I.K. (2010) Quantitative methods for structural characterization of proteins based on deep UV resonance Raman spectroscopy. *Methods* 52:23-37.

30. Asher, S. A.; Ianoul, A.; Mix, G.; Boyden, M. N.; Karnoup, A.; Diem, M.; Schweitzer-Stenner, R. (2001) Dihedral ψ angle dependence of the amide III vibration: a uniquely sensitive UV resonance Raman secondary structural probe. *J. Am. Chem. Soc.* 123:11775-11781.

31. Mikhonin, A. V.; Bykov, S. V.; Myshakina, N. S.; Asher, S. A. (2006) Peptide secondary structure folding reaction coordinate: correlation between UV Raman amide III frequency, ψ Ramachandran angle, and hydrogen bonding. *J. Phys. Chem. B* 110:1928-1943.

32. Popova, L. A.; Kodali, R.; Wetzel, R.; Lednev, I. K. Structural variations in the cross-β core of amyloid β fibrils revealed by deep UV resonance Raman spectroscopy. *J. Am. Chem. Soc.* 132:6324-6328.

33. Siamwiza, M. N.; Lord, R. C.; Chen, M. C.; Takamatsu, T.; Harada, I.; Matsuura, H.; Shimanouchi, T. (1975) Interpretation of the doublet at 850 and 830 cm^{-1} in the Raman spectra of tyrosyl residues in proteins and certain model compounds. *Biochemistry* 14:4870-4876.

34. Wang, Y.; Petty, S.; Trojanowski, A.; Knee, K.; Goulet, D.; Mukerji, I.; King, J. (2010) Formation of amyloid fibrils in vitro from partially unfolded intermediates of human γC-crystallin. *Invest. Ophthalmol. Visual Sci.* 51:672-678.

35. Chen, M. C.; Lord, R. C.; Mendelsohn, R. (1973) Laser-Excited Raman spectroscopy of biomolecules IV. Thermal denaturation of aqueous lysozyme. *Biochim. Biophys. Acta* 328:252-260.

36. Miura, T.; Takeuchi, H.; Harada, I. (1988) Characterization of individual tryptophan side chains in proteins using Raman spectroscopy and hydrogen-deuterium exchange kinetics. *Biochemistry* 27:88-94.

37. Hiramatsu, H.; Lu, M.; Matsuo, K.; Gekko, K.; Goto, Y.; Kitagawa, T. (2010) Differences in the molecular structure of β2-Microglobulin between two morphologically different amyloid fibrils. *Biochemistry* 49:742-751.

38. Li, T.; Chen, Z.; Johnson, J. E.; Thomas, G. J., Jr. (1990) Structural studies of bean pod mottle virus, capsid, and RNA in crystal and solution states by laser Raman spectroscopy. *Biochemistry* 29:5018-5026.

39. Miura, T.; Takeuchi, H.; Harada, I. Tryptophan Raman bands sensitive to hydrogen bonding and side-chain conformation. *J. Raman Spectrosc.* **1989**, *20*, 667-671.

40. Bhattacharya, M.; Jain, N.; Mukhopadhyay, S. (2011) Insights into the mechanism of aggregation and fibril formation from bovine serum albumin. *J. Phys. Chem. B* 115:4195-4205.

41. Tanaka, N.; Morimoto, Y.; Noguchi, Y.; Tada, T.; Waku, T.; Kunugi, S.; Morii, T.; Lee, Y.-F.; Konno, T.; Takahashi, N. (2011) The mechanism of fibril formation of a non-inhibitory serpin ovalbumin revealed by the identification of amyloidogenic core regions. *J. Biol. Chem.* 286:5884-5894.

42. Morel, B.; Varela, L.; Azuaga, A. I.; Conejero-Lara, F. (2010) Environmental conditions affect the kinetics of nucleation of amyloid fibrils and determine their morphology. *Biophys. J.* 99:3801-3810.

43. Hill, S. E.; Miti, T.; Richmond, T.; Muschol, M. (2011) Spatial extent of charge repulsion regulates assembly pathways for lysozyme amyloid fibrils. *PLoS One 6:*e18171.

44. Juarez, J.; Lopez, S. G.; Cambon, A.; Taboada, P.; Mosquera, V. (2009) Influence of electrostatic interactions on the fibrillation process of human serum albumin *J. Phys. Chem. B* 113:10521-10529.

45. Putnam C. Protein Calculator version 3.3 http://www.scripps.edu/cgi-bin/cdputnam/protcalc3.

46. If the networks comprising extensive disulfide crosslinks were formed prior to and during aggregation, it is expected that the Raman band corresponding to disulfide bond at ~510 cm^{-1} would be visible and become prominent as a function of aggregation. However, no such band was observed during the entire course of ovalbumin aggregation.

Chapter 5

Chain Collapse of an Amyloidogenic Intrinsically Disordered Protein

This work has been published in *Biophysical Journal*

Reference: **N. Jain**, M. Bhattacharya and S. Mukhopadhyay. Chain collapse of an myloidogenic intrinsically disordered protein. *Biophys. J.* **2011**, *101*, 1720-1729.

5.1 Introduction

Intrinsically disordered proteins (IDPs) confront the conventional sequence-structure-function paradigm owing to their structural attributes, which are in contrast to the uniquely folded globular proteins.[1-4] Bioinformatic analyses have indicated that over 30% of eukaryotic proteins are disordered.[1-5] It has been documented that despite being devoid of a well-defined, ordered 3D structure, IDPs carry out important cellular functions such as molecular recognition, replication, signaling etc.[3,6-8] Comparison between the amino acid compositions of IDPs and globular proteins has revealed that the sequence and frequent occurrence of disorder- promoting amino acid residues with high flexibility index, low hydrophobicity, and high net charge are accountable for the conformational plasticity observed in IDPs. Also, IDPs can be empirically sub-classified into pre-molten globule, structured molten globule, collapsed disordered ensemble and extended disordered ensemble which undergo non-cooperative conformational transitions.[1-8] Such inherent structural randomness and conformational heterogeneity pose a major bottleneck in the structural characterization of the IDPs by X-ray crystallography, which has been one of the primary techniques used to elucidate high resolution structure of biomolecules. However, nuclear magnetic resonance[9,10], circular dichroism[3,4,11], vibrational[12, 13] and fluorescence spectroscopic studies[3, 14-16] have yielded important structural insights into the dynamic ensembles of the IDPs. Recent single-molecule fluorescence experiments have revealed the dynamic conformational behavior of IDPs that have intrinsic property to undergo chain collapse.[17-19]

Recent structural investigations of IDPs have gained tremendous importance in amyloid research, since most (misfolded) amyloidogenic proteins adopt a disordered state in their monomeric form, either continuously or transiently, prior to oligomerization and amyloid formation that is implicated in a variety of neurodegenerative disorders.[8,20,21] These proteins

include amyloid-β (Alzheimer's), α-synuclein (Parkinson's), polyglutamine (Huntington's), N-terminal disordered segment of prion proteins (mad cow and transmissible spongiform encephalopathy) and functional amyloid proteins such as yeast prion proteins[22,23] and pMel[24] that are unrelated to disease. Some of these amyloidogenic IDPs have been theoretically predicted, and experimentally demonstrated, to undergo a reversible chain collapse from an extended form in good solvents (denaturant) to compact form in poor solvents (water).[17,25,27] The chain collapse phenomenon of IDPs in water is observed when the favorable interaction between (intramolecular) chain and chain is stronger than that between chain and solvent at an infinitely dilute protein solution in water.[25-28] An unstructured collapsed globule ensues when the intrachain interactions are favourable, with a concomitant gain in the solvent entropy due to poor chain solvation. At higher protein concentrations, the chain-chain interactions between collapsed, yet disordered, protein molecules can promote intermolecular association leading to unstructured oligomers that conformationally mature into ordered amyloid fibrils.[25]

In the following work, we used bovine κ-casein as a readily available archetypal IDP that has been previously shown to assemble into amyloid fibrils under carefully controlled laboratory conditions.[29-31] Based on the bioinformatic predictions and a variety of spectroscopic tools, we first established that κ-casein undergoes a chain collapse under the native condition and then demonstrated that the excimer formation from κ-casein covalently-labeled with two pyrene moieties can be utilized as a simple, convenient, and elegant approach to study the chain collapse of an amyloidogenic IDP under both equilibrium and kinetic conditions.

5.2 Experimental Section

5.2.1 Materials

Bovine κ–casein, guanidinium chloride, urea, dithiothreitol (DTT), iodoacetic acid, ANS (8-anilinonaphthalene-1-sulfonic acid ammonium salt), acrylamide, sodium phosphate (monobasic and dibasic), potassium chloride, sodium citrate and Tris-HCl were procured from Sigma (St. Louis, MO) and used without any further purification. N-(1-Pyrene) maleimide and 5-((2-((iodoacetyl)amino)ethyl)amino)naphthalene-1-sulfonic acid (IAEDANS) were purchased from Molecular Probes (Eugene, OR) and DMSO (dimethylsulfoxide) was obtained from Merck and used as received. Milli-Q water (Millipore, Billercia, MA) was used for the preparation of buffers and other aqueous solutions. The pH of the buffers was checked and adjusted using 1 N HCl or NaOH on Metrohm (Herisau, Switzerland) 827 pH meter at ~24 °C.

5.2.2 Monomerization of κ-casein

To prepare monomeric κ-casein (reduced and carboxymethylated: RCM), a previously described procedure[31] was used with slight modifications. Briefly, 1 mM κ-casein solution was prepared in 6 M GdmCl (pH 8, 100 mM Tris-Cl), to which 10 mM DTT was added. To ensure complete reduction (cleavage of intra- and interdisulfide linkages) and denaturation, the reaction mixture was stirred for one hour at 37 °C at a speed of 45 rpm. Next, 50 mM iodoacetic acid (freshly prepared in DMSO) was added into the reaction mixture to react with the thiol groups of the resulting free cysteines, and the mixture was further stirred for another 30 min. After the reaction was complete, traces of free iodoacetic acid were removed and the protein was

concentrated using AMICON YM-10 (10 kDa cut-off; Millipore) by washing it extensively with 6 M GdmCl (pH 7, 50 mM phosphate buffer). Accurate concentration of RCM κ-casein was determined by measuring the tryptophan absorbance at 280 nm by UV-Vis spectrophotometer (Perkin Elmer, Waltham, MA) using molar extinction coefficient of 11,500 $M^{-1}cm^{-1}$.[31] RCM κ-casein was prepared freshly before each spectroscopic measurement.

5.2.3 Fluorescence experiments with RCM κ-casein under denatured and native conditions

Freshly prepared RCM κ-casein (6 M GdmCl, pH 7) was incubated separately in (a) 8 M urea solution prepared in 5mM phosphate buffer, pH 7, to form urea-denatured RCM κ-casein**;** (b) 5 mM KCl-HCl, pH 1.6, to form acid-denatured protein; and (c) 5 mM phosphate buffer, pH 7 (native), to a final protein concentration of 20 μM each for an hour at room temperature after which the Trp fluorescence intensity and anisotropy of denatured and native κ-casein were measured.

5.2.4 Fluorescence quenching experiments with RCM κ-casein

To carry out the tryptophan quenching experiments, a stock of 2 M acrylamide was prepared in three sets at pH 7, 5 mM phosphate buffer; pH 1.6, 5 mM KCl-HCl; and 8 M urea prepared in 5 mM phosphate buffer, pH 7. Stock of 1 mM RCM κ-casein (6 M GdmCl, pH 7) was diluted in different concentrations of acrylamide (0-500 mM) to get a final protein concentration of 20 μM at room temperature and the tryptophan fluorescence intensity was recorded as a function of acrylamide concentration under native (pH 7) and denatured (acid- and urea) conditions. The quenching graphs were plotted using OriginPro software, version 8, and fitted using the linear regression equation to estimate the Stern-Volmer constant. The

accessibility of tryptophan was determined by using Stern-Volmer equation: $F_0/F = 1 + K_{sv}$ where F_0 and F are the tryptophan fluorescence intensity in the absence and presence of quencher, respectively, and K_{sv} is the Stern-Volmer quenching constant.

5.2.5 Fluorescence labeling of κ-casein with IAEDANS

The labeling of the free thiol groups of two cysteines in denatured and reduced κ-casein was carried out in pH 7, 50 mM phosphate buffer, pH 7. Initially, 1 mM κ-casein solution was prepared in 6 M GdmCl (50 mM phosphate buffer, pH 7), to which an aqueous solution of 10 mM DTT was added. The resulting solution was stirred for one hour at 37 °C at a speed of 45 rpm. Approximately 50 equivalents of IAEDANS, dissolved in dry DMSO, was added into the reduced κ-casein solution and the reaction mixture was stirred again for an hour at 37 °C. After the labeling reaction was complete, the labeled protein was purified and concentrated using AMICON YM-10 whereby the free, unreacted dye was removed. The concentrated protein was diluted in 6 M GdmCl (50 mM phosphate buffer, pH 7), and its concentration was checked by measuring the absorbance at both 280 (tryptophan) and 337 nm (AEDANS). The concentration of the labeled protein was determined by subtracting the absorption contribution of AEDANS at 280 nm. The molar extinction coefficients of IAEDANS at 280 nm and 337 nm are 1060 $M^{-1}cm^{-1}$ [32] and 6100 $M^{-1}cm^{-1}$ [33], respectively.

5.2.6 Fluorescence labeling of κ-casein with N-(1-Pyrene) maleimide

Two cysteines in denatured and reduced κ-casein were covalently labeled by pyrene maleimide, a thiol-reactive probe, using a literature protocol[34] with slight modifications. Briefly, to a solution of chemically denatured κ-casein (1 mM prepared in 6 M GdmCl, pH 7, 50 mM

phosphate buffer), an aqueous solution of 5 mM DTT was added. The reaction was allowed to stir for one hour at 37 °C at a speed of 45 rpm. After one hour, 50 mM pyrene maleimide (freshly dissolved in DMSO) was added into the reaction mixture and stirred for another three hours at 37 °C. Once the reaction was complete, the free dye was removed by washing the reaction mixture exhaustively with 6 M GdmCl (50 mM phosphate, pH 7) using AMICON YM-10. The absorbance of filtrates and concentrated labeled protein were measured as a ratio at 280 nm and 340 nm for pyrene-labeled κ-casein. The degree of labeling was determined using molar extinction coefficient of 40,000 $M^{-1}cm^{-1}$ for pyrene at 340 nm.[35]

5.2.7 Fluorescence experiments with labeled κ-casein under denatured and native conditions

For experiments under urea-denatured conditions, a stock solution of urea (8 M) was prepared in phosphate buffer (pH 7, 50 mM) and its pH was adjusted to pH 7 at 24–25 °C. 1 mM stock solution of labeled (either pyrene or AEDANS) κ-casein (in 6 M GdmCl, pH 7) was diluted 100-fold into varying concentrations of urea (from 8 M to 0 M) to yield a final protein concentration of 10 μM. The solutions were incubated for 1 h at 25 °C to ensure denaturation at that particular concentration of urea. Also, 1 mM stock solution of labeled (either pyrene or AEDANS) κ-casein (in 6 M GdmCl, pH 7) was diluted 100-fold into pH 7 and pH 1.6 buffers separately. The urea- and acid denatured as well as the natively unfolded states of labeled κ-casein were monitored by measuring the intensity and anisotropy of covalently attached pyrene and/or AEDANS.

5.2.8 Fluorescence measurements

(i) Steady-state experiments

All the steady-state fluorescence measurements were performed on a Perkin Elmer LS 55 fluorimeter using 10-mm pathlength quartz cuvette. The steady-state fluorescence anisotropy (r_{ss}) is given as:

$$r_{ss} = (I_{ll}-I_{\perp}G)/(I_{ll}+2I_{\perp}G) \quad \text{---(1)}$$

r_{ss} was recorded from the parallel (I_{ll}) and perpendicular ($I_{\perp}$) intensity components with G-factor correction. An integration time of 30 seconds was used for anisotropy measurements. The final protein concentration was 10 μM in all the experiments except for tryptophan fluorescence measurements, where it was fixed at 20 μM. The excitation bandpass was fixed at 2.5 nm for all experiments. For Trp fluorescence: λ_{ex} = 290 nm and λ_{em} = 350 nm (bandpass 4 nm). For Trp anisotropy: λ_{ex} = 300 nm, λ_{em} = 350 nm (bandpass 15 nm). For AEDANS fluorescence intensity: λ_{ex} = 375 nm; λ_{em} = 475 nm (bandpass 4 nm). For AEDANS anisotropy, the emission bandpass was 7 nm. For pyrene fluorescence, λ_{ex} was 340 nm and the spectra were scanned from 350-550 nm (bandpass of 3.5 nm). For ANS-binding studies on κ-casein, the samples were excited at 350 nm and the fluorescence spectra were recorded from 460-550 nm (bandpass 2 nm and 4 nm, respectively). All the emission spectra were recorded with a scan speed of 10 nm/min and averaged over three scans. The final concentration of α-lactalbumin, κ-casein and ANS were 20 μM for each. The fluorescence resonance energy transfer (FRET) experiments (Trp→AEDANS) and ANS binding were carried out on Chirascan spectrometer (Applied Photophysics, Leatherhead, United Kingdom).

(ii) Stopped-flow experiments

The kinetics of conformational changes of RCM and pyrene labeled κ-casein was monitored by the change in total fluorescence intensity of tryptophan and pyrene excimer, respectively as a result of pH jump from acid denatured state (pH 1.6, 5 mM KCl-HCl buffer) to the native state (pH 7, 50 mM phosphate buffer) with a spectrometer (Chirascan, Applied Photophysics) equipped with a stopped-flow apparatus (Applied Photophysics). Initially, the required volume of chemically denatured protein was equilibrated at pH 1.6 for acid denaturation at room temperature. The acid-denatured protein solution and the refolding buffer of pH 7 were rapidly mixed in 1 : 2.5 ratio (dead time ~1.8 ms) and the renaturation kinetics was monitored. For Trp fluorescence, the final protein concentration was 20 μM. The samples were excited at 290 nm (bandpass 4 nm) and fluorescence was collected using a 320 nm long pass filter. For experiments with pyrene-labeled κ-casein, the final protein concentration was 10 μM. Pyrene was excited at 340 nm (bandpass 4 nm) and the excimer fluorescence was collected using a 395 nm long pass filter to separate the contribution from monomer emission. The stopped-flow data were acquired for 0.5 sec with 10,000 samples per point and the traces were collected in triplicates for five times and averaged to get a satisfactory signal-to-noise ratio. The baseline was also collected with acidic pH under the same experimental conditions to determine the burst phase amplitude. The fluorescence traces were fitted to a biexponential function using the Chirascan Pro-Data Software (Applied Photophysics), and the apparent rate constants were estimated. The goodness of the fit was determined by the residual plots.

(iii) Time-resolved experiments

Time-resolved fluorescence decay measurements of the samples were made using a picosecond laser coupled to a time-correlated single photon counting (TCSPC) setup. A mode-locked frequency-doubled Nd:YAG laser (Spectra Physics, Mount View, CA) of 1 ps pulse width was used to pump a dye (Rhodamine 6G) laser and the generated dye-laser pulses were frequency doubled using a KDP crystal. A wavelength of 295 nm was used for our experiments to excite Trp. The instrument response function (IRF) at 295 nm was collected using a dilute colloidal suspension of dried non-dairy whitener. The width of the IRF was ~40 ps. The Trp fluorescence emission was collected using a microchannel plate photomultiplier (Model 2809u; Hamamatsu Corp., Hamamatsu City, Japan). The emission monochromator was fixed at 350 nm with a bandpass of 10 nm. A long-pass filter of 345 nm was placed just after the sample to block any scattering from the sample. For anisotropy decay measurements, the emission data were collected at 0° and 90° with respect to the excitation polarization and the anisotropy decays were analyzed by globally fitting $I_{II}(t)$ and $I_{\perp}(t)$ as follows:

$$I_{II}(t) = I(t)[1+2r(t)]/3 \quad \text{---(2)}$$

$$I_{\perp}(t) = I(t)[1-r(t)]/3 \quad \text{---(3)}$$

The perpendicular component of the fluorescence decay was corrected for the *G*-factor of the spectrometer. $I(t)$ is the fluorescence intensity collected at magic angle (54.7°) at time *t*. The anisotropy decays were analyzed using a biexponential decay model describing fast and slow rotational correlation times as follows:

$$r(t) = r_0 [\beta_{fast} \exp(-t/\phi_{fast}) + \beta_{slow} \exp(-t/\phi_{slow})] \quad \text{---(4)}$$

where r_0: Intrinsic fluorescence anisotropy; ϕ_{fast}: fast rotational correlation time; ϕ_{slow}: slow rotational correlation time; β_{fast}: amplitude associated with fast correlation time and $\beta_{slow:}$ amplitude associated with slow correlation time.

The global (slow) rotational correlation time (ϕ_{slow}) is related to viscosity (η) and molecular volume (V) by the Stoke's-Einstein relationship as follows:

$$\phi_{slow} = \eta V/kT \quad \text{---(5)}$$

where $V = {}^{4}/_{3}\,\pi R_h^3$ ---(6)

where R_h : hydrodynamic radius of the molecule.

5.2.9 Circular dichroism measurements

Far UV-CD spectra of RCM κ-casein (10 μM) were collected under both native and acid denatured conditions in a quartz cuvette of 2 mm pathlength using a Chirascan CD spectrometer (Applied Photophysics) with a scan range of 200-260 nm. The spectra were recorded with a scan speed of 0.1 nm/s and averaged over five scans. All the CD spectra were buffer subtracted and smoothened using Pro-Data software provided with the instrument. All the graphs were plotted using the commercially available OriginPro Version 8 software. The mean residue molar ellipticity was calculated as described in the literature.[36]

5.2.10 Dynamic light scattering measurements

The dynamic light scattering (DLS) experiments were performed on a Delsa Nano C particle analyzer instrument (Beckman Coulter, Brea, CA) at 25 ºC. Before the DLS experiments, both the phosphate buffer (pH 7) and 6 M GdmCl solution were filtered through 0.22 μm Millipore

syringe filters. Freshly prepared RCM κ-casein was added to the filtered pH 7 phosphate buffer and 6 M GdmCl solutions separately to a final protein concentration of 10 μM each. Each dataset was a collection of at least 30 scattering intensities. All the data were collected using Delsa Nano software provided with the instrument and were subsequently analyzed using the CONTIN method. The viscosity of 6 M GdmCl was taken from the literature.[37]

5.3 Results

5.3.1 Spectroscopic characterizations of the disordered state

Caseins are relatively small, extremely flexible proteins which belong to the class of IDPs that lack specific secondary structure.[3, 38] Usually they have a tendency to self-associate, leading to micelle formation and amyloid-like deposits in bovine mammary glands.[39] Matured signal-peptide cleaved κ-casein is a 169-residue, 18.9 kDa protein that has a single Trp (residue 76) and two Cys (residues 11 and 88) (Figure 5.1a). Our bioinformatic analyses of κ-casein led to the prediction that the protein adopts a disordered and collapsed conformer under physiological conditions (Figure 5.1b,c).

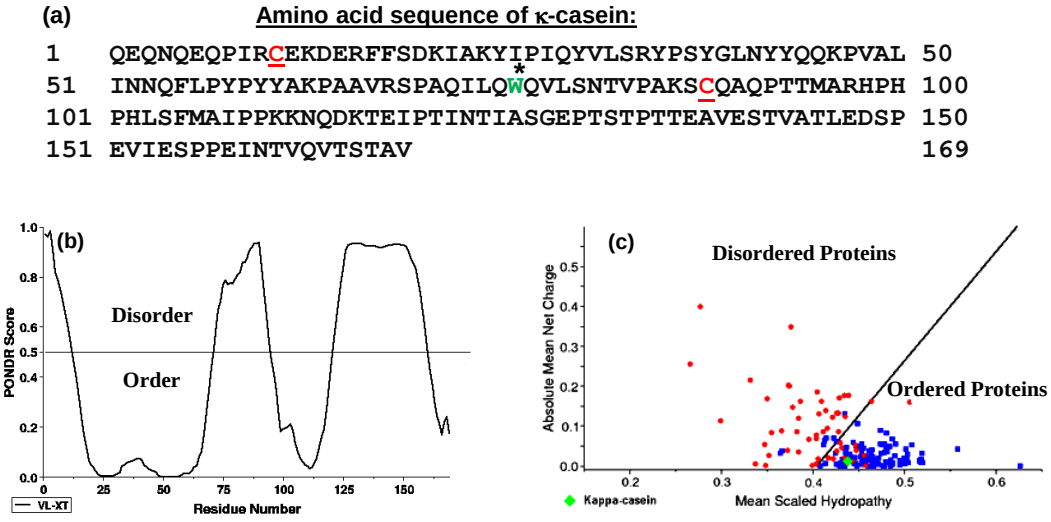

Figure 5.1 (a) The amino acid sequence of κ-casein. Trp 76 and two Cys are shown with asterisk and underscoring, respectively. (b) PONDR® score for κ-casein plotted using VL-XT predictor (Molecular Kinetics, Inc. IN, USA). Most of the amino acid residues lie in the disordered region (PONDR® score above 0.5). (c) Plot between mean hydropathy and mean net charge (CH plot using VL-XT predictor) which places κ-casein (green dot) among ordered proteins. It has been reported that a protein predicted to be ordered by CH plot might have the properties of a collapsed chain and can occur in pre-molten globule form.

Naturally occurring κ-casein exists in micellar form due to the presence of intra- and intermolecular disulfide bonds. Therefore, prior to embarking upon conformational studies under different solution conditions, we first prepared monomeric RCM κ-casein. To do this, we carried out reduction of disulfides followed by carboxymethylation of κ-casein under the denatured condition. To confirm monomerization we performed ANS-binding experiments that suggested that the monomeric form had a much weaker affinity for ANS compared to the micellar form of κ-casein and the archetypal molten-globule form of bovine α-lactalbumin (Figure 5.2a,b).

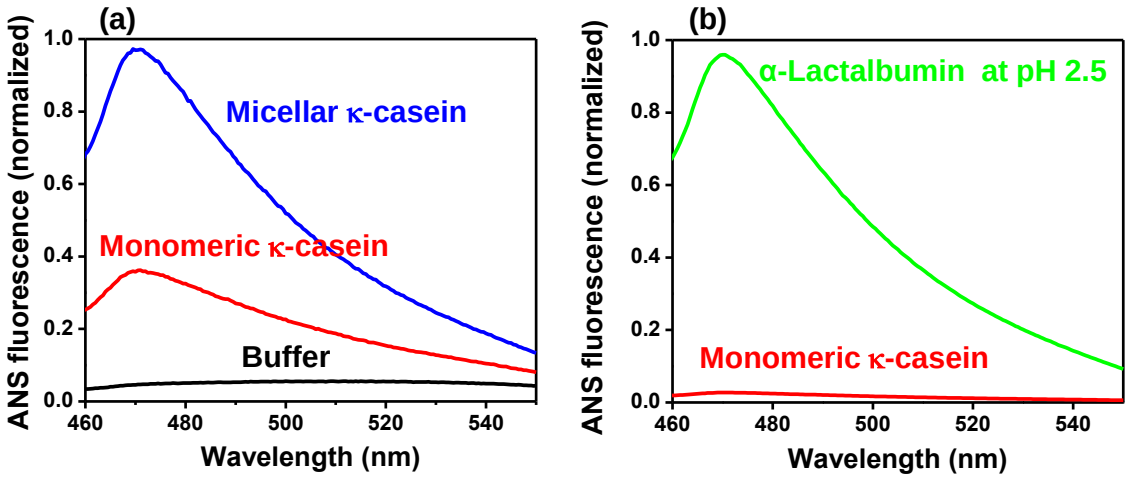

Figure 5.2 ANS-binding studies on κ-casein. (a) Fluorescence spectra of ANS in micellar κ-casein and monomeric RCM κ-casein under the native condition (pH 7 buffer) showing that the monomeric-form has a much weaker affinity for ANS compared to the micellar-form. (b) The comparison of ANS-binding to monomeric κ-casein with that of the molten-globule form of bovine α-lactalbumin (20 μM, pH 2.5) indicates that the collapsed (pre-molten globule like) state of κ-casein is less hydrophobic than the archetypal molten-globule state. The final concentration of both protein and ANS were 20 μM each.

We next probed the fluorescence properties of the single tryptophan (Trp^{76}) that is located in the central region of the polypeptide chain. The fluorescence emission of Trp is sensitive to the environment.[40] Under urea denatured condition of RCM κ-casein, the Trp emission spectrum exhibited a band with a maximum at ~ 355 nm, which is consistent with exposed Trp under unfolded condition. Upon transfer to a refolding buffer, the emission maximum underwent a blue-shift to ~ 347 nm, indicating a lower solvent accessibility around Trp^{76} (Figure 5.3a). In addition to the spectral shift, we observed a small but measurable decrease in the tryptophan fluorescence intensity under native conditions (Figure 5.3a), suggesting a structural change from an expanded to a compact state that results in more efficient quenching of tryptophan fluorescence by proximal amino acid quenchers located on the polypeptide chain. The structural rigidification around Trp is further supported by more restricted rotational motion of Trp, as evidenced by a significant rise in the tryptophan fluorescence anisotropy upon renaturation (Figure 5.3b).

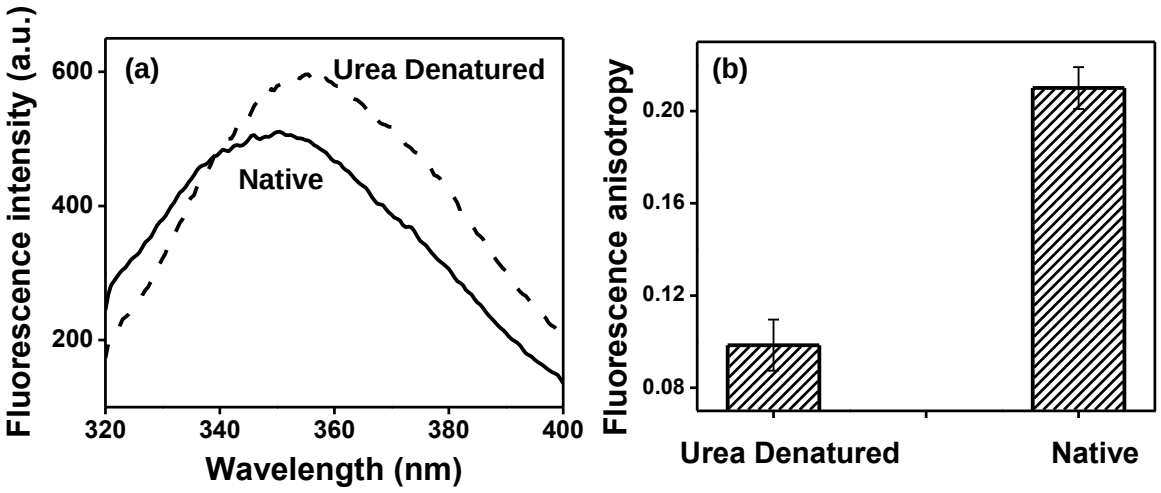

Figure 5.3 (a) Tryptophan fluorescence spectra of 20 μM κ-casein under urea-denatured (dashed line) and native conditions (solid line). (b) The increase in tryptophan fluorescence anisotropy of κ-casein upon transfer from urea-denatured to native conditions.

Next we performed quenching experiments, to measure the Stern-Volmer quenching constant[40] of Trp fluorescence by using acrylamide as a quencher, which again indicated that the native κ-casein is less efficiently quenched as expected for a protected Trp (Figure 5.4a). Figure 5.4b depicts Stern-Volmer plot for κ-casein under native and urea denatured conditions as a function of acrylamide. The nonlinearity in the quenching plot can be attributed to both static and dynamic quenching and presumably heterogeneous conformational distribution on the timescale of tryptophan fluorescence lifetime.

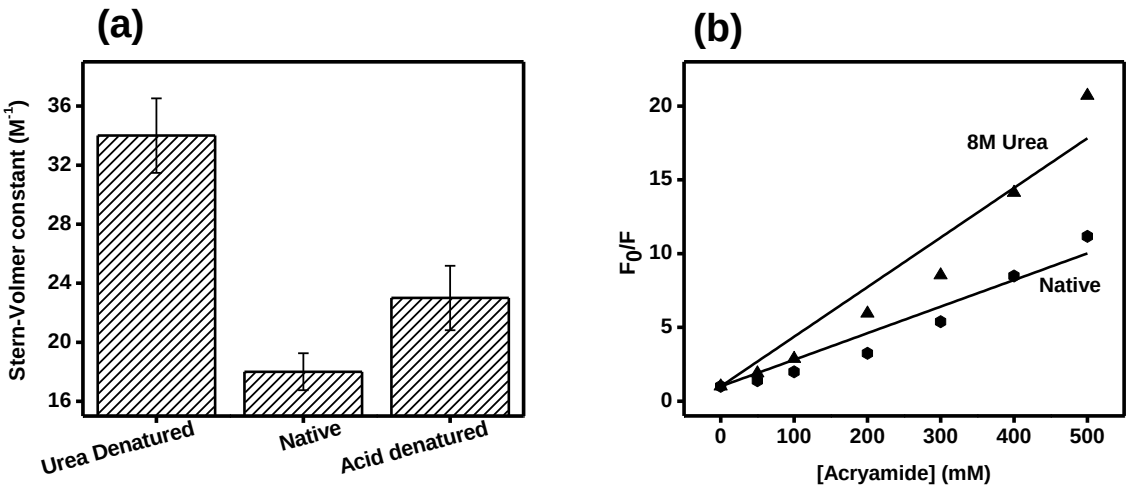

Figure 5.4 (a) The Stern-Volmer quenching constant of Trp of 20 μM κ-casein with acrylamide quencher under different conditions. (b) Stern-Volmer plot for κ-casein under native (filled hexagon) and urea denatured (filled triangle) conditions as a function of acrylamide (quencher) concentration obtained from tryptophan fluorescence quenching experiments. F_0 and F are the tryptophan fluorescence intensity in the absence and presence of acrylamide (quencher), respectively. The solid line indicates linear fit of the quenching data.

Using CD, we showed that the native state is devoid of detectable elements of secondary structure (Figure 5.5). Taken together, our tryptophan fluorescence and far-UV CD data indicated structural compaction in the native state of κ-casein that remains disordered. This

compact, yet disordered, state can respond to acid denaturation as indicated by extensive tryptophan fluorescence quenching without much change in secondary structural contents at low pH (Figure 5.4a). All of the above experiments provide initial experimental support in favor of monomeric κ-casein adopting a compact conformation under native condition.

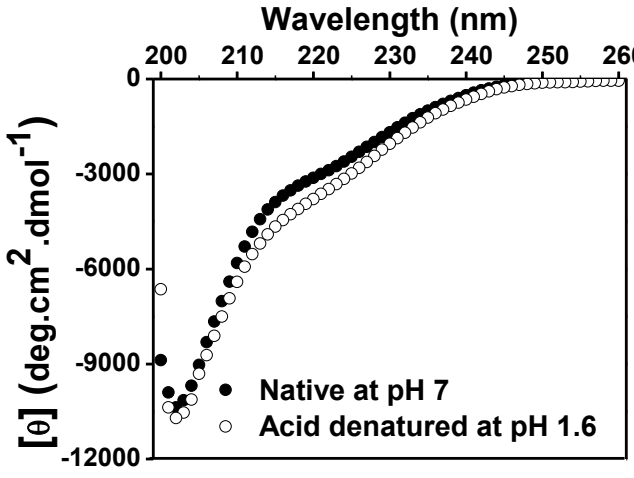

Figure 5.5 Far UV CD spectra of 10 μM κ-casein under native (filled circles) and acid-denatured (open circles) forms. Under native condition, $[\theta]_{222}$ and $[\theta]_{200}$ were -2880 and -8880 deg.cm^2.dmol^{-1}, respectively.

5.3.2 Chain collapse observed by fluorescence resonance energy transfer (FRET)

The intrinsic tryptophan fluorescence properties are likely to depict a more local structure formation around the tryptophan residue under the native condition. We next investigated whether the chain collapse is a locally restricted phenomenon around the Trp residue or globally felt among other residues along the polypeptide chain. We took advantage of two cysteine residues (Cys^{11} and Cys^{88}). We labeled them using IAEDANS, a thiol-labeling fluorescent probe that is highly environment-sensitive.[40] Fluorescence spectra of the AEDANS-κ-casein conjugate showed progressive blue-shift (490 nm → 480 nm) and a concomitant increase in fluorescence intensity from the denatured to native state that is consistent with a non-polar microenvironment of the fluorophore (Figure 5.6a inset). Fluorescence anisotropy of AEDANS also exhibited a

distinct increase upon lowering of denaturant concentration, again suggesting restricted environment around the probe (Figure 5.6a). These results prompted us to investigate the fluorescence resonance energy transfer (FRET) from Trp → AEDANS to probe the changes in intrachain distances as a result of compaction under native condition. Initially, the FRET efficiency from Trp → AEDANS was low under urea-denatured condition, as expected for a random coil. Upon transferring into the native buffer, an increase in AEDANS (acceptor) fluorescence with a concomitant decrease in Trp (donor) emission indicated an increase in FRET efficiency that revealed a global intrachain compaction under native condition (Figure 5.6b). Taken together, the aforementioned experiments revealed that the disordered polypeptide chain of κ-casein is likely to be globally collapsed under the native buffer condition.

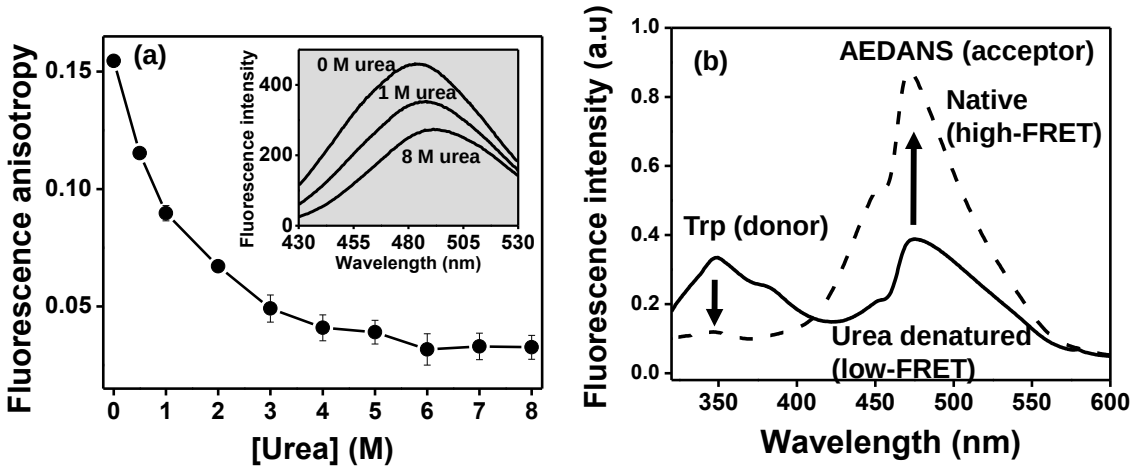

Figure 5.6 (a) The increase in AEDANS fluorescence anisotropy upon refolding of fluorescently-labeled 10 μM κ-casein from urea denatured state. The inset shows AEDANS fluorescence spectra as a function of denaturant concentration. (b) FRET between Trp (donor) and AEDANS (acceptor) under denatured and native conditions.

5.3.3 Chain dynamics and dimension observed by time-resolved fluorescence anisotropy and dynamic light scattering

We have carried out picosecond time-resolved fluorescence anisotropy measurements that provide insights into the local and global dynamics of proteins.[40, 41] Global dynamics is represented by a slow rotational correlation time (ϕ_{slow}) that is generally related to the size (hydrodynamic radius) of the protein (Eq. 4). In the denatured-form, κ-casein showed two rotational correlation times. The fast rotational correlation time, ϕ_{fast} (~ 0.2 ns), represents the local dynamics of Trp, whereas ϕ_{slow} (~ 2.7 ns) could indicate the segmental mobility of the unfolded polypeptide chain (Figure 5.7a). For an unfolded protein, ϕ_{slow} is related to segmental flexibility and does not depend on the protein size, since the segmental conformation fluctuations depolarize the fluorescence much more rapidly than the global tumbling of polypeptide chain.[41] Upon transferring into the native buffer, ϕ_{slow} increased to ~ 7 ns, which may corresponds to a hydrodynamic radius (R_h) of 1.9 nm for the collapsed globule (Figure 5.7 and Eq. 4 & 5). This is also corroborated with R_h obtained from our DLS data (1.9 ± 0.3 nm). On the other hand, the DLS data of the denatured form of κ-casein showed R_h of 4.6 ± 0.7 nm, which is in accordance with calculated R_h (~ 4.1 nm) for a 169-residue unfolded protein using a previously reported empirical relationship.[42] Taken together, time-resolved fluorescence anisotropy and DLS data provide a quantitative description of chain collapse of monomeric κ-casein that undergoes a change in the mean hydrodynamic radius from ~4.6 nm (denatured) to ~1.9 nm (native).

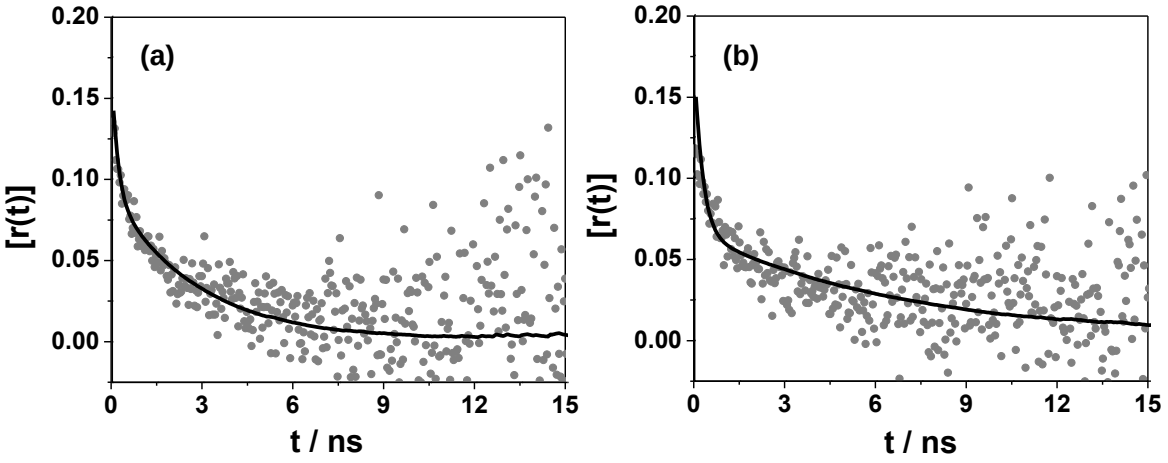

Figure 5.7 Picosecond time-resolved fluorescence anisotropy decays [$r(t)$] of Trp in denatured (a) and native (b) κ-casein. The solid line is the biexponential fit (Eq. 4). The recovered rotational correlation times with associated amplitudes are given as follows: (a) ϕ_{fast} = 0.2 ± 0.1; β_{fast} = 0.53 ± 0.02; ϕ_{slow} = 2.7 ± 0.8; β_{slow} = 0.47 ± 0.02 for denatured κ-casein (b) ϕ_{fast} = 0.2 ± 0.1; β_{fast} = 0.65 ± 0.03; ϕ_{slow} = 7.1 ± 0.6; β_{slow} = 0.35 ± 0.03 for native κ-casein.

5.3.4 Pyrene excimer formation upon polypeptide chain collapse

Our next goal of the study was to directly watch the chain collapse using a strategy that allowed us to monitor the changes in the intramolecular distances at short length-scales. One such proximity indicator is pyrene excimer (excited-state dimer), that is observed when two proximal pyrene moieties interact below 5 Å distance within the excited state lifetime of pyrene (~ 100 ns). [40, 43] Excimer formation provides a direct handle to monitor conformational changes at a much shorter length-scale compared to more commonly utilized FRET technique that offers structural information at much longer length-scale ranging from 20-80 Å. Recently, pyrene excimer fluorescence has been successfully utilized to gain important insights into the protein conformational changes and aggregation.[44-47]

Reduced κ-casein has two free cysteines that are well separated (by 77 residues) in the primary sequence. We labelled the cysteines with two molar equivalents of thiol-reactive pyrene [N-(1-Pyrene) maleimide]. We conjectured that upon chain collapse, the internal distance between residues 11 and 88 would decrease, as a result of which we would see high excimer fluorescence. To gain information about conformational transitions, we recorded the pyrene fluorescence spectra of urea-denatured protein sequentially transferred to native buffer. Monomer fluorescence emission of pyrene ranges between 370 and 400 nm with vibronic bands, whereas a single excimer band is observed between 450 and 480 nm (Figure 5.8a). As we decreased the urea concentration, the excimer emission band increased at the expense of the monomer emission band. The excimer/monomer ratio increased in a noncooperative fashion from < 1 (denatured) to 4 (native), suggesting progressive collapse of the polypeptide chain (Figure 5.8b,c). We point out also that there was residual excimer intensity present even at the fully denatured condition. This might indicate that the polypeptide chain undergoes rapid nanosecond fluctuations given that the fluorescence lifetime of pyrene is ~ 100 ns. Upon renaturation, the pyrene excimer contribution grew significantly, indicating a substantial decrease in inter-pyrene distance arising from chain collapse. To eliminate the possibility of excimer formation by oligomeric aggregates, we performed experiments at different protein concentrations under native condition and obtained the same excimer/monomer ratio (Figure 5.8d).

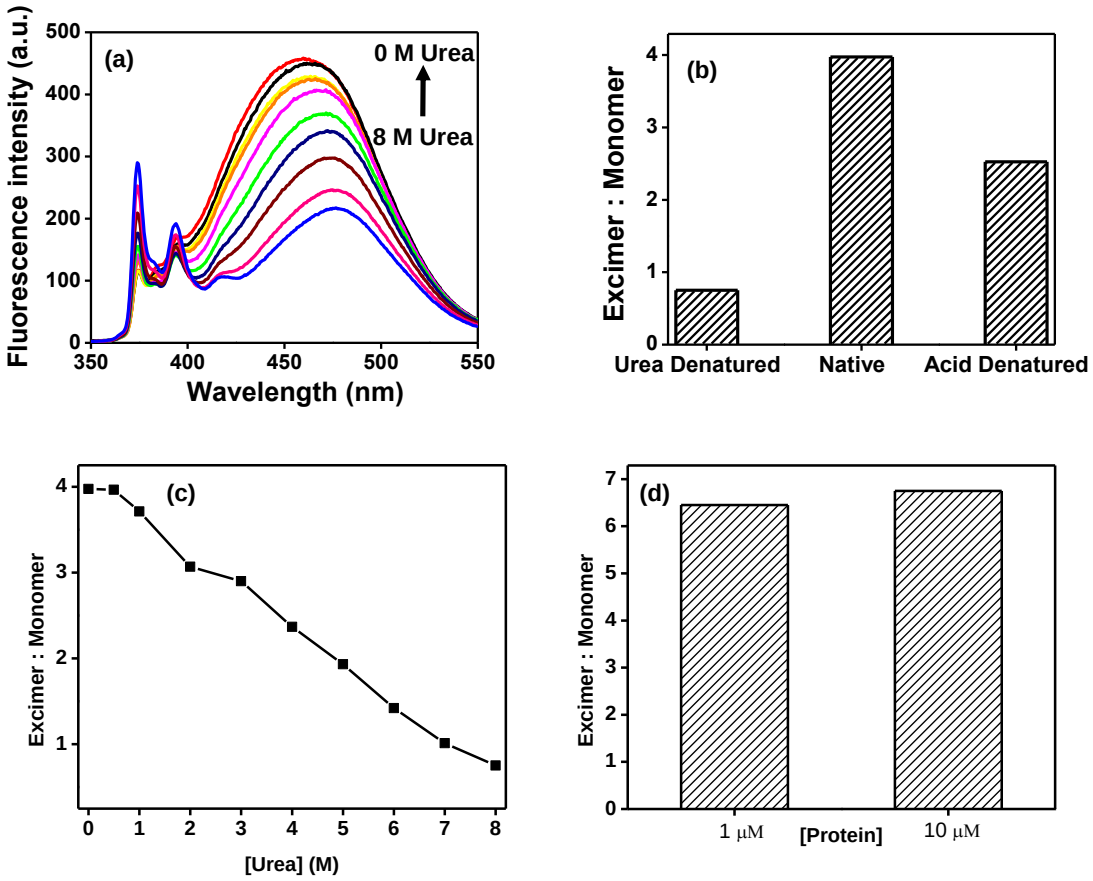

Figure 5.8 (a) Pyrene excimer formation of dual-labeled 10 μM κ-casein upon renaturation from urea. (b) The excimer to monomer ratio of pyrene under urea-denatured, native and acid-denatured conditions. (c) The excimer to monomer ratio of pyrene in pyrene labeled κ-casein as a function of urea concentration, showing highest excimer intensity at the natively unfolded (0 M urea, pH 7) state of κ-casein. (d) The excimer to monomer ratio of pyrene as a function of pyrene labeled κ-casein concentration under native conditions.

These experiments confirmed that excimer formation is solely due to the chain collapse of the monomeric protein. Additionally, a gradual blue-shift of the excimer band from 475 nm (denatured) to 460 nm (native) is indicative of the change in pyrene micro-environment from

polar to non-polar. Taken together, these results provide direct evidence in favor of chain collapse of disordered κ-casein in water (Figure 5.9).

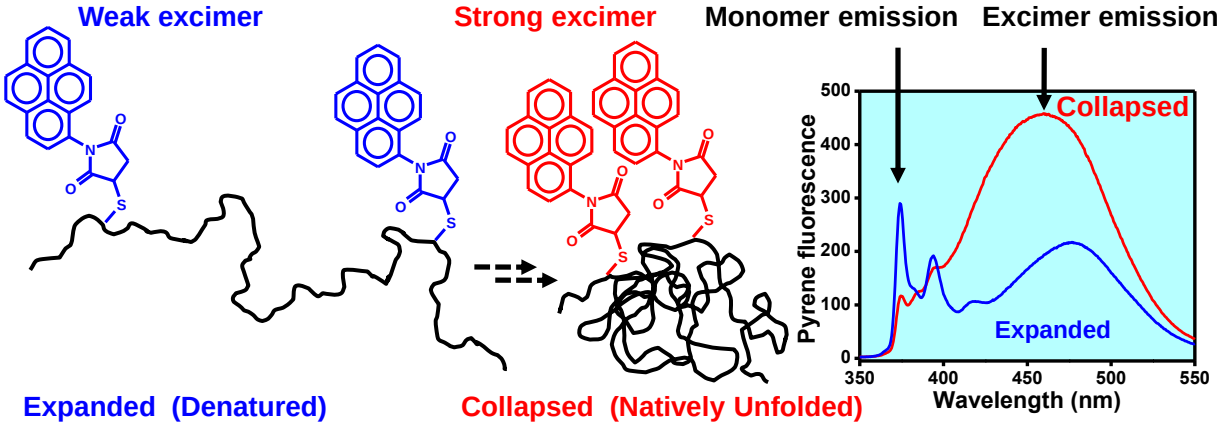

Figure 5.9 A schematic of excimer formation upon polypeptide chain collapse.

5.3.5 Kinetics of chain collapse

After establishing the above equilibrium experiments on chain collapse of κ-casein, we directed our efforts to study the kinetics of conformational change from the extended to the collapsed state using stopped-flow pH-jump from acid denatured (pH 1.6) to natively unfolded state at neutral pH (pH 7). As discussed previously, natively unfolded κ-casein undergoes pH-induced unfolding (Figure 5.5) because of the change in net-charge from -1.4 at pH 7 to +17.9 at pH 1.6. Therefore, reversible transitions between compact and expanded can be monitored simply by changing pH of the solution without using high concentration of denaturant. Figure 5.10a shows the steady-state fluorescence spectra of the single tryptophan (Trp^{76}) in carboxymethylated κ-casein both at neutral and at low pH, suggesting significant decrease in Trp emission as a result of acid denaturation (pH 7 → 1.6). Using stopped-flow fluorescence with a

pH-jump from 1.6 to 7, we observed time-dependent recovery of total Trp fluorescence upon renaturation of acid-denatured κ-casein (Figure 5.10b). The Trp fluorescence kinetics revealed that there is > 50% burst phase that could not be resolved within the dead-time of mixing of a millisecond or so. This submillisecond kinetic phase is followed by a slow phase with a relaxation time of ~ 20 ms. These results indicated that the chain collapse is likely to occur in at least in two phases, a fast (sub-millisecond) phase and a slower phase with a relaxation time of ~ 20 ms that increases with the increase in solvent viscosity, as expected for chain collapse. This biphasic relaxation kinetics comprising submillisecond and millisecond components observed for the chain collapse is consistent with previous results on expansion and collapse of a polypeptide.[48] We next undertook pH-induced kinetic experiments using dual-pyrene labeled κ-casein. Figure 5.10c shows the steady-state pyrene emission spectra of pyrene labeled κ-casein under both neutral and low pH conditions showing an increase in pyrene excimer emission at pH 7 with a concurrent decrease in monomer fluorescence. To selectively monitor the time-evolution of pyrene excimer fluorescence upon renaturation kinetics, we used an optical filter (395 nm long pass) on the emission path. Here again, as expected, we observed a significant fraction of burst phase along with a slow phase with a relaxation time of ~ 20 ms that corroborated with the stopped-flow Trp fluorescence data (Figure 5.10d). The fast component, hidden in the burst phase, could arise due to rapid chain collapse, whereas, the 20 ms component could reveal the slow conformational reorganization of the collapsed globules into pre-molten globules. There was another much slower component with a small amplitude, which can be attributed to a slow conformational reorganization of pre-molten globule conformers comprising a small degree of secondary structural elements. This slow component was not a contribution

from aggregation as confirmed by stopped-flow experiments at different final protein concentrations.

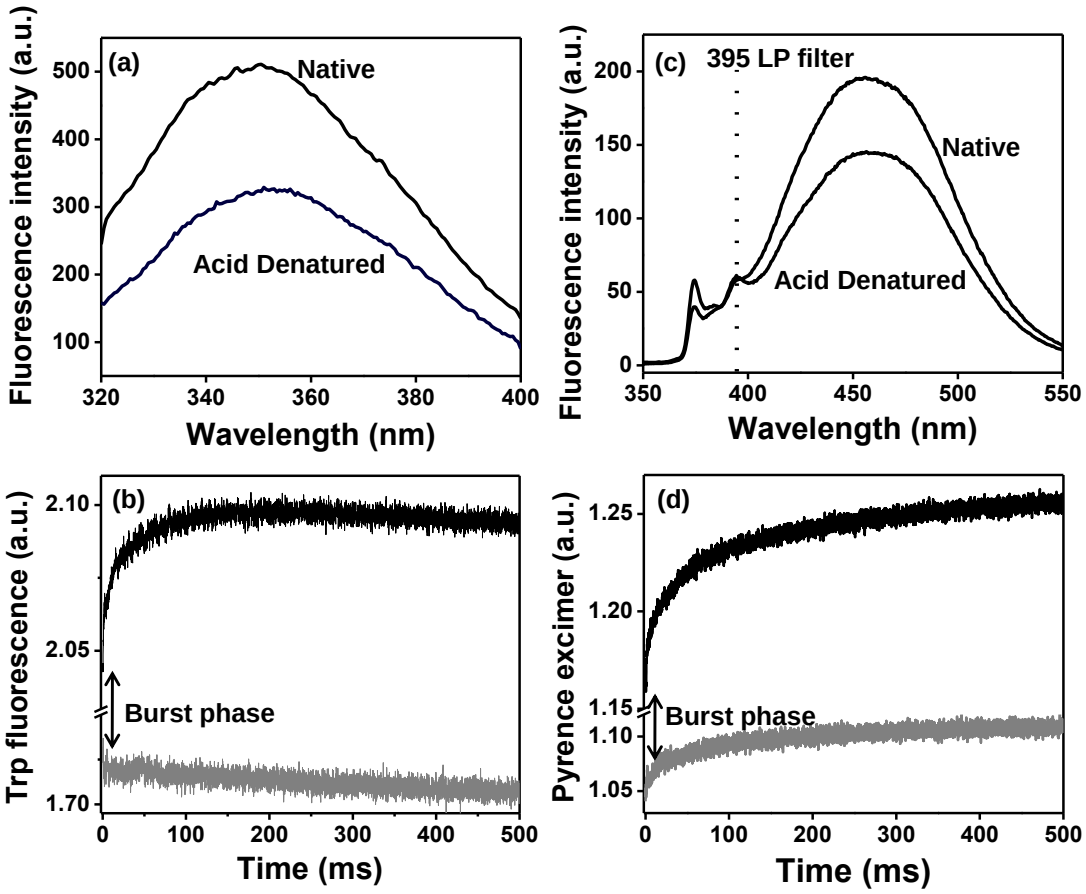

Figure 5.10 (a) Trp fluorescence spectra of 20 μM κ-casein under acid-denatured and native conditions. (b) Stopped-flow kinetics of Trp fluorescence upon acid-renaturation of κ-casein from pH 1.6 to 7. An optical filter (320 nm long pass) was used to collect total Trp fluorescence. The baseline is shown in gray. (c) Pyrene emission spectra of dual-labeled 10 μM κ-casein under acid-denatured and native conditions. (d) Stopped-flow kinetics of pyrene excimer formation upon acid-renaturation. The optical filter (395 nm long pass) used to selectively collect excimer fluorescence in the stopped-flow experiment is shown by a dotted line in Figure 5.10c.

5.4 Discussion

In this work, using a variety of spectroscopic techniques, we have provided compelling evidences in favor of our hypothesis that a model amyloidogenic IDP, κ-casein, adopts a collapsed, yet disordered, pre-molten globule-like conformation, under the native condition. This pre-molten globule-like disordered state may contain very small elements of secondary structure, as indicated by the CD 'double-wavelength plot'[11] and has much lower hydrophobicity compared to an archetypal molten globule such as the low-pH form of α-lactalbumin (Figure 5.2b). We have shown for the first time, to the best of our knowledge, that pyrene excimer formation can be used as a simple, convenient, and elegant tool to study the chain collapse behavior of IDPs (Figure 5.11). Since we observed strong excimer fluorescence upon chain collapse, the inter-pyrene distance must approach 5 Å. It is likely that due to backbone dynamics, there is conformational fluctuation faster than the fluorescence lifetime of pyrene (~ 100 ns) that may bring the pyrene moieties temporarily to a very close proximity. In addition, pre-molten globule formation could also contribute to further shortening of the inter-pyrene distance. The contribution of hydrophobic association of the pyrene moieties leading to the chain collapse could be a concern in this type of study. However, this is not a problem in our case since a variety of fluorescence experiments on the unlabeled protein involving the intrinsic tryptophan fluorescence also indicated the chain collapse phenomenon. Therefore, we suggest that to use the pyrene excimer methodology, it is important to independently verify the chain collapse behavior using other methods, such as intrinsic protein fluorescence (spectral position, anisotropy and quenching).

The observed chain collapse is likely to be largely driven by the entropic factors, since water acts as a poor solvent for the polypeptide chain. We believe that the enthalpic contributions may also be important. A closer look at the κ-casein sequence revealed that the well-known disorder promoting residues proline (P) and glutamine (Q) have more than double (P ~ 12 % and Q ~ 9 %) their frequency of occurrence in globular proteins (P ~ 5 % and Q ~ 4 %) which is in keeping with the observed conformational flexibility under physiological conditions. The unusually high occurrence of glutamine in κ-casein makes this protein very unique and interesting for aggregation studies, since polyglutamine repeats and glutamine-rich yeast prion have also been shown to undergo chain collapse, that has been implicated in amyloid aggregation.[17,26] The chain collapse phenomenon of IDPs is consistent with the emerging polymer physics perspective of protein aggregation and amyloid formation.[25] In this work, we have also shown that chain collapse can be studied by pH-induced renaturation because of the decrease in the net-charge of the protein, which allows favorable intrachain interactions through both hydrophobic effect and hydrogen bonding. The collapsed state of the protein is likely to be stabilized by ⟩C=O⋯⋯H–N⟨ hydrogen bonding between the side-chain amides of glutamines. Such hydrogen bonding-mediated chain collapse of disordered peptides has been described previously.[27] Recent reports indicate that water serves as a poor solvent for generic polypeptides.[49,50] One biologically important amyloidogenic IDP, α-synuclein, has also been demonstrated to adopt collapsed conformational ensemble in water.[51,52]

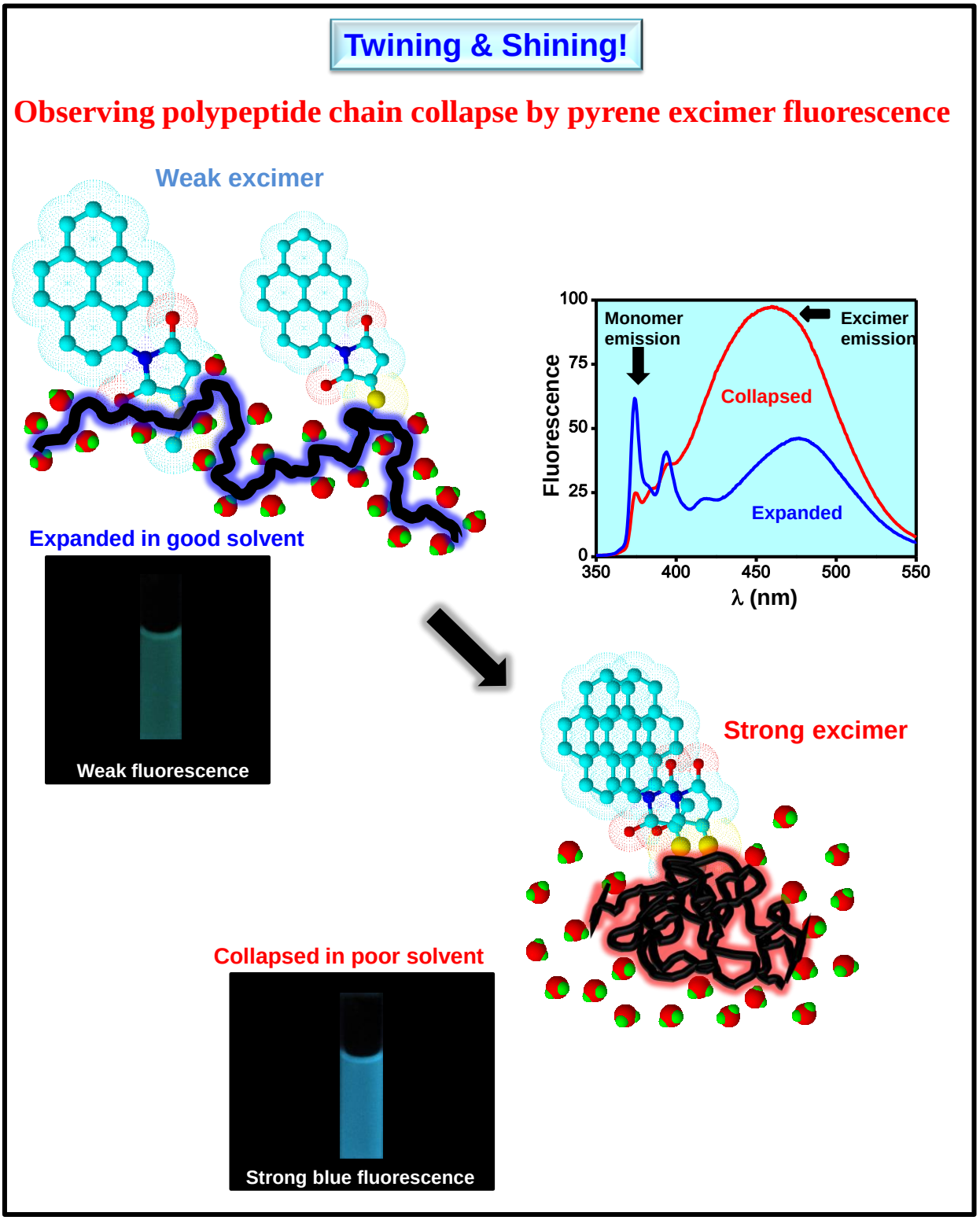

Figure 5.11 Direct observation of polypeptide chain collapse by pyrene excimer.

5.5 Conclusion

Overall, our results described in this work clearly demonstrate that water acts as a poor solvent for disordered κ-casein that assumes a collapsed premolten globule-like conformation. Our results indicate a change in the mean hydrodynamic radius from ~4.6 nm to ~1.9 nm upon polypeptide chain collapse. This collapsed conformer may be a reminiscent of early ″burst-phase″ intermediate formed during the folding of many globular proteins. We suggest that at a high protein concentration, polypeptide chains from different protein molecules will interact in an intermolecular fashion and will form oligomers to avoid unfavorable contacts with water molecules. Subsequently, the β-rich amyloidogenic conformers will be sequestered within the oligomers, which will conformationally mature into amyloid fibrils as described by the nucleated conformational conversion model.[23] We would like to point out that the pyrene excimer methodology is easy to apply and is applicable to any IDP, either wild-type containing two cysteines or dual-cysteine mutants. We anticipate that the pyrene excimer methodology will serve as a complementary and perhaps better readout of chain collapse than FRET, since the collapse is expected to bring different segments of the polypeptide chain at a much closer proximity. In addition, this method involves one-step preparation of the labeled protein, unlike FRET-studies, wherein extensive purification is required at each step of both donor and acceptor labeling. In summary, the pyrene excimer methodology offers a robust and convenient spectroscopic tool to study IDPs and can eventually be extended to two-color (monomer/excimer) ratiometric imaging to monitor IDP chain collapse in complex environments such as liposomes and cells.

5.6 References

1. Uversky, V. N.; Dunker, A. K. (2010) Understanding protein non-folding. *Biochim. Biophys. Acta* 1804:1231-1264.

2. Dunker, A. K.; Lawson, J. D.; Brown, C. J.; Williams, R. M.; Romero, P.; Oh, J. S.; Oldfield, C. J.; Campen, A. M.; Ratliff, C. M.; Hipps, K. W.; Ausio, J.; Nissen, M. S.; Reeves, R.; Kang, C.; Kissinger, C. R.; Bailey, R. W.; Griswold, M. D.; Chiu, W.; Garner, E. C.; Obradovic, Z. (2001) Intrinsically disordered protein. *J. Mol. Graph. Model*. 19:26-59.

3. Tompa, P. (2010) Structure and function of intrinsically disordered proteins. 1st ed.; CRC Press: Boca Raton, FL, U.S.A.

4. Uversky, V. N. (2009) Intrinsically disordered proteins and their environment: effects of strong denaturants, temperature, pH, counter ions, membranes, binding partners, osmolytes, and macromolecular crowding. *Protein J*. 28:305-326.

5. Radivojac, P.; Iakoucheva, L. M.; Oldfield, C. J.; Obradovic, Z.; Uversky, V. N.; Dunker, A. K. (2007) Intrinsic disorder and functional proteomics. *Biophys. J*. 92:1439-1456.

6. Dyson, H. J.; Wright, P. E. (2005) Intrinsically unstructured proteins and their functions. *Nat. Rev. Mol. Cell. Biol*. 6:197-208.

7. Tompa, P. (2005) The interplay between structure and function in intrinsically unstructured proteins. *FEBS Lett*. 579:3346-3354.

8. Dunker, A. K.; Silman, I.; Uversky, V. N.; Sussman, J. L. (2008) Function and structure of inherently disordered proteins. *Curr. Opin. Struct. Biol*. 18:756-764.

9. Dyson, H. J.; Wright, P. E. (2004) Unfolded proteins and protein folding studied by NMR. *Chem. Rev*. 104:3607-3622.

10. Dedmon, M. M.; Lindorff-Larsen, K.; Christodoulou, J.; Vendruscolo, M.; Dobson, C. M. (2005) Mapping long-range interactions in α-synuclein using spin-label NMR and ensemble molecular dynamics simulations. *J. Am. Chem. Soc*. 127:476-477.

11. Uversky, V. N. (2002) Natively unfolded proteins: a point where biology waits for physics. *Protein Sci*. 11:739-756.

12. Smyth, E.; Syme, C. D.; Blanch, E. W.; Hecht, L.; Vasak, M.; Barron, L. D. (2001) Solution structure of native proteins with irregular folds from Raman optical activity. *Biopolymers* 58:138-151.

13. Syme, C. D.; Blanch, E. W.; Holt, C.; Jakes, R.; Goedert, M.; Hecht, L.; Barron, L. D. (2002) A Raman optical activity study of rheomorphism in caseins, synucleins and tau. *Eur. J. Biochem*. 269:148-156.

14. Jeganathan, S.; von Bergen, M.; Brutlach, H.; Steinhoff, H. J.; Mandelkow, E. (2006) Global hairpin folding of tau in solution. *Biochemistry* 45:2283-2293.

15. Szilvay, G. R.; Blenner, M. A.; Shur, O.; Cropek, D. M.; Banta, S. (2009) A FRET-based method for probing the conformational behavior of an intrinsically disordered repeat domain from Bordetella pertussis adenylate cyclase. *Biochemistry* 48:11273-11282.

16. Grupi, A.; Haas, E. (2011) Segmental conformational disorder and dynamics in the intrinsically disordered protein α-synuclein and its chain length dependence. *J. Mol. Biol*. 405:1267-1283.

17. Mukhopadhyay, S.; Krishnan, R.; Lemke, E. A.; Lindquist, S.; Deniz, A. A. (2007) A natively unfolded yeast prion monomer adopt an ensemble of collapsed and rapidly fluctuating structures. *Proc. Natl. Acad. Sci. U.S.A.* 104:2649-2654.

18. Ferreon, A. C. M.; Gambin, Y.; Lemke, E. A.; Deniz, A. A. (2009) Interplay of alpha-synuclein binding and conformational switching probed by single-molecule fluorescence. *Proc. Natl. Acad. Sci. U.S.A.* 106:5645-5650.

19. Ferreon, A. C. M.; Moran, C. R.; Gambin, Y.; Deniz, A. A. (2010) Single-molecule fluorescence studies of intrinsically disordered proteins. *Methods Enzymol*. 472:179-204.

20. Uversky, V. N. (2008) Amyloidogenesis of natively unfolded proteins. *Curr. Alzheimer Res*. 5:260-287.

21. Turoverov, K. K.; Kuznetsova, I. M.; Uversky, V. N. (2010) The protein kingdom extended: ordered and intrinsically disordered proteins, their folding, supramolecular complex formation, and aggregation. *Prog. Biophys. Molec. Biol*. 102:73-84.

22. Scheibel, T.; Lindquist, S. L. (2001) The role of conformational flexibility in prion propagation and maintenance for Sup35p. *Nat. Struct. Biol*. 8:958-962.

23. Serio, T. R.; Cashikar, A. G.; Kowal, A. S.; Sawicki, G. J.; Moslehi, J. J.; Serpell, L.; Arnsdorf, M. F.; Lindquist, S. L. (2000) Nucleated conformational conversion and the replication of conformational information by a prion determinant. *Science.* 289:1317-1321.

24. Fowler, D. M.; Koulov, A. V.; Balch, W. E.; Kelly, J. W. (2007) Functional amyloid from bacteria to humans. *Trends Biochem. Sci.* 32:217-224.

25. Pappu, R. V.; Wang, X.; Vitalis, A.; Crick, S. L. (2008) A polymer physics perspective on driving forces and mechanisms for protein aggregation. *Arch. Biochem. Biophys*. 469:132-141.

26. Crick, S. L.; Jayaraman, M.; Frieden, C.; Wetzel, R.; Pappu, R. V. (2006) Fluorescence correlation spectroscopy shows that monomeric polyglutamine molecules form collapsed structures in aqueous solutions. *Proc. Natl. Acad. Sci. U.S.A.* 103:16764-16769.

27. Mao, A. H.; Crick, S. L.; Vitalis, A.; Chicoine, C. L.; Pappu, R. V. (2010) Net charge per residue modulates conformational ensembles of intrinsically disordered proteins. *Proc. Natl. Acad. Sci. U.S.A.* 107:8183-8188.

28. Möglich, A.; Joder, K.; Kiefhaber, T. (2006) End-to-end distance distributions and intrachain diffusion constants in unfolded polypeptide chains indicate intramolecular hydrogen bond formation. *Proc. Natl. Acad. Sci. U.S.A.* 103:12394-12399.

29. Thorn, D. C.; Meehan, S.; Sunde, M.; Rekas, A.; Gras, S. L.; MacPhee, C. E.; Dobson, C. M.; Wilson, M. R.; Carver, J. A. (2005) Amyloid fibril formation by bovine milk κ-casein and its inhibition by the molecular chaperones α_S- and β-casein. *Biochemistry.* 44:17027-17036.

30. Ecroyd, H.; Koudelka, T.; Thorn, D. C.; Williams, D. M.; Devlin, G.; Hoffmann, P.; Carver, J. A. (2008) Dissociation from the oligomeric state is the rate-limiting step in fibril formation by κ-casein. *J. Biol. Chem*. 283:9012-9022.

31. Leonil, J.; Henry, G.; Jouanneau, D.; Delage, M. M.; Forge, V.; Putaux, J. L. (2008) Kinetics of fibril formation of bovine κ-casein indicate a conformational rearrangement as a critical step in the process. *J. Mol. Biol*. 381:1267-1280.

32. Atanasiu, C.; Su, T. J.; Sturrock, S. S.; Dryden, D. T. F. (2002) Interaction of the ocr gene 0.3 protein of bacteriophage T7 with EcoKI restriction/modification enzyme. *Nucl. Acids Res.* 30:3936-3944.

33. Hudson, E. N.; Weber, G. (1973) Synthesis and characterization of two fluorescence sulfhydryl reagents. *Biochemistry* 12:4154-4161.

34. Campioni, S.; Mannini, B.; Zampagni, M.; Pensalfini, A.; Parrini, C.; Evangelisti, E.; Relini, A.; Stefani, M.; Dobson, C. M.; Cecchi, C.; Chiti, F. (2010) A causative link between the structure of aberrant protein oligomers and their toxicity. *Nat. Chem. Biol.* 6:140-147.

35. Han, M. K.; Knutson, J. R.; Roseman, S.; Brand, L. (1990) Sugar transport by the bacterial phosphotransferase system. Fluorescence studies of subunit interactions of enzyme I *J. Biol. Chem.* 265:1996-2003.

36. Corrêa, D. H. A.; Ramos, C. H. I. (2009) The use of circular dichroism spectroscopy to study protein folding, form and function. *African J. Biochem. Res.* 3:164-173.

37. Kawahara, K.; Tanford, C. (1966) Viscosity and Density of Aqueous Solutions of Urea and Guanidine Hydrochloride. *J. Biol. Chem.* 241:3228-3232.

38. Holt, C. (1992) Structure and stability of bovine casein micelles. *Adv. Protein Chem*. 43:63-151.

39. Reid, I. M. (1972) Corpora amylacea of the bovine mammary gland: histochemical and electron microscopic evidence for their amyloid nature. *J. Comp. Pathol*. 82:409-413.

40. Lakowicz, J. R. (2006) Principles of fluorescence spectroscopy. 3rd ed.; Springer: New York, U.S.A.

41. Saxena, A.; Udgaonkar, J. B.; Krishnamoorthy, G. In Applications of Fluorescence Spectroscopy; Hof, M., Hutterer R., and Fidler, V. (Eds.); (2005) Springer-Verlag: New York.

42. Wilkins, D. K.; Grimshaw, S. B.; Receveur, V.; Dobson, C. M.; Jones, J. A.; Smith, L. J. (1999) Hydrodynamic radii of native and denatured proteins measured by pulse field gradient NMR techniques. *Biochemistry*, 38:16424-16431.

43. Turro, N. J. (1991) *Modern molecular photochemistry*. 1st ed.; University Science Books: Sausalito, CA, U.S.A.

44. Krishnan, R.; Lindquist, S. L. (2005) Structural insights into a yeast prion illuminate nucleation and strain diversity. *Nature* 435:765-772.

45. Drury, J. D.; Narayanaswami, V. (2005) Examination of lipid bound conformation of apolipoprotein E4 by pyrene excimer fluorescence. *J. Biol. Chem*. 280:14605-14610.

46. Patel, A. B.; Khumsupan, P.; Narayanaswami, V. (2010) Pyrene fluorescence analysis offers new insights into the conformation of the lipoprotein-binding domain of human apolipoprotein E. *Biochemistry* 49:1766-1775.

47. Thirunavukkuarasu, S.; Jares-Erijman, E. A.; Jovin, T. M. (2008) Multiparametric fluorescence detection of early stages in the amyloid protein aggregation of pyrene-labeled alpha-synuclein. *J. Mol. Biol*. 378:1064-1073.

48. Hagen, S. J.; Eaton, W. A. (2000) Two-state expansion and collapse of a polypeptide. *J. Mol. Biol*. 301:1019-1027.

49. Tran, H.T.; Mao, A.; Pappu, R.V. (2008) Role of backbone-solvent interactions in determining conformational equilibria of intrinsically disordered polypeptides. *J. Am. Chem.Soc.* 130: 7380-7392.

50. Teufel, D. P.; Johnson, C. M.; Lum, J. K.; Neuweiler, H. (2011) Backbone-Driven Collapse in Unfolded Protein Chains. *J. Mol. Biol*. 409:250–262.

51. Morar, A. S.; Olteanu, A.; Young, G. B.; Pielak, G. J. (2001) Solvent-induced collapse of α-synuclein and acid-denatured cytochrome C. *Protein Sci*. 10:2195-2199.

52. Lee, J. C.; Langen, R.; Hummel, P. A.; Gray, H. B.; Winkler, J. R. (2004) Alpha-synuclein structures from fluorescence energy-transfer kinetics: implications for the role of the protein in Parkinson's disease. *Proc. Natl. Acad. Sci. U.S.A.* 101:16466-16471.

Chapter 6

Dynamic Hydration Map Reveals Key Structural Insights into Membrane-bound α-synuclein

6.1 Introduction

α-Synuclein is a small 140-residue soluble presynaptic protein that is predominantly expressed in the human brain and is localized in presynaptic nerve terminals.[1,2] The precise physiological function of α-synuclein still remains elusive, however, it is conjectured to be involved in vesicle trafficking,[3] synaptic plasticity,[4] learning,[5] SNARE complex assembly[6] and neurotransmission[7]. In addition to its poorly understood functional aspects, aggregation of α-synuclein is implicated in a number of disorders like Parkinson's disease, Alzheimer's disease and many other neurodegenerative diseases.[8,9] Structurally, α-synuclein belongs to the class of Intrinsically Disordered Proteins (IDPs). α-Synuclein has 3 distinct modular domains: (i) positively charged N-terminal region (residues 1-60) has propensity to bind membranes[10]; (ii) hydrophobic non-amyloid β (NAC) domain (residues 61-95) is responsible for aggregation,[11] (iii) negatively charged C-terminal region (residues 96-140) is highly flexible and facilitates interaction with Ca^{2+} ion and other biomolecules.[12] The N-terminal and NAC domains have 7 imperfect 11-residue repeats.

Numerous elegant studies based on circular dichroism,[13,14] nuclear magnetic resonance,[15-17] electron paramagnetic resonance,[18-20] and fluorescence experiments[21-23] have shown that α-synuclein undergoes a profound conformational transition from random coil to α-helix upon interaction with membrane mimetic such as sodium dodecyl sulphate (SDS) and anionic phospholipid membranes. The synuclein-membrane interactions have implications in biological functions and disease pathology.[24-26] Upon interaction with negatively charged surface (micelle or membrane), α-synuclein can adopt two major conformations namely broken horseshoe-type helix and/or extended helix. Recent single molecule studies provide direct evidence for the switch between the two conformations.[27-29] Many reports have

suggested that the binding is facilitated by N-terminus with the involvement of repeat regions.[30] A recent study has addressed the penetration depth of the N-terminal end into the outer leaflet of the lipid layer.[31] However, there is still a deficit in the information on the residue-specific localization of the entire chain of α-synuclein on the membrane surface. The knowledge on immersion depths of different residues at the membrane surface is an important structural aspect in the context of both functional and pathological roles of α-synuclein.

In the present study, we have made an attempt to gain the residue-specific resolution of α-synuclein under micelle- and membrane-bound conditions. As a prelude, we initiated our efforts on SDS-bound states and then embarked upon studies on model lipid membranes. We have utilized a variety of spectroscopic techniques to monitor site-specific positioning of the bound form of α-synuclein. We have taken advantage of the fact that the wild-type α-synuclein is devoid of tryptophan and incorporated ten single Trp mutants at different locations. We deciphered the localization of Trp residues by monitoring ultraslow relaxation of water molecules located at the interfaces of micelle-water as well as membrane-water. Our results permitted us to construct a dynamic hydration map indicating the positions of different residues of α-synuclein with respect to the interfaces.

6.2 Experimental section

6.2.1 Materials

All the chemicals (except lipids) were purchased from Sigma (St. Louis, MO) and used as received.

6.2.2 Mutagenesis, expression and purification

Recombinant human α-synuclein cloned in pT7-7 plasmid was kindly provided by Prof. V. Subramaniam (University of Twente, Netherlands). We incorporated single tryptophan(s) at ten different locations (F4W, A27W, Y39W, A56W, A69W, A78W, A90W, A107W, A124W, and A140W) using site-directed mutagenesis kit from Stratagene (La Jolla, CA) with slight modification in the PCR protocol. The primers were designed and checked using the freely available software "Gene Runner". All the constructs were confirmed by DNA sequencing. The primer sequence for site directed mutation is mentioned below.

Primer sequence for site-directed mutagenesis

Mutants	Primer	Sequence (5'→3')	No. of Bases	T_m	% GC
A69W	Forward	5'GACAAATGTTGGAGGATGGGTGGTGACG3'	28	60.1	53.6
A69W	Reverse	5'CACCCGTCACCACCCATCCTCCAAC3'	25	59.7	64
A27W	Forward	5'CCAAACAGGGTGTGTGGGAAGCAGCAGG3'	28	63.7	60.7
A27W	Reverse	5'GTCTTTCCTGCTGCTTCCCACACACCCTG3'	29	62.5	58.6
A56W	Forward	5'GGTGTGGCAACAGTGTGGGAGAAGACC3'	27	58.6	59.3
A56W	Reverse	5'GCTCTTTGGTCTTCTCCCACACTGTTGC3'	28	57.6	53.6
A90W	Forward	5'CAGGGAGCATTGCATGGGCCACTGGC3'	26	65.2	65.4
A90W	Reverse	5'CAAAGCCAGTGGCCCATGCAATGCTCC3'	27	64.4	59.3

A78W	Forward	5'GGTGTGACAGCAGTATGGCAGAAGACAG3'	28	55.3	53.6
A78W	Reverse	5'CTCCACTGTCTTCTGCCATACTGCTGTC3'	28	54.7	53.6
A107W	Forward	5'GCAAGAATGAAGAAGGATGGCCACAGGAAG3'	30	61	50
A107W	Reverse	5'CAGAATTCCTTCCTGTGGCCATCCTTCTTC3'	30	60.3	50
A124W	Forward	5'GGATCCTGACAATGAGTGGTATGAAATGCC3'	30	58.1	46.7
A124W	Reverse	5'CCTCAGAAGGCATTTCATACCACTCATTGTC3'	31	57.8	45.2
Y39W	Forward	5'GACAAAAGAGGGTGTTCTCTGGGTAGGCTCC3'	31	60.6	54.8
Y39W	Reverse	5'GGTTTTGGAGCCTACCCAGAGAACACCC3'	28	59.2	57.1
F4W	Forward	5' CATATGGATGTATGGATGAAAGGAC3'	25	45.4	40
F4W	Reverse	5' GTCCTTTCATCCATACATCCATATG3'	25	45.4	40
A140W	Forward	5'GACTATGAACCTGAATGGTAAGAAATATCTTTGC3'	34	55	35.3
A140W	Reverse	5'GAGCAAAGATATTTCTTACCATTCAGGTTCATAG3'	34	55.1	35.3

Expression and purification of wild-type and mutant proteins:

The wild-type and mutants were purified using the protocol described previously[32] with minor modifications. Briefly, 1% of the overnight grown culture was transferred in fresh media and induced with 0.8 mM IPTG (Isopropyl β-D-1-thiogalactopyranoside) for four hours after the O.D. of the culture reached to 0.6. The induced cells were pelleted at 4,000 rpm and resuspended in lysis buffer (10 mM Tris, 1 mM EDTA, pH 7.5). The lysed cells were then boiled at 95 °C for 15-20 min and centrifuged at 11,000 rpm for 20 min. The supernatant was thoroughly mixed with 10% streptomycin sulfate solution (136 µL/ml) and glacial acetic acid (228 µL/ml). The solution was centrifuged at 11,000 rpm for 30 min. To the clear supernatant, equal volume of saturated ammonium sulphate was added and incubated at 4°C for an hour with an intermittent mixing. The precipitated protein was

separated by centrifuging it at 11,000 rpm for 30 min. The pellet was dissolved in equal volume of absolute ethanol (chilled) and 100 mM ammonium acetate. Finally, the pellet was washed twice with absolute ethanol and resuspended in 10 mM Tris pH 7.4 followed by ion-exchange chromatography. The fractions of pure protein eluted at ~ 300 mM NaCl were checked on SDS-PAGE (Figure 6.1a) and the molecular weight was confirmed by Mass Spectrometry. The pure fractions were pooled and dialysed against buffer (10 mM HEPES and 50 mM NaCl; pH 7.4). The concentration of wild-type protein was determined using ε_{280}=5,600 $M^{-1}cm^{-1}$.[32] Concentration for all the mutants (except Y39W) was determined using ε_{280} =10,810 $M^{-1}cm^{-1}$; ε_{280} = 9,970 $M^{-1}cm^{-1}$ (Y39W).[31] The purified proteins were stored at -80°C.

6.2.3 Preparation of SDS solution

The stock of 1 M SDS was prepared in acetate buffer (0.2 mM NaCl, 10 mM NaH_2PO_4, 10 mM glycine and 10 mM sodium acetate; pH 7). The different concentrations of SDS were prepared by diluting the stock in the same buffer.

6.2.4 Preparation of small unilamellar vesicles (SUVs)

Chloroform solutions of (1-palmitoyl-2-oleoyl-sn-glycero-3-phospho-L-serine) POPS, (1-palmitoyl-2-oleoyl-sn-glycero-3-phosphocholine) POPC and (1-palmitoyl-2-oleoyl-sn-glycero-3-phospho(1'-rac-glycerol)) POPG were purchased from Avanti Polar Lipids (Alabaster, AL) and used without further purification. Lipid vesicles (SUVs) were prepared using previously reported procedure[19] with slight modifications. Briefly, appropriate amount of lipid was taken in a round bottom flask and purged with a gentle stream of nitrogen

followed by vacuum desiccation for two hours to ensure complete removal of the organic solvent. The dried lipid film was then hydrated in DPBS (Dulbecco's phosphate buffer saline: 2.67 mM KCl, 1.47 mM KH_2PO_4, 138 mM NaCl, and 8.06 mM Na_2HPO_4; pH 7.4) buffer to get a final lipid concentration of 10 mM. Hydration was carried out for one hour with intermittent vortexing which resulted in a turbid solution, characteristic of large multilamellar vesicles (MLVs). Liposomes were then subjected to five freeze thaw cycles alternating between liquid nitrogen and water bath (preset at 42°C) for one minute each. MLVs were subjected to sonication in a bath sonicator for one hour to obtain SUVs. The size of SUVs was determined using DAWN 8 Helios MALS system (Wyatt Technology). The average hydrodynamic radius of SUVs was found to be 35 ± 10 nm. Vesicles were prepared fresh for each set of experiments.

6.2.5 Preparation of protein samples

Prior to every experiment, the protein samples were filtered through 50 kDa AMICON to remove oligomers (if any) and then concentrated using 3 kDa AMICON (procured from Millipore) to get a concentration of ~ 500 µM. The accurate concentration was then checked on an absorption spectrometer. The protein concentration was fixed to 20 µM for SDS experiments and 50 µM for lipids experiments.

6.2.6 Circular dichroism (CD) measurements

The CD spectra for wild-type and the mutants (25 µM) were recorded on Chirascan CD machine (Applied Photophysics) with a scan range of 200 - 260 nm. The data were collected with a scan rate of 1 nm/s. The final spectra were averaged over 3 scans; buffer subtracted

and smoothened using 'ProData viewer' software provided with the instrument. CD spectra of protein were collected in absence and presence of SDS and lipid vesicles under identical conditions.

6.2.7 Steady state fluorescence measurements

All the spectroscopic measurements were performed on Fluoromax-4 (Horiba Jobin Yvon, NJ). For all fluorescence experiments, the concentration of SUVs was fixed to 2 mM (lipid: protein = 40). Following parameters were adjusted to measure tryptophan intensity in absence and presence of SDS and lipid vesicles; λ_{ex} = 295 nm and λ_{em} = 315-400 nm with 0.5 nm and 3 nm bandpass, respectively with an integration time of 1 s. For anisotropy measurements, excitation wavelength and bandpass were fixed to 295 nm and 1 nm, respectively, whereas emission wavelength was fixed at the maxima for each Trp mutant. The steady-state anisotropy is given by $r_{ss} = (I_{\parallel} - I_{\perp}G) / (I_{\parallel} + 2I_{\perp}G)$, where $I_{\parallel}$ and $I_{\perp}$ are fluorescence intensities collected using parallel and perpendicular geometry of the polarizers, respectively, with an integration time of 5 s. The perpendicular components were corrected using respective G-factors. For collecting the tryptophan spectral scans for REES measurements, following parameters were adjusted: λ_{ex} = 280/295/305 nm and λ_{em} (scan range) = 310-400 nm. The excitation bandpass was adjusted to 0.5 nm (for λ_{ex} = 280 and 295 nm) and 1 nm (for λ_{ex} = 305 nm). The emission bandpass was fixed to 3 nm. All the spectra were integrated for 1 s and averaged over 3 scans except for λ_{ex} = 305 where five scans were averaged over 3 s. All the spectra were buffer subtracted and plotted using OriginPro Version 8.5 software. To measure spectral-shifts, all the spectra were normalized. All the measurements were done at

25°C. Protein samples were incubated for 10 min with SDS and vesicles at room temperature (~ 25°C) prior to the measurements.

6.2.8 Time resolved measurements

Time-resolved fluorescence decay measurements of the samples were made using a time-correlated single-photon-counting (TCSPC) setup (Fluorocube, Horiba Jobin Yvon, NJ). For all the decay measurements, 295 nm LED was used as the excitation source. Lifetime measurement for A56W mutant (50 µM) in presence of 0.8 mM SDS was collected using a photomultiplier tube (Hamamatsu Corp) at emission wavelength of 335 nm and 12 nm slit-width. Ludox solution in water (10%) was used to record instrument response function (IRF ~ 1.1 ns). Lifetime experiments were done in a cuvette with pathlength of 10x10 mm. A good signal-to-noise ratio was ensured by fixing the counts to 10,000 in the highest channel. For time resolved emission shift (TRES) measurements the emission spectra were collected from 320 - 400 nm. All the data were collected at magic angle (54.7°).

6.2.9 Stopped-flow CD experiments

The kinetics of conformational changes of α-synuclein upon SDS interaction was monitored by the change in ellipticity. The Trp variant (A56W) was transferred from buffer to SDS and change in ellipticity at 222nm was monitored with a spectrometer (Chirascan, Applied Photophysics) equipped with a stopped-flow apparatus (Applied Photophysics) in 2 mm pathlength cuvette. The final protein concentration was fixed at 40 µM and SDS concentration was 880 µM. The data were acquired for 0.5 sec with 10,000 samples per point

and the traces were collected in triplicates for five times and averaged to get a satisfactory signal-to-noise ratio.

6.2.9 Data analysis

The intensity decays were deconvoluted with respect to IRF and analysed by fitting them to a sum of exponentials. The spectral reconstruction for TRES measurement was done by slicing the data with 4 channels per slice using DAS software provided with the instrument. The spectra were normalized and fitted to logarithm normal function at each delay point using OriginPro version 8.5 software. The fits were used to construct the TRES that represents spectral change at different wavelengths and time during the fluorescence decay. The corresponding hydration correlation function $C(t)$, was determined using the following relation[33]:

$$C(t) = [\upsilon_{max}(t) - \upsilon_{max}(\infty)]/[\upsilon_{max}(0) - \upsilon_{max}(\infty)]$$

The values for maximum fluorescence, $\upsilon_{max}(t)$ in cm^{-1}, for each delay point were obtained from logarithm normal fits. In the present observation, the spectral evolution related to solvation was completed by 11 ns, therefore it was used to define $\upsilon_{max}(\infty)$. The $\upsilon_{max}(0)$ was considered as 32,170 cm^{-1} (320 nm) as reported in previous studies.[33] The correlation function was fitted single exponentially to get an estimate of solvent relaxation time.

6.3 Results

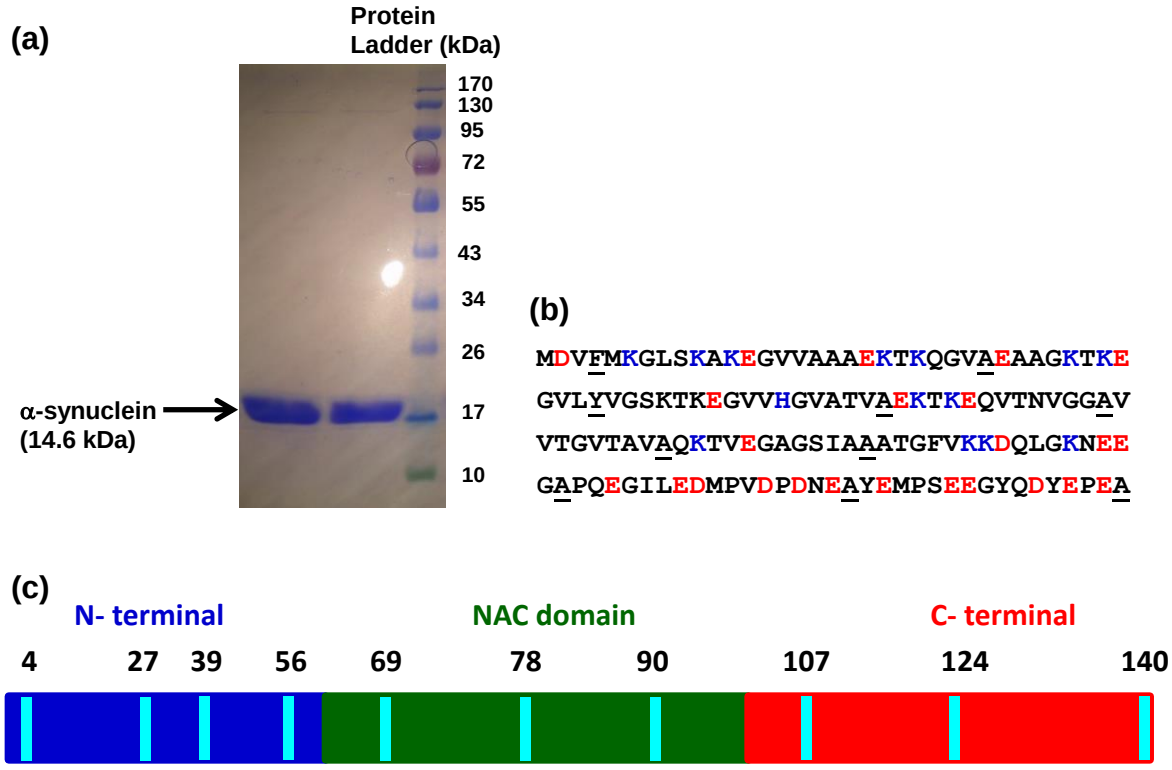

Figure 6.1 SDS-PAGE, amino acid sequence and mutational sites of α-synuclein. (a) The SDS-PAGE of wild-type α-synuclein. (b) Amino acid sequence showing negatively (red) and positively (blue) charged amino acids. The mutational sites for incorporating Trp are shown as underscored. (c) Various regions of the protein: N-terminal (blue), NAC-domain (green) and C-terminal (Red). Trp mutant positions are shown in cyan.

6.3.1 α-synuclein interaction with SDS

6.3.1.1 Binding induced folding monitored by circular dichroism (CD)

CD spectroscopy was employed to monitor α-synuclein interaction with SDS. We observed progressive increase in the helicity at an expense of random coil with the increase in the concentration of SDS (Figure 6.2a). We next performed the stopped-flow experiments to follow the kinetics of the conformational change. The process was found to be faster than the

dead time of the mixer (~ 2 ms) (Figure 6.2b). These preliminary results from CD spectroscopy prompted us to perform more detailed fluorescence-based experiments on α-synuclein interaction with SDS to shed light on residue-specific binding-induced folding.

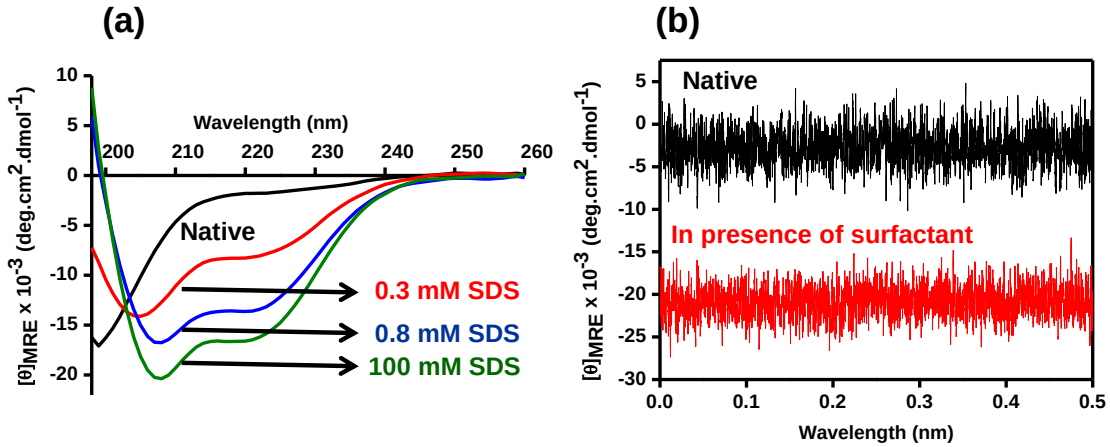

Figure 6.2 CD spectra of wild-type α-synuclein. (a) Changes in the secondary structure from random coil (black; Native IDP state) to α-helix with varying SDS concentrations (red, blue and green). (b) Stopped-flow CD measurements depicting fast kinetics of conformational change in presence of 0.8 mM SDS (red trace). Black trace represents the protein in native (IDP) form.

6.3.1.2 Residue-specific structural insights into the SDS-bound state

Next, we embarked upon fluorescence properties of substituted tryptophans at different locations. For incorporating Trp, the residue positions at 4, 39, 69, 90, 124 and 140 were chosen based on earlier reports that demonstrated no alteration in the conformational properties of α-synuclein[34] (Figure 6.1b,c). Additionally, we made four single Trp mutants (27, 56, 78 and 107) (Figure 6.1b,c). The wild-type protein and all the mutants exhibited random coil under native conditions (Figure 6.3a). Tryptophan emission shift and anisotropy were measured in the absence and presence of SDS at different concentrations with all α-synuclein mutants. In the absence of SDS, all the mutants exhibited fluorescence maxima at ~

348 nm (Figure 6.3b) and low anisotropy values (r_{ss} = 0.05 ± 0.02) (Figure 6.3c) indicating that the tryptophan(s) are exposed to water in the free disordered form of the protein.

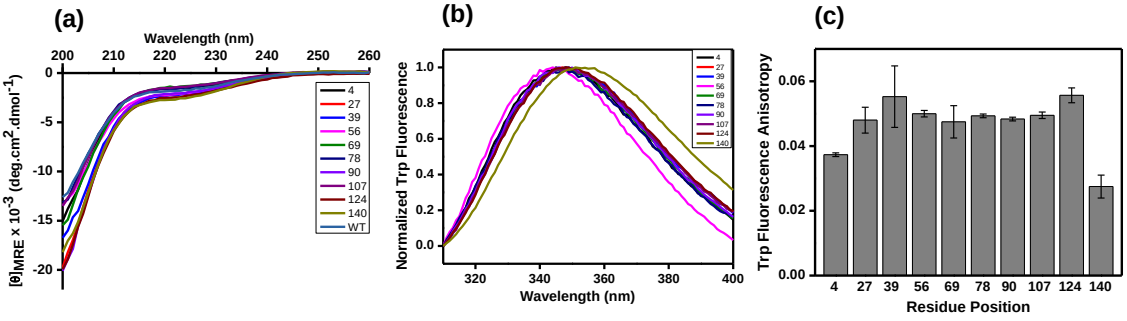

Figure 6.3 Native (IDP) state of all Trp mutants confirmed by (a) CD, (b) Tryptophan fluorescence emission maxima and (c) Tryptophan fluorescence anisotropy.

However, upon incubation with different concentrations of SDS, Trp fluorescence emission maxima and anisotropy showed changes along the sequence (Figure 6.4a). The Trp emission maxima exhibited blue shift for all the mutants except the positions at the C-terminal segment at all the SDS concentrations. The blue-shift in the emission maxima indicated that the Trp residues get buried. Next, we probed the structure formation around the tryptophan(s) by measuring the fluorescence anisotropy, which is an indicator of structural rigidification around the probe. The anisotropy of tryptophan(s) varied as a function of SDS concentrations and residue positions (Figure 6.4b). At low SDS concentrations, the variants in N-terminus (except Trp 39) and NAC domain showed moderate increase in anisotropy whereas at higher concentrations all the mutants showed significant rise in anisotropy indicating dampening of tryptophan motion. The anisotropy for the variants located at C-terminus (Trp 107, 124, 140) remained unaltered at all the concentrations of SDS. From the 3D plot (Figure 6.4b), it can be inferred that SDS at low concentration behaves as small unilamellar vesicles (SUVs) having high surface curvature and thus α-synuclein can twine

around to form a broken-helix like (horseshoe-type) structure, whereas, at high concentrations, SDS molecules may arrange themselves to form a rod like structure akin to large unilamellar vesicles where protein gets larger surface area for interaction and thus exists as an extended helix.[27]

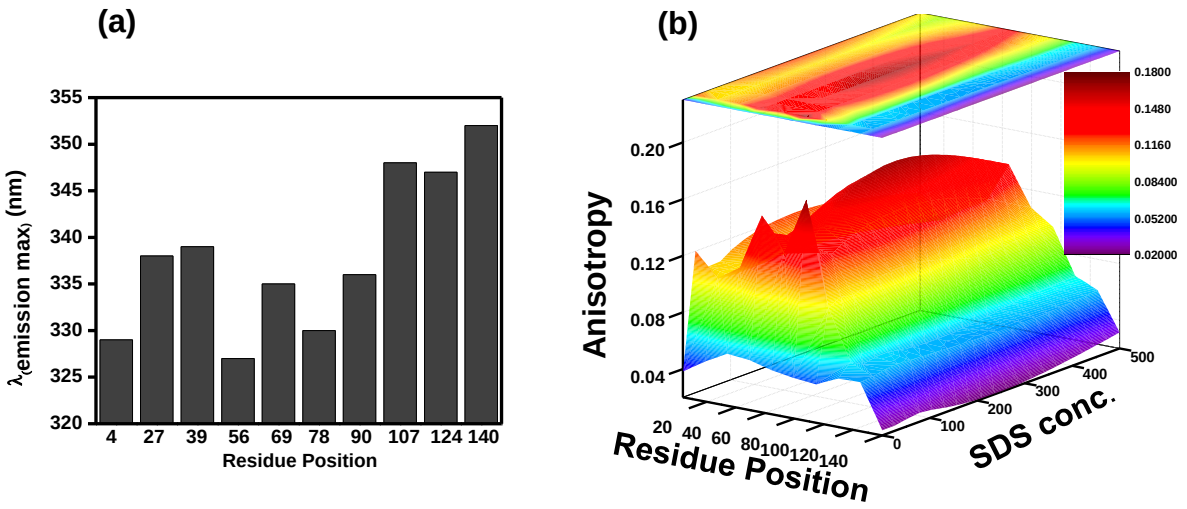

Figure 6.4 Tryptophan fluorescence of α-synuclein single Trp mutants. (a) Emission maxima of Trp located at different residues in the presence of SDS (0.8 mM). (b) Variation in tryptophan fluorescence anisotropy as a function of SDS concentration along the chain.

6.3.1.3 Depth-profile of different residues of α-synuclein at micelle-water interface

We next asked the question: How do the different parts of the protein localize themselves with respect to the SDS-water interface? In order to answer this question, we set out to perform experiments that would allow us to distinguish the proximal and distal tryptophans from the SDS surface. Here we took the advantage of the fact that the solvation dynamics of restricted water molecules around the membrane-bound protein is different from that of bulk water. The membrane interface comprises a thin (~ 15 Å) layer of motionally restrained water molecules that create highly ordered and viscous micro-environment. We conjectured that the residues that are localized in this thin layer of highly ordered water

molecules will report its fluorescence readout that is sensitive to micro-viscosity. One of such "wavelength-selective" approach is the red-edge excitation shift (REES) that is applied to monitor the dynamics of restricted water molecules at the membrane interface.[35-37] In bulk non-viscous media, fluorescence emission maxima is independent of excitation wavelength since the timescale of water reorientation is much faster (picoseconds) compared to the fluorescence decay timescale (nanoseconds). However in a viscous micro-environment, such as in membrane-interface, the water reorientation time is slowed down by orders of magnitude and competes with the fluorescence lifetime. Under such conditions, the emission maxima exhibit a progressive shift towards the longer wavelength when the excitation wavelength is gradually shifted to the red edge of the absorption band. Tryptophan fluorescence has also been shown to demonstrate REES under restricted environment. Since SDS is a well characterized membrane mimetic that consists of motionally restricted water molecules at the micelle-water interface, we carried out REES experiments on single Trp α-synuclein constructs in the absence and in the presence of SDS.

In the disordered (unbound) state of α-synuclein, Trp residues placed along the sequence showed no appreciable shift in the emission maxima when excited at three different wavelengths (280 nm, 295 nm and 305 nm) at the red-edge of the tryptophan absorption maxima (Figure 6.5a,b; top panel). However, in the SDS-bound form, different residue positions demonstrated a varied extent of REES. With the addition of SDS, a progressive shift in emission maxima as a function of excitation wavelength was observed for the residues in N-terminus and NAC domain whereas no change was observed for C-terminal residues (Figure 6.5a,b; bottom panel). At the N-terminus and NAC-domain, the residues Trp 56 and Trp 78 showed maximum shift of ~ 23 nm and ~ 18 nm, respectively suggestive of

slow reorientation of water molecules in the vicinity of embedded tryptophan(s) inside SDS. The mutants Trp 4 and Trp 90 exhibited moderate REES of ~ 12 nm which implies the partial exposure of tryptophans to the bulk water. A low REES was observed for Trp 27, Trp 39 and Trp 69 indicating exposure of these tryptophan(s) to the bulk to a much greater extent.

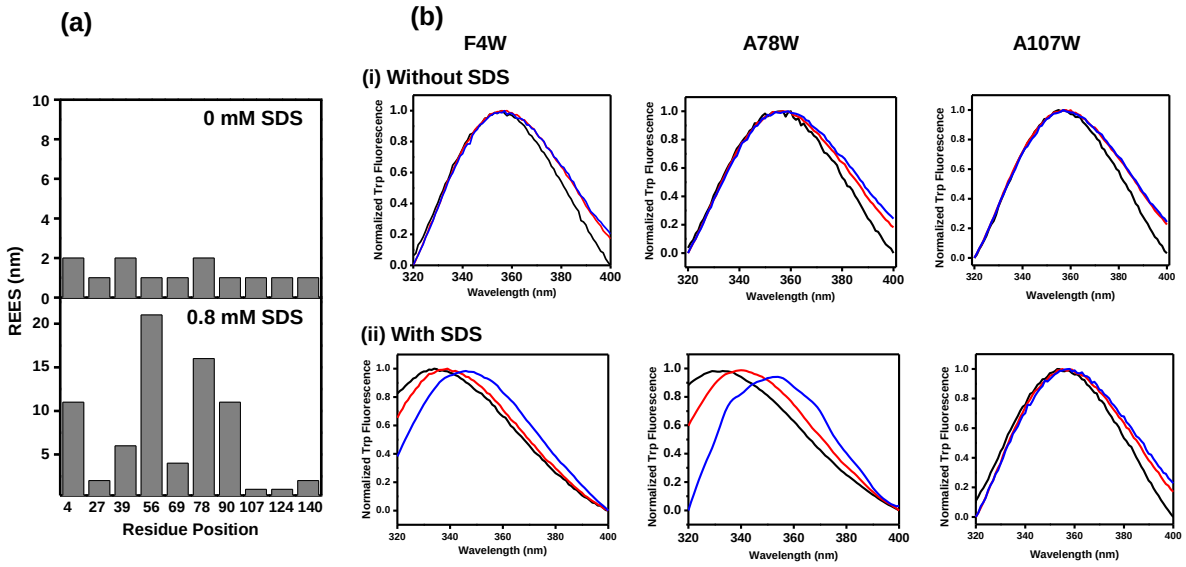

Figure 6.5 Red-edge excitation shift (REES) of tryptophans in α-synuclein. (a) Extent of REES observed in the absence (top panel) and in the presence of 0.8 mM SDS (bottom panel). (b) Fluorescence emission spectra with progressive change in excitation wavelength (λ_{ex}= 280 nm: black; 295 nm: red; 305 nm: blue) in the absence (panel i) and the presence of 0.8 mM SDS (panel ii) for representative locations at the N-terminal segment (Trp 4), NAC-domain (Trp 78) and C-terminal segment (Trp 107).

As mentioned earlier, that REES arises due to the slow reorientation dynamics of water that is either comparable to or slower than fluorescence lifetime. In order to directly monitor the water dynamics, we next embarked upon studying the timescale of hydration dynamics of α-synuclein in the presence of SDS (0.8 mM) using time-resolved emission spectra (TRES) that measures the time-dependent Stokes shift (TDSS) on the nanosecond timescale. In order to perform TRES experiments, we chose Trp 56 variant which lies in the

N-terminus and demonstrated the maximum extent of REES. The mean lifetime obtained from the decay (Figure 6.6a) for Trp 56 in the presence of SDS (0.8 mM) was found to be ~ 3.6 ns. Figure 6.6b shows the time-resolved decay of Trp fluorescence monitored at different emission wavelength. The fluorescence decays become progressively longer with an increase in the average fluorescence lifetime as a function of emission wavelength and provides a clear signature of slow solvent relaxation at the excited state. The correlation time from the decay analysis exhibited TDSS on the nanosecond timescale which is comparable to the lifetime of the fluorophore (Figure 6.6a,c). These results provide compelling evidence in favour of ultraslow water relaxation arising out of localization of the Trp-residue at SDS-water interface comprising a highly ordered water layer with a constrained mobility.

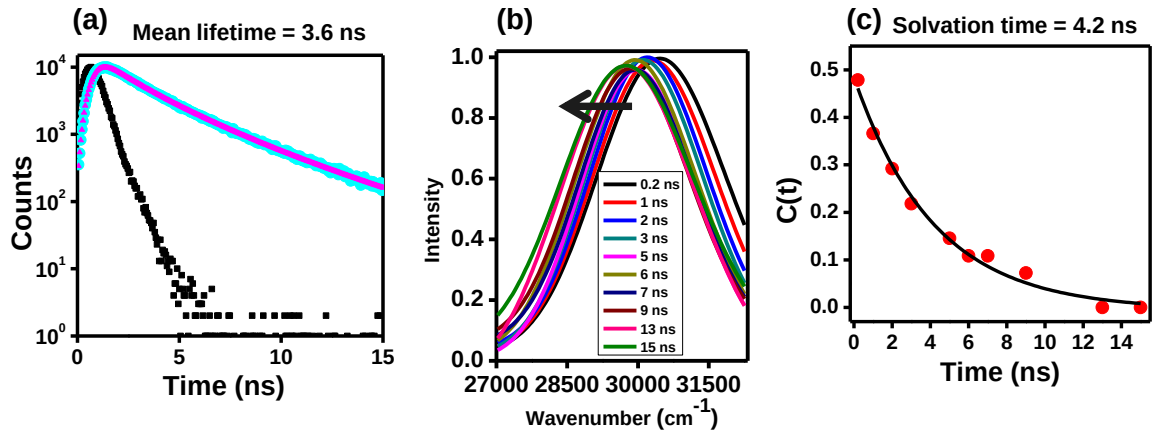

Figure 6.6 Time-resolved fluorescence studies to monitor ultraslow hydration dynamics. (a) Time-resolved decay of Trp 56 of α-synuclein in the presence of 0.8 mM SDS. (b) The time-resolved emission spectra (TRES) of Trp 56 of α-synuclein in the presence 0.8 mM SDS showing gradual shift of the spectra on the nanosecond timescale confirming ultraslow water relaxation in the excited state of Trp. (c) Correlation function derived from TRES data.

Our REES results coupled with the anisotropy data indicate that the N-terminus and NAC domain interact with the micelle surface, whereas, the C-terminal segment owing to high negative charge remains completely exposed to the bulk water. These preliminary

results prompted us to embark upon our studies on membrane-bound α-synuclein. We next performed these experiments using lipid membranes.

6.3.2 α-synuclein interaction with synthetic membranes

6.3.2.1 Membrane-induced conformational change monitored by CD

We first monitored binding-induced folding behaviour of α-synuclein in the presence of small unilamellar vesicles (SUVs) from synthetic phospholipids with varied head-group chemistry. We have used SUVs for our experiments since the size of SUVs is comparable to presynaptic vesicles where α-synuclein is known to be localized.[2] Circular dichroism (CD) spectroscopic studies indicated conformational transition from an intrinsically disordered state to a highly helical state upon binding to phospholipid SUVs. Negatively charged POPG SUVs were able to induce the most significant structural changes under the physiological

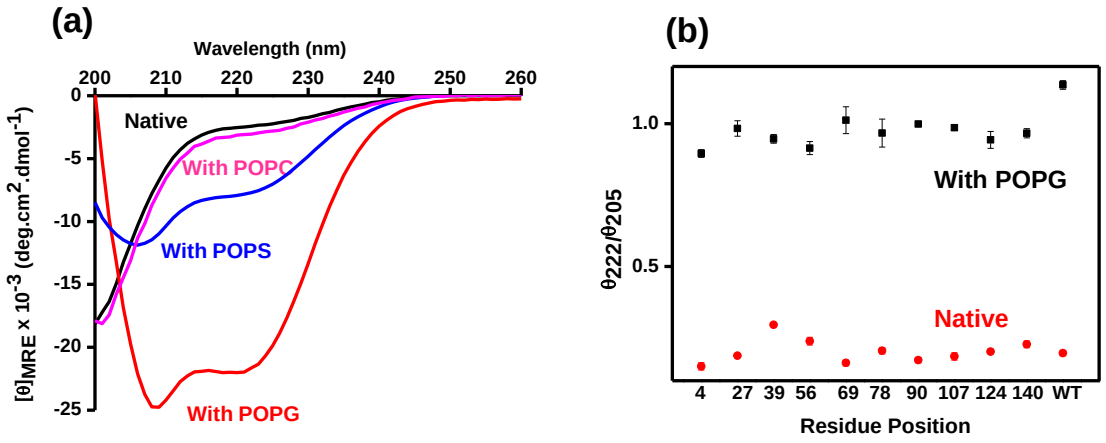

Figure 6.7 Changes in the secondary structure of α-synuclein monitored by CD. (a) Trp 78 variant in presence of different phospholipids. (b) The ratio of ellipticity ($\theta_{222}/\theta_{205}$) for all Trp mutants in the absence and presence of POPG SUVs. (Lipid: Protein = 40).

condition among the SUVs derived from POPC, POPS and POPG (Figure 6.7a). These results corroborated with a previous report where NMR data also demonstrates highest binding affinity of α-synuclein to POPG.[17] For all our subsequent experiments, we have used POPG SUVs. All the Trp mutants showed conformational change to similar extent upon binding with membrane derived from POPG (Figure 6.7b). This set of results indicated that natively unfolded α-synuclein, upon binding to negatively charged membrane, undergoes a profound conformational change.

6.3.2.2 Structural and dynamical insights into the membrane-bound state

Next, we monitored the changes in Trp fluorescent properties of the protein upon interaction with POPG SUVs. Upon binding to POPG SUVs, different locations showed varied blue-shift indicating membrane-interaction and structure formation at the N-terminal segment and the NAC domain, whereas, the Trp residues placed at the C-terminal end did not undergo any detectable blue-shift that is consistent with the fact that predominantly acidic C-terminus does not bind to negatively charged membrane (Figure 6.8a,b).

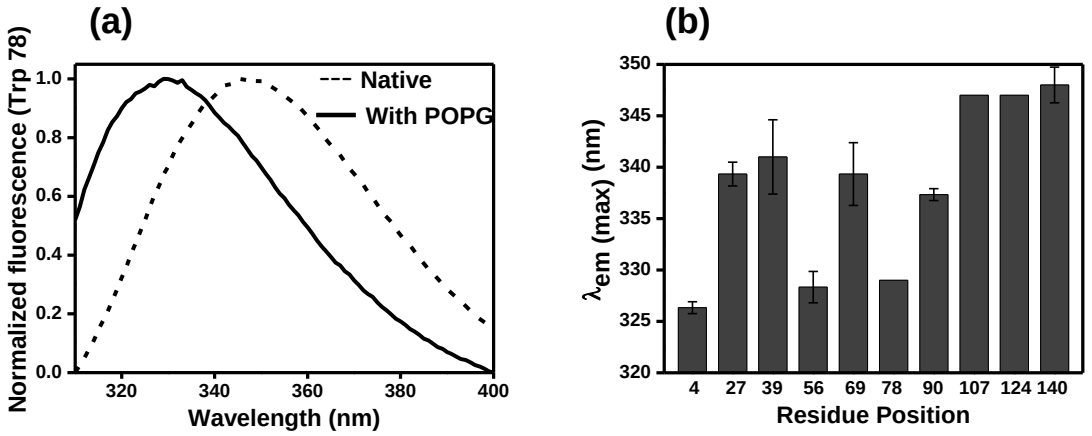

Figure 6.8 (a) Tryptophan (A78W) fluorescence emission in absence and presence of POPG SUVs. (b) Emission maxima for all the Trp mutants in presence of POPG SUVs (λ_{ex} = 295 nm).

Next, we took one of the NAC-domain locations (Trp 78) and carried out fluorescence polarization experiments, in which measured steady-state fluorescence anisotropy reports the rotational mobility at a given residue position. The idea behind this experiment is that the binding-induced folding would impart considerable conformational restriction at a given region of the polypeptide chain containing Trp and would result in a sharp increase in fluorescence anisotropy. We then validate our approach by monitoring fluorescence anisotropy of Trp 78 in the free- and lipid-bound states. These experiments showed that anisotropy increases from ~ 0.05 (free disordered protein) to ~ 0.18 (membrane-bound) and confirmed the strongest binding of α-synuclein with POPG among the lipids we have studied (Figure 6.9a). Also, the anisotropy experiments indicated lower binding affinity at high salt concentrations that is consistent with earlier reports (Figure 6.9b).[22]

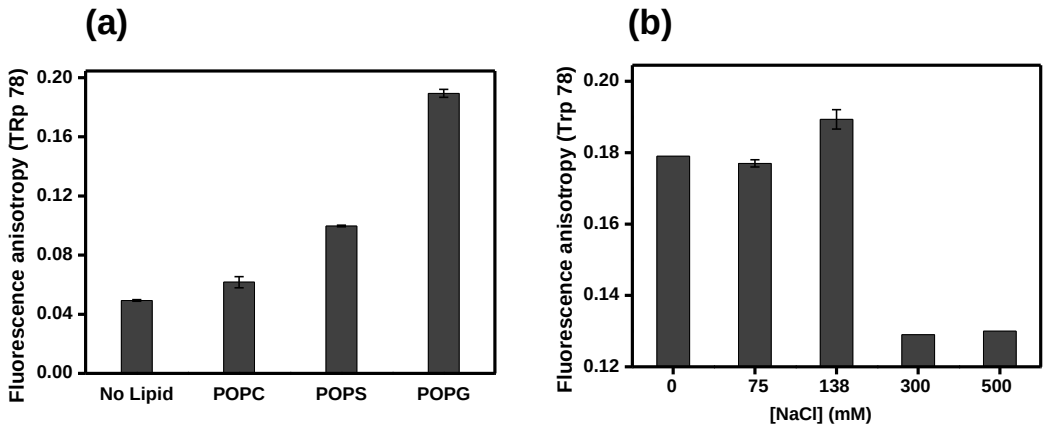

Figure 6.9 (a) Fluorescence anisotropy of Trp 78 in the absence and presence of chemically different SUVs. (b) Fluorescence anisotropy of Trp 78 in the presence of POPG SUVs at different salt concentrations.

After demonstrating that the Trp anisotropy is a robust reporter of membrane binding-induced acquisition of structure, we then carried out anisotropy experiments for all 10 single-Trp variants of α-synuclein along the sequence to map the restriction in the rotational

dynamics from the N- to the C-terminal end. In the free form, anisotropy was low (0.05 ± 0.01) for all the positions in α-synuclein indicating an intrinsically disordered state devoid of any specific structural propensity. In the lipid-bound form, the anisotropy values along the sequence showed varied extent of dampening of dynamics as a result of gain in the structure at different regions of the protein (Figure 6.10). Based on the measured anisotropy at various residue positions, we constructed the anisotropy map, which revealed that the N-terminal end is tightly bound and structured, whereas, C-terminal end does not seem to participate in the folding event. The middle region of the N-terminal segment (Trp 27 and 39) showed lower degree of structure, while the region juxtaposing the N- and the NAC-domain (Trp 56) is highly structured as indicated by high anisotropy. Interestingly, the NAC-domain also showed different degrees of structural organization. The initial region (Trp 69) showed a lower degree of structure as compared to the middle region (Trp 78). The structural organization in the region between the NAC-domain and C-terminal segment (Trp 90) is lower compared to Trp 78 and progressively diminishes as Trp is moved from the NAC- to the C-terminal region. Taken together, these experiments provide residue-specific structural organization of the membrane-bound α-synuclein.

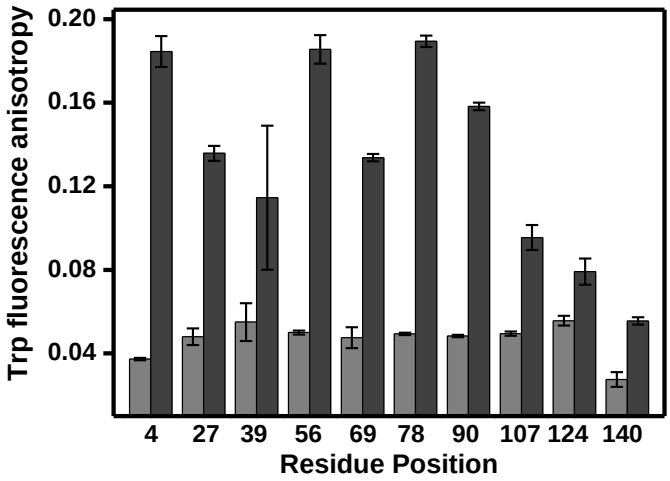

Figure 6.10
Change in anisotropy for all the Trp mutants in absence (light grey) and presence (dark grey) of POPG SUVs.

Taken together, our CD and fluorescence measurements on α-synuclein revealed a profound conformational change from random-coil to α-helix upon binding to the membrane. Additionally, residue-specific structural alterations along the polypeptide chain could be extracted from tryptophan fluorescence spectral-shifts and anisotropy data.

6.3.2.3 Depth-profile of different segments of α-synuclein from the membrane surface

The dynamics of solvent relaxation mirrored in the shift of Trp's fluorescence spectrum, was thus utilized to elucidate the proximal and distal positions of different residues with respect to the membrane surface. We observed that different residues demonstrated a varied extent of REES indicating their proximal and distal positioning with respect to the membrane interface. Figure 6.11a,b show the fluorescence emission spectra for POPG-bound α-synuclein (Trp 78 and 140) recorded by progressively shifting the excitation wavelength (280 nm, 295 nm and 305 nm). These spectra clearly indicated progressive shift in the emission maxima for Trp 78 variant as a function of excitation wavelength. However, Trp 140 that is located at the end of C-terminus did not show any shift. We then plotted the REES (in nm) for each residue position in the membrane-bound form to construct a *dynamic hydration map* that depicts the regions that are localized within the 15 Å layer of motionally restrained water molecules at the membrane interface (Figure 6.11c). Initial part of the N-terminal sequence (Trp 4) demonstrated a large extent of the REES (~13 nm), whereas, the middle region (Trp 27 and 39) exhibited much lower REES. In the NAC-domain, residues 56, 78 and 90 showed a significant REES (~13 nm, 15 nm and 11 nm, respectively), whereas, the residue 69 exhibited much lower REES (~ 5 nm). The C-terminal residues did not show any significant REES.

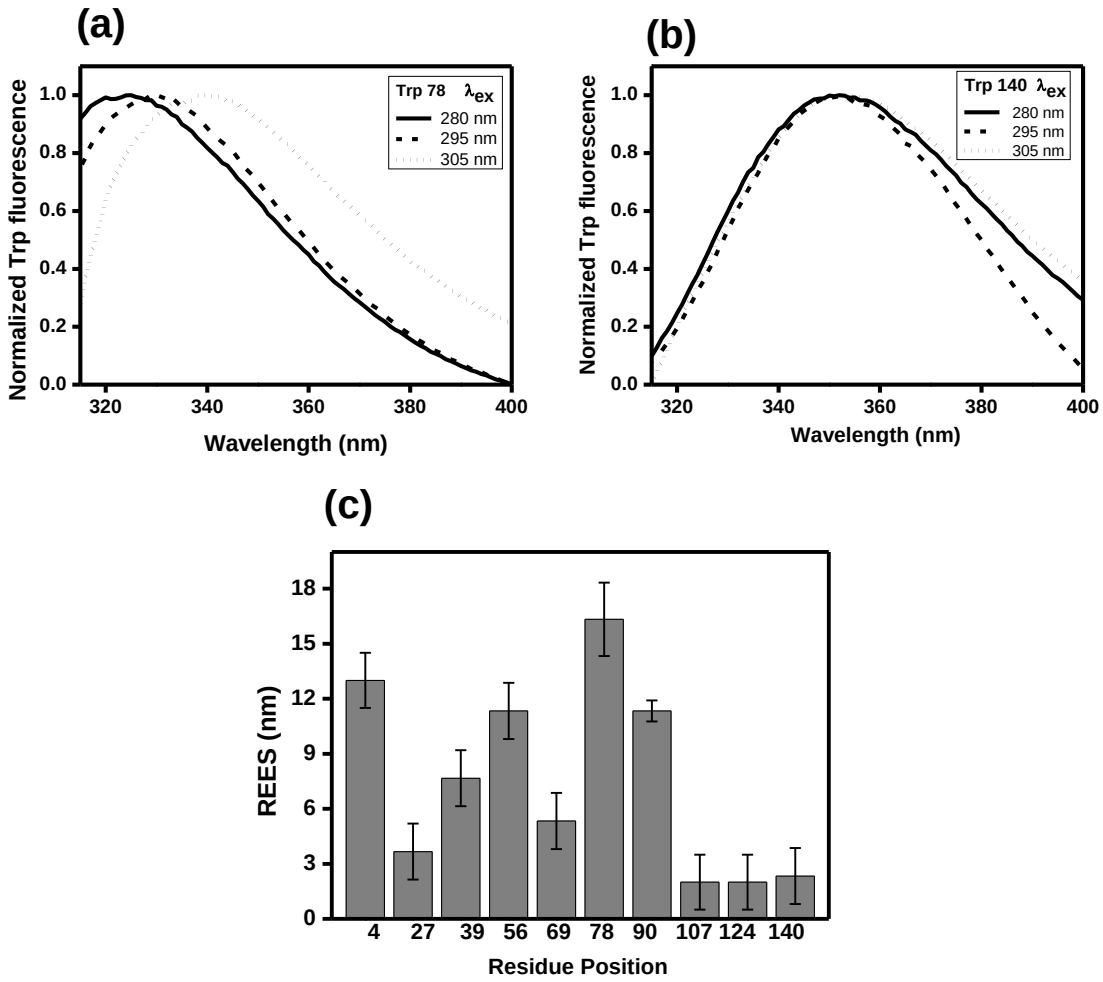

Figure 6.11 Red-edge excitation shift (REES) of tryptophans in α-synuclein. (a) Fluorescence emission spectra of Trp 78 by varying excitation wavelength from 280 to 305 nm in the presence of SUVs. (b) Fluorescence emission spectra of Trp 140 by varying excitation wavelength from 280 to 305 nm in the presence of SUVs. (c) REES observed at different residue positions along the sequence of α-synuclein in the presence of POPG SUVs.

6.4 Discussion

α-Synuclein undergoes a large-scale disordered-to-helix conformational transition in the presence of lipid membrane. However, it has been difficult to elucidate the high-resolution structural details, especially, the extent of penetration-depth at the residue-specific level in the membrane-bound form. Using single Trp mutants generated along the sequence

of α-synuclein from the N- to the C-termini, we have been able to gain structural and dynamical insights at specific locations of the protein on the SDS surface and membranes. The selective insight from each of these residues allowed us to construct a conformational map of the protein on the SDS-surface and lipid membrane. For instance, the anisotropy map lends support to the broken-helix model at low SDS concentration where the initial N-terminal segment and the NAC-domain are structured, whereas, the structure gets progressively lost as one moves to the end of C-terminus. Similar results were obtained with POPG SUVs. However, at high SDS concentration, the N-terminal segment and NAC domain are completely structured resembling the extended helix formed on membrane surface. The anisotropy map provides crucial structural insights at the residue-specific level but lacks the information about the depth-profile of the α-synuclein chain on the membrane. In order to obtain the precise localization of different residues at different immersion depths near the membrane surface, we utilized a unique and reliable indicator, such as REES, that reports the hydration dynamics around a fluorophore. The membrane-water interface comprises a ~15 Å thick water layer having strongly bound (restrained) water. This type of ordered water, also termed as '*biological water*', has been conjectured to play a variety of crucial biomolecular processes.[33,38] The extent of REES depends on whether or not the residues are localized in the outer leaflet of the bilayer comprising ordered water layer. Therefore, our REES studies, report on otherwise 'optically silent' water molecules[36] that are important to characterize the structural details of α-synuclein traversing the membrane surface. Based on our results and the constructed dynamic hydration map, we provide a structural model of α-synuclein in the membrane-bound form (Figure 6.12).

This model depicts the following salient features: The N-terminal end of the chain is embedded deeper into the membrane-interface. Our results on this part of α-synuclein provide support to an earlier model postulated based on fluorescence quenching and neutron reflectometry measurements coupled with molecular dynamics simulations.[31] The region near residues 27-39 traverses out to bulk water presumably because of a break in the helix in this region. The region around 56 again gets immersed into the ordered water layer. The early part of the NAC-domain containing residue 69 bulges out of the membrane-interface, the region around residue 78 traverses back into the interface and then the chain progressively starts emanating out of the membrane surface. The C-terminal residues do not localize themselves anywhere near the membrane surface. Taken together, our results elucidate the intriguing molecular details of the binding mode of α-synuclein to negatively charged membrane surface.

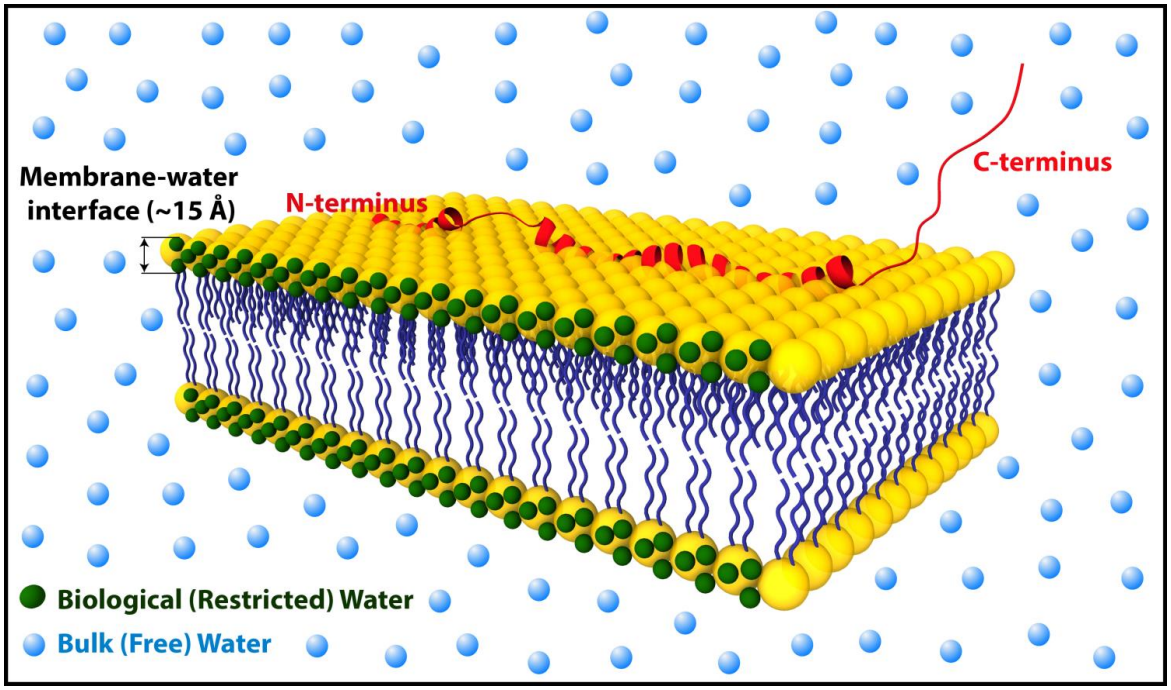

Figure 6.12 A proposed structural model of membrane-bound α-synuclein obtained from the dynamic hydration map.

Our results have important implications in the biology of α-synuclein. The mode of membrane binding may be of prime importance to its function. Site-specific binding of α-synuclein to the membrane surface not only leads to its conformational change but also influences the membrane stability and fluidity. These structural modulations in both α-synuclein and biological membranes could also be related to the fusion propensity of presynaptic vesicles. Besides the involvement in physiological function, α-synuclein-vesicle interaction might turn to be counterproductive leading to membrane permeabilization and cytotoxicity. From the interpretation of our data we can speculate that certain residues embedded in the membrane may alter the surface topology and lipid packing leading to increase in membrane permeability. These residues may serve as template for accumulation of protein that can promote α-synuclein aggregation. The segments sticking out of the membrane can also promote protein aggregation. It is interesting to note that a mutant related to Parkinson's disease (A30P) is located in the flexible region encompassing residue 27-39 that expels out of the membrane surface.

6.5 Conclusion

In summary, our results shed light into lipid-protein interaction in a residue-specific manner. The insight gained from the present study provides an important structural aspect in the understanding of synuclein-membrane interaction in the context of normal physiological functions as well as disease progression. We believe that our methodologies and results will find a broad application in the study of membrane binding of other amyloidogenic proteins.

6.6 References

1. Marques, O.; Outeiro, T. F. (2012) Alpha-synuclein: from secretion to dysfunction and death. *Cell Death Dis.* 3:e350; doi:10.1038/cddis.2012.94.

2. Goedert, M. (2001) Alpha-synuclein and neurodegenerative diseases. *Nat. Rev. Neurosci.* 2:492-501.

3. Cooper, A. A.; Gitler, A. D.; Cashikar, A.; Haynes, C. M.; Hill, K. J.; Bhullar, B.; Liu, K.; Xu, K.; Strathearn, K. E.; Liu, F.; Cao, S.; Caldwell, K. A.; Caldwell, G. A.; Marsischky, G.; Kolodner, R. D.; LaBaer, J.; Rochet, J.-C.; Bonini, N. M.; Lindquist, S. (2006) α-Synuclein blocks ER-Golgi traffic and Rab1 rescues neuron loss in Parkinson's models. *Science* 313:324-328.

4. Watson, J. B.; Hatami, A.; David, H.; Masliah, E.; Roberts, K.; C. E. Evans, C. E.; Levine, M. S. (2009) Alterations in corticostriatal synaptic plasticity in mice over-expressing human α-synuclein neuroscience. *Neurosci.* 159:501-513.

5. George, J. M.; Jin, H.; Woods, W. S.; Clayton, D. F. (1995) Characterization of a novel protein regulated during the critical period for song learning in the zebra finch. *Neuron* 15:361-372.

6. Burre, J.; Sharma, M.; Tsetsenis, T.; Buchman, V.; Etherton, M. R.; Sudhof, T. C. (2010) Alpha-synuclein promotes SNARE-complex assembly in vivo and in vitro. *Science* 329:1663-1667.

7. Abeliovich, A.; Schmitz, Y.; Fariñas, I.; Choi-Lundberg, D.; Ho, W.-H.; Castillo, P. E.; Shinsky, N.; Verdugo, J. M. G.; Armanini, M.; Ryan, A.; Hynes, M.; Phillips, H.; David Sulzer, D.; Rosenthal, A. (2000) Mice lacking α-synuclein display functional deficits in the nigrostriatal dopamine system. *Neuron* 25:239-252.

8. Waxman, E. A.; Giasson, B. I. (2009) Molecular mechanisms of α-synuclein neurodegeneration. *Biochim. Biophys. Acta* 1792:616-624.

9. Spillantini, M. G.; Schmidt, M. L.; Lee, V. M.-Y.; Trojanowski, J. Q.; Jakes, R.; Goedert,

M. (1997) α-Synuclein in Lewy bodies. *Nature* 388:839-840.

10. Bartels, T.; Ahlstrom, L. S.; K. Beyer. (2010) The N-terminus of the intrinsically disordered protein α-synuclein triggers membrane binding and helix folding. *Biophys. J.* 99:2116-2124.

11. Weinreb, P. H.; Zhen, W.; Poon A. W.; Conway, K. A.; Lansbury Jr., P. T. (1996) NACP, a protein implicated in Alzheimer's disease and learning, is natively unfolded. *Biochemistry* 35:13709-13715.

12. Tamamizu-Kato, S.; Kosaraju, M. G.; Narayanaswami, V. (2006) Calcium-triggered membrane interaction of the α-synuclein acidic tail. *Biochemistry* 45:10947-10956.

13. Perrin, R. J.; Woods, W. S.; Clayton, D. F.; George, J. M. (2000) Interaction of human α-synuclein and Parkinson's disease variants with phospholipids. *J. Mol. Biol.* 275: 34393-34398.

14. Ferreon, A. C. M.; Deniz, A. A. (2007) α-Synuclein multistate folding thermodynamics: Implications for protein misfolding and aggregation. *Biochemistry* 46:4499-4509.

15. Eliezer, D.; Kutluay, E.; Browne, G. (2001) Conformational properties of α-synuclein in its free and lipid-associated states. *J. Mol. Biol.* 307:1061-1073.

16. Ulmer, T. S.; Bax, A.; Cole, N. B.; Nussbaum, R. L. (2005) Structure and dynamics of micelle-bound human α-synuclein. *J. Mol. Biol.* 280:9595-9603.

17. Wang, G.-F.; Li, C.; Pielak, G. J. (2010) ^{19}F NMR studies of α-synuclein-membrane interactions. *Prot. Sci.*19:1686-1691.

18. Christine, C. J.; Der-Sarkissian, A.; Chen, J.; Langen, R. (2004) Structure of membrane-bound α-synuclein studied by site-directed spin labelling. *Proc. Natl. Acad. Sci. U.S.A.* 101:8331-8336.

19. Drescher, M.; Veldhuis, G.; van Rooijen, B. D.; Milikisyants, S.; Subramaniam, V.;

Huber, M. (2008) Antiparallel arrangement of the helices of vesicle-bound α-synuclein, *J. Am. Chem. Soc.* 130:7796-7797.

20. Robotta, M.; Braun, P.; Rooijen, B. V.; Subramaniam, V.; Huber, M.; Drescher, M. (2011) direct evidence of coexisting horseshoe and extended helix conformations of membrane-bound alpha-synuclein. *Chem. Phys. Chem.* 12:267-269.

21. Lee, J. C.; Langen, R.; Hummel, P. A.; Gray, H. B.; Winkler, J. R. (2004) α-Synuclein structures from fluorescence energy transfer kinetics:Implications for the role of the protein in Parkinson's disease. *Proc. Natl. Acad. Sci. U.S.A.* 101:16466-16471.

22. Rhoades, E.; Ramlall, T. F.; Webb, W.W.; Eliezer, D. (2006) Quantification of α-Synuclein binding to lipid vesicles using fluorescence correlation spectroscopy. *Biophys. J.* 90:4692-4700.

23. Shvadchak, V. V.; Falomir-Lockhart, L. J.; Yushchenko, D. A.; Jovin, T. M (2011) specificity and kinetics of α-synuclein binding to model membranes determined with fluorescent Excited State Intramolecular Proton Transfer (ESIPT) Probe. *J. Biol. Chem.* 286:13023-13032.

24. Pfefferkorn, C. M.; Jiang, Z.; Lee, J. C. (2012) Biophysics of α-synuclein membrane interactions. *Biochim. Biophys. Acta* 1818:162-171.

25. Auluck, P. K.; Caraveo, G.; Lindquist, S. (2010) α-Synuclein: Membrane interactions and toxicity in Parkinson's disease. *Annu. Rev. Cell Dev. Biol*. 26:211-233.

26. Butterfield, S. M.; Lashuel, H. A. (2010) Amyloidogenic protein–membrane interactions: Mechanistic insight from systems. *Angew. Chem. Int. Ed.* 49:5628 -5654.

27. Ferreon, A.; Gambin, Y.; Lemke, E. L.; Deniz, A. A. (2009) Interplay of α-synuclein binding and conformational switching probed by single molecule fluorescence. *Proc. Natl. Acad. Sci. U. S. A.* 106:5645-5650.

28. Trexler, A. J.; Rhoades, E. (2009) α -Synuclein binds large unilamellar vesicles as an extended helix. *Biochemistry* 48: 2304-2306.

29. Ferreon, A. C. M.; Moran, C. R.; Ferreon, J. C.; Deniz, A. A. (2010) Alteration of the α-synuclein folding landscape by a mutation related to Parkinson's disease. *Angew. Chem. Int. Ed.* 49:3469 -3472.

30. Vamvaca, K.; Volles, M. J.; Lansbury Jr., P. T. (2009) The First N-terminal Amino Acids of α-Synuclein are essential for α-helical structure formation in vitro and membrane binding in yeast. *J. Mol. Biol.* 389:413-424.

31. Pfefferkorn, C. M.; Heinrich, F.; Sodt, A. J.; Maltsev, A. S.; Pastor, R. W.; Lee, J. C. (2012) Depth of α-synuclein in a bilayer determined by fluorescence, neutron reflectometry, and computation. *Biophys. J.* 102:613-621.

32. van Raaij, M. E.; Ine M. J. Segers-Nolten, I. M. J.; Subramaniam, V. (2006) Quantitative morphological analysis reveals ultrastructural diversity of amyloid fibrils from α-synuclein mutants. *Biophys. J. Biophys. Lett.* L96-98.

33. Pal, S. K.; Peon, J.; Zewail, A. H. (2002) Biological water at the protein surface: Dynamical solvation probed directly with femtosecond resolution. *Proc. Natl. Acad. Sci. U. S. A.* 99:1763-1768.

34. Rooijen, B. D. V.; Leijenhorst-Groener, K. A. V.; Claessens, M. M. A. E.; Subramaniam, V. (2009) Tryptophan fluorescence reveals structural features of α-synuclein oligomers *J. Mol. Biol.* 394:826–833.

35. Demchenko, A. P. (2008) Site-selective Red-Edge effects. *Methods Enzymol.* 450:59-78.

36. Haldar, S.; Chaudhuri, A.; Chattopadhyay, A. (2011) Organization and dynamics of membrane probes and proteins utilizing the red edge excitation shift. *J. Phys. Chem. B* 115:5693-5706.

37. Haldar, S.; Chattopadhyay, A. (2012) Hydration dynamics of probes and peptides in captivity. *Reviews in Fluorescence 2010* (Geddes, C.D., Ed.), Springer, New York pp. 155-172.

38. Pal, S. M.; Zewail, A. H. (2004) Dynamics of water in biological recognition. *Chem. Rev.* 104:2099−2123.